



NAVAL POSTGRADUATE SCHOOL

MONTEREY, CALIFORNIA

THESIS

**OPERATIONAL ANALYSIS OF TIME-OPTIMAL
MANEUVERING FOR IMAGING SPACECRAFT**

by

Wenjie Yeau

March 2013

Thesis Co-Advisors:

Mark Karpenko
I. Michael Ross

Approved for public release; distribution is unlimited

THIS PAGE INTENTIONALLY LEFT BLANK

REPORT DOCUMENTATION PAGE			Form Approved OMB no. 0704-0188	
Public reporting burden for this collection of information is estimated to average 1 hour per response, including the time for reviewing instruction, searching existing data sources, gathering and maintaining the data needed, and completing and reviewing the collection of information. Send comments regarding this burden estimate or any other aspect of this collection of information, including suggestions for reducing this burden, to Washington headquarters Services, Directorate for Information Operations and Reports, 1215 Jefferson Davis Highway, Suite 1204, Arlington, VA 22202-4302, and to the Office of Management and Budget, Paperwork Reduction Project (0704-0188) Washington DC 20503.				
1. AGENCY USE ONLY (Leave blank)		2. REPORT DATE March 2013		3. REPORT TYPE AND DATES COVERED Master's Thesis
4. TITLE AND SUBTITLE OPERATIONAL ANALYSIS OF TIME-OPTIMAL MANEUVERING FOR IMAGING SPACECRAFT			5. FUNDING NUMBERS	
6. AUTHOR(S) Wenjie Yeau				
7. PERFORMING ORGANIZATION NAME(S) AND ADDRESS(ES) Naval Postgraduate School Monterey, CA 93943-5000			8. PERFORMING ORGANIZATION REPORT NUMBER	
9. SPONSORING /MONITORING AGENCY NAME(S) AND ADDRESS(ES) N/A			10. SPONSORING/MONITORING AGENCY REPORT NUMBER	
11. SUPPLEMENTARY NOTES The views expressed in this thesis are those of the author and do not reflect the official policy or position of the Department of Defense or the U.S. Government. IRB Protocol number ____N/A____.				
12a. DISTRIBUTION / AVAILABILITY STATEMENT Approved for public release; distribution is unlimited			12b. DISTRIBUTION CODE	
13. ABSTRACT (maximum 200 words) There is currently a gap in translating the performance enhancements made possible by new maneuver strategies into operational benefits derived for spacecraft missions. In the context of imaging satellites, slew time is one of the key factors that influences the economic performance of image collection operations. To analyze the operational benefits associated with adopting time-optimal maneuver strategies to reduce slew times, this thesis studies two different operational scenarios based on the Singapore-developed X-SAT imaging spacecraft. The analysis is facilitated through the use of AGI's Systems Tool Kit (STK) software. An Analytic Hierarchy Process (AHP)-based framework is proposed to evaluate, from a business analytic point of view, the impact of incorporating time-optimal maneuvers as part of X-SAT imaging operations. The business case analysis is focused on assessing key performance indicators such as image collection volume, collected image resolution and economic revenue. The findings presented herein suggest that time-optimal maneuvers can enhance the value of imaging operations and provide additional revenue for satellite operators. Moreover, the proposed AHP hierarchy model was found to provide a convenient and methodical means for quantifying the operational advantages and economic Return on Investment (ROI) that can be obtained when incorporating new maneuver strategies into spacecraft operations.				
14. SUBJECT TERMS Operational Analysis, Time-Optimal Attitude Maneuvers, Spacecraft, Business Case Analysis, Imaging Satellites, Analytic Hierarchy Process			15. NUMBER OF PAGES 135	
			16. PRICE CODE	
17. SECURITY CLASSIFICATION OF REPORT Unclassified	18. SECURITY CLASSIFICATION OF THIS PAGE Unclassified	19. SECURITY CLASSIFICATION OF ABSTRACT Unclassified	20. LIMITATION OF ABSTRACT UU	

THIS PAGE INTENTIONALLY LEFT BLANK

Approved for public release; distribution is unlimited

**OPERATIONAL ANALYSIS OF TIME-OPTIMAL MANEUVERING FOR
IMAGING SPACECRAFT**

Wenjie Yeau

Civilian, Defence Science Technology Agency (DSTA), Singapore

B.Eng (Hons), National University of Singapore, 2006

M.Sc, National University of Singapore, 2010

Submitted in partial fulfillment of the
requirements for the degree of

MASTER OF SCIENCE IN SPACE SYSTEMS OPERATIONS

from the

**NAVAL POSTGRADUATE SCHOOL
March 2013**

Author: Wenjie Yeau

Approved by: Mark Karpenko
Thesis Co-Advisor

I. Michael Ross
Thesis Co-Advisor

Rudy Panholzer
Chair, Space Systems Academic Group

THIS PAGE INTENTIONALLY LEFT BLANK

ABSTRACT

There is currently a gap in translating the performance enhancements made possible by new maneuver strategies into operational benefits derived for spacecraft missions. In the context of imaging satellites, slew time is one of the key factors that influences the economic performance of image collection operations. To analyze the operational benefits associated with adopting time-optimal maneuver strategies to reduce slew times, this thesis studies two different operational scenarios based on the Singapore-developed X-SAT imaging spacecraft. The analysis is facilitated through the use of AGI's Systems Tool Kit (STK) software. An Analytic Hierarchy Process (AHP)-based framework is proposed to evaluate, from a business analytic point of view, the impact of incorporating time-optimal maneuvers as part of X-SAT imaging operations. The business case analysis is focused on assessing key performance indicators such as image collection volume, collected image resolution and economic revenue. The findings presented herein suggest that time-optimal maneuvers can enhance the value of imaging operations and provide additional revenue for satellite operators. Moreover, the proposed AHP hierarchy model was found to provide a convenient and methodical means for quantifying the operational advantages and economic Return on Investment (ROI) that can be obtained when incorporating new maneuver strategies into spacecraft operations.

THIS PAGE INTENTIONALLY LEFT BLANK

TABLE OF CONTENTS

I.	INTRODUCTION.....	1
A.	SPACECRAFT SLEWING CAPABILITIES	4
B.	MOTIVATION FOR THESIS	5
C.	RESEARCH OBJECTIVES AND OUTCOME.....	6
II.	IMAGING SATELLITES FOR REMOTE SENSING.....	9
A.	CIVILIAN AND SCIENTIFIC APPLICATIONS.....	10
1.	Maritime Applications	10
a.	<i>Oil Spill Detection</i>	10
b.	<i>Sea State Monitoring</i>	11
c.	<i>Bathymetry Data Acquisition</i>	11
2.	Climate Monitoring	12
3.	Forestry and Agriculture Monitoring	13
4.	Natural Disaster and Hazard Assessment.....	14
B.	MILITARY APPLICATIONS.....	16
C.	CHARACTERIZATION OF SATELLITE IMAGING RESOLUTION...	17
1.	Spatial Resolution	18
2.	Temporal Resolution	19
3.	Spectral Resolution	20
4.	Commercially Available Satellite Imagery Sources	21
5.	Resolution Trade-off.....	23
D.	OTHER CRITERIA AFFECTING QUALITY OF SATELLITE IMAGES	24
1.	Elevation Angle.....	24
2.	Sun Angle	25
3.	Cloud Cover	26
E.	MISSION PLANNING FOR SATELLITE IMAGERY COLLECTION..	27
F.	OPTIMIZING SATELLITE IMAGERY COLLECTION	30
III.	SATELLITE ATTITUDE CONTROL	33
A.	MANEUVERING REQUIREMENTS.....	33
B.	TIME-OPTIMAL SPACECRAFT MANEUVERS	35
1.	ON-ORBIT TIME-OPTIMAL MANEUVER DEMONSTRATION	36
C.	OPERATONAL ANALYSIS	38
D.	OPERATIONAL SCENARIO SETUP.....	39
1.	Operational Scenario 1.....	41
2.	Operational Scenario 2.....	43
IV.	ANALYSIS OF OPERATIONAL SCENARIO 1	45
A.	PRELIMINARY WORK	45
B.	DETERMINATION OF IDEAL COLLECTION ROUTE	46
C.	IMPACT OF TIME-OPTIMAL MANEUVER STRATEGIES.....	47
1.	Imaging Window Period	53

2.	Mission Completion Time	54
3.	Resolution of Satellite Imagery Collected	55
4.	In-Track Stereo Imaging Opportunities	58
D.	CONCLUSIONS DRAWN FROM OS1 ANALYSIS.....	60
V.	A FRAMEWORK FOR BUSINESS CASE ANALYSIS.....	61
A.	ANALYTIC HIERARCHY PROCESS.....	62
B.	AHP-BASED ANALYSIS OF IMAGING SPACECRAFT OPERATIONS.....	64
1.	Motivation for using AHP Technique	64
2.	An AHP Hierarchy for Imaging Operations.....	65
VI.	AHP ANALYSIS OF OPERATIONAL SCENARIO 2.....	71
A.	EXTRACTING RELEVANT DATA FOR ANALYSIS	71
B.	APPLICATION OF AHP TECHNIQUE FOR OS2 ANALYSIS.....	75
C.	IMPACT OF TIME-OPTIMAL MANEUVER STRATEGIES.....	80
D.	BUSINESS CASE ANALYSIS OF X-SAT IMAGING OPERATIONS IN OS2.....	85
VII.	CONCLUSION AND FUTURE WORK.....	89
A.	CONCLUSION	89
B.	FUTURE WORK.....	90
	APPENDIX A. STK DATA AND BENEFIT SCORES FOR BASELINE SLEW PERFORMANCE	93
	APPENDIX B. STK DATA AND BENEFIT SCORES FOR 50% IMPROVEMENT IN SLEW PERFORMANCE	99
	APPENDIX C. BENEFIT SCORE COMPARISON BETWEEN BASELINE SLEW PERFORMANCE VERSUS 50% IMPROVEMENT IN SLEW PERFORMANCE	105
	LIST OF REFERENCES.....	111
	INITIAL DISTRIBUTION LIST	117

LIST OF FIGURES

Figure 1.	In-Track Stereo Satellite Image Collection. From [7]	3
Figure 2.	NASA MODIS Terra Satellite Image of Oil Slick Surrounding the Mississippi Delta due to BP oil spill. From [23]	11
Figure 3.	Bathymetry Data Expressed in Shaded Relief Visualization of Ocean Bottom Topography. From [25]	12
Figure 4.	Sea Surface Height Data Obtained from Active Radar Remote Sensing Equipment. From [27]	13
Figure 5.	Forestation Coverage Map of Tropical Rainforests in Southeast Asia. From [30]	14
Figure 6.	Satellite Image of Japan's Fukushima Nuclear Power Plant during the Nuclear Meltdown Incident in March 2011. From [32]	16
Figure 7.	Spatial Resolution Differences. From [38]	19
Figure 8.	Electromagnetic Spectrum. From [39]	20
Figure 9.	Three Dimensions for Resolution Trade-Off. From [40]	24
Figure 10.	Illustration of Elevation Angle. After [38]	25
Figure 11.	Solar Elevation Angle. After [42]	26
Figure 12.	Mission Planning Workflow for Satellite Imagery Collection. After [43]	28
Figure 13.	Singapore-developed X-SAT. From [53]	40
Figure 14.	X-SAT Technical Specifications and Orbital Parameters. From [53] ..	41
Figure 15.	Southeast Asia Geographic Map	42
Figure 16.	Target Cities in Operational Scenario 1	42
Figure 17.	Target Cities in Operational Scenario 2	44
Figure 18.	Screenshot of Imaging Window Assignment in STK	46
Figure 19.	Screenshot of X-SAT Imaging Bangkok City (arrow shows direction of satellite motion along the ground track)	46
Figure 20.	25% Reduction in Maneuvering Time	48
Figure 21.	50% Reduction in Maneuvering Time	49
Figure 22.	Slew Angle Calculation Example	50
Figure 23.	Slew Time from Phnom Penh to Bangkok for Baseline X-SAT Slew Performance	51
Figure 24.	Elevation Angle from Respective Target Cities to X-SAT during Image Collection in OS1	56
Figure 25.	Position of X-SAT at the start of Collecting Vientiane Imagery	57
Figure 26.	In-Track Stereo Imaging of Vientiane in OS1	59
Figure 27.	Generic AHP Hierarchy model	63
Figure 28.	Generic AHP Hierarchy Model with Assigned Weights	64
Figure 29.	AHP Hierarchy Model for Imaging Spacecraft Operations	67
Figure 30.	AHP Hierarchy Model for Imaging Spacecraft Operations with Assigned Weights	68
Figure 31.	Screenshot from STK for Generating the Satellite Access Time in OS2	72

Figure 32.	Screenshot from STK for Generating the AER data in OS2	73
Figure 33.	Screenshot of X-SAT Satellite Access Time Data from STK	73
Figure 34.	Sample Screenshot of Azimuth, Elevation and Range (AER) Data for Manila City	74
Figure 35.	Illustration of Difference between Imaging Time and Satellite Access Time.....	76
Figure 36.	Modified AHP Hierarchy Model for X-SAT Imaging Operations.....	77
Figure 37.	AHP Hierarchy Model for X-SAT Imaging Operations Updated with Assigned Weights.....	77

LIST OF TABLES

Table 1.	High-Res and Medium-Res satellite Imagery Sources. From [41].....	22
Table 2.	X-SAT Slewing Angles and Slewing Time in OS1	51
Table 3.	X-SAT Slewing Rate in OS1.....	52
Table 4.	Additional Imaging Time with Varying Improvement in Slewing Performance.....	53
Table 5.	Mission Completion Time for Imaging Five Target Cities	54
Table 6.	Relevant Data Obtained from STK for Possible Collection Routes in OS2	78
Table 7.	Results from Application of AHP Hierarchy Model for X-SAT Imaging Operations for OS2.....	79
Table 8.	Relevant Data Obtained from revised STK simulation of OS2 with 50% Improvement in X-SAT slewing performance	81
Table 9.	Application of AHP Hierarchy Model for X-SAT Imaging Operations in OS2 with 50% Improvement in Slewing Performance	82
Table 10.	Benefit Score Comparison for Image Resolution between Baseline and Time-Optimal Maneuvers	84
Table 11.	Computed Economic Benefit Score for All Collection Route Permutations in OS2	87

THIS PAGE INTENTIONALLY LEFT BLANK

LIST OF ACRONYMS AND ABBREVIATIONS

LEO	Low Earth orbit
EOS	Earth Observing Satellite
EPS	Electrical Power System
AOI	Area of Interest
ROI	Return on Investment
AHP	Analytic Hierarchy Process
EO	Electro Optical
IR	Infrared
SAR	Synthetic Aperture Radar
CMG	Control Moment Gyroscope
FOV	Field of View
GSD	Ground Sample Distance
STK	Systems Tool Kit
OS1	Operational Scenario 1
OS2	Operational Scenario 2
EBS	Economic Benefit Score

THIS PAGE INTENTIONALLY LEFT BLANK

ACKNOWLEDGMENTS

The author would like to thank Professor Mark Karpenko for his patient and meticulous review of the thesis from start until completion. We shared many fruitful discussions. Through these discussions, the exchanges help to spark the inquisitive thoughts in me and drive me to make my thesis more complete.

At the same time, the author would also like to thank Professor Mike Ross for his invaluable support and guidance towards the completion of this thesis. I am grateful for the confidence that Professor Mike Ross showed in me. He was always positive that I would be able to do a good job.

Last, but not least, the author would also like to thank his beloved wife, Yolanda Tan, who was with him in Monterey, and his respectful parents back in Singapore. Without my wife's loving support and selfless sacrifices, I would not be able to devote my time to completing this thesis. My parents have been a great influence in my life, and I hope I have made them proud.

THIS PAGE INTENTIONALLY LEFT BLANK

I. INTRODUCTION

The field of remote sensing relates to the “acquisition of information about an object from a distance” [1]. During the 19th century, one of the earliest forms of remote sensing was the practice of taking photographs from hot-air balloons in the sky. This laid the foundation for other remote sensing applications, which have since then mostly leveraged aerial imageries captured from an overhead position.

In the early 1900s, the practice of aerial photography proceeded to make its way into the aircraft platform and thus led to a dramatic growth in the number of aerial photos that could be collected. Usage of these aerial imagery data was further promulgated and eventually made its way to military applications (e.g., intelligence gathering and surveillance). Aerial imagery proved to be an important source of intelligence information during the two World Wars [2].

The development of satellite technology towards the latter half of the 20th century has further advanced the state of remote sensing applications. Aerial image collection can now take place from satellite platforms that are located hundreds of miles above Earth’s surface in Low Earth Orbits¹ (LEOs). With the advancement of satellite sensing technology and communications, humankind can now easily access satellite imagery, by simply downloading satellite images of worldwide locations from the Internet using applications such as Google Earth. Companies which require high-resolution satellite imagery can also procure these data directly from the various commercial companies that collectively own and operate sophisticated constellations of high-resolution commercial earth imaging satellites such as Quickbird, IKONOS, Worldview, GeoEye-1, RapidEye and Pléiades.

¹ A Low Earth Orbit is generally defined as an orbit below an altitude of 2,000 kilometres (1,200 miles) [3].

Earth Observing Satellites (EOSs) constantly traverse the globe collecting images using sensors and other equipment designed for remote sensing purposes. Today, EOSs have become an important means for Earth reconnaissance and Earth resources research. Although the number of EOSs is continuously increasing, the demand for remote sensing data is increasing at an even higher rate. From the satellite operators' perspective, the limited resources of EOSs are therefore extremely valuable. Efficient operation of imaging satellites is vital to make replete use of the EOSs imaging resources and to derive maximum operational benefit in terms of enhancing the value of imaging satellite operations. This allows for the collection of the highest quality geospatial data so as to achieve best economic returns. The majority of companies operating imaging satellites today are able to offer the following technical capabilities in their production of high-resolution imagery:

- a. *Large image collection capacity:* DigitalGlobe's Worldview-2 (launched on October 2009), is capable of collecting satellite imagery up to 1 million km² in a 24-hour period [4] while RapidEye claims an image collection capacity of 4 million km² per day [5].
- b. *High geo-location accuracy:* Modern commercial imaging satellites such as Worldview-1 and Worldview-2, are able to track and target an Area of Interest (AOI) with precision down to within 10-meter accuracy [4]. RapidEye offers 6.5-meter accuracy [5].
- c. *Large swath width:* Imaging satellites capable of collecting images with large swath width sensing characteristics are desired for efficient imaging coverage of large geographical regions. Worldview-1 and Worldview 2 are capable of collecting swath widths of more than 15 km at nadir [4] while Pléiades can provide imaging swath of 20 km [6].
- d. *Rapid targeting:* An agile attitude control system can provide the spacecraft with fast maneuvering capability in order to move from one target to the

next as quickly as possible. Worldview-1 and Worldview-2 are able to provide up to 3.5 degrees per second of slew agility [4] and Pléiades can also slew more than 3 degrees per second [6].

- e. *In-track stereo collection*: This concept refers to the capability of imaging satellites whereby stereo satellite images² are collected in the same orbit and acquired at angles optimal for stereo viewing and processing [7]. An example of in-track stereo satellite image collection is illustrated in Figure 1.

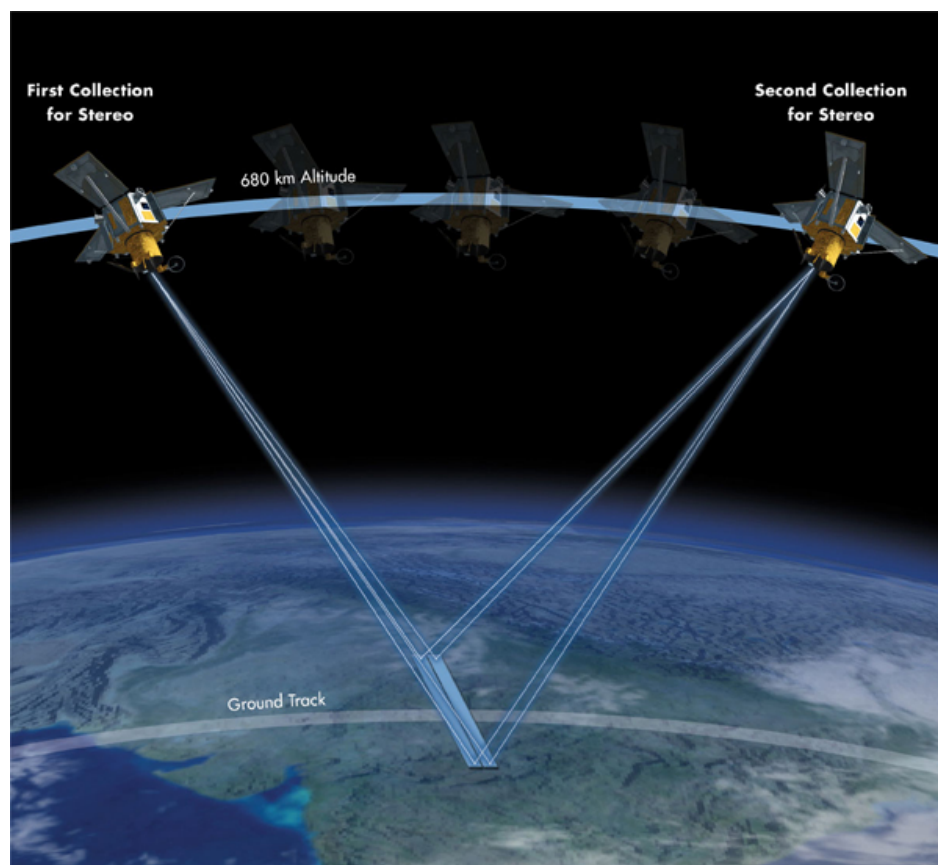


Figure 1. In-Track Stereo Satellite Image Collection. From [7]

² Stereo satellite images are a pair of images collected by the imaging satellite along the same ground path just a short duration apart at high-definition angles, in order to maintain the consistency of the images' color tone to enable better image quality [4].

The overall effectiveness of imaging satellites is largely dependent on the imagery collection capability, which in turn hinges on the duration of satellite access time and slew time from target to target. As the spacecraft revolves around Earth in LEO, the slewing capability of the spacecraft will affect the speed of the imaging satellite's target acquisition for satellite imagery collection.

A. SPACECRAFT SLEWING CAPABILITIES

In the context of spaceflight, slews are defined as “re-orientation or movement in reference to a plane or fixed position such as Earth, the Sun or another celestial body or another reference point in space” [8]. Controlling the orientation of a spacecraft system is vital for accomplishing many requirements of a spacecraft's mission. For example, slew maneuvers are required in the following operations:

- a. Orienting a high-gain antenna towards Earth for transmitting and receiving telemetry data and commands.
- b. Orienting the spacecraft towards the Sun for balancing the thermal heating and cooling of the spacecraft subsystems.
- c. Angling solar arrays towards the Sun for solar power absorption to reduce spacecraft systems' reliance on internal Electrical Power System (EPS).
- d. Targeting imaging equipment and sensor systems at AOIs for image acquisition.

While all of the operations mentioned above are critical for ensuring spaceflight mission success, the last factor is especially critical for satellite imagery providers in their endeavors to maximize economic returns. Potentially significant benefits can be reaped through the enhancement of the slewing capability of the spacecraft in terms of either reducing slew time or power consumption.

Modern commercial Earth-imaging satellites, including the recently launched Worldview-2 satellite, are equipped with rapid rotational maneuverability for high-resolution image collection. Instead of sweeping the imaging sensors from side to side (whisk-broom or push-broom mode³), the entire spacecraft body is able to turn rapidly in order to point the spacecraft towards the targeted AOI. This type of operation allows the imaging system to achieve a greater definition and thus improves the resolution of the collected imageries. Given that the overall cost-effectiveness of satellite imagery collection missions is greatly affected by the average retargeting time, development of intelligent control algorithms for rapid slewing and retargeting capabilities is crucial to the mission success and operational sustainability [9].

Retargeting maneuvers are subject to the physical limits of actuators, sensors, spacecraft structural rigidity, and other mission constraints [9]. The logic of large-angle control of most spacecraft is, however, generally restricted “by actuator momentum limits as well as torque saturation, rather than by sensor measurement limits or alignment” [10]. To simplify spacecraft control, it is usually desired to maintain rotation of the spacecraft body about an inertial-fixed axis during the target-acquisition mode. The imaging sensor can then acquire the desired target for imagery capture [11]. Optimal control theory can also be applied towards enabling rapid target-to-target acquisition in order to extend the capability of imaging satellites.

B. MOTIVATION FOR THESIS

In the study of optimal control theory for application to spacecraft maneuvering, the most fundamental issue was concerned with “determining the extreme case of the optimal control problems developed for non-singular and singular controls” [12]. Since the 1990s, there has been a resurgence of research interest in the design of controllers for spacecraft reorientation maneuvers.

³ Sensors sweep across the satellite’s track in whisk broom mode and along the satellite’s track in push-broom mode.

Among these studies, the optimization objectives have included the maneuver time, the fuel consumed and the weighted fuel/time cost function [13], [14], [15], [16].

The success of a spacecraft mission hinges on several key parameters and the definition of mission success can also differ from scenario to scenario. For imaging satellites, the volume of satellite imagery collected during a particular collection route reflects the economic Return on Investment (ROI) for that mission. Time-optimal maneuver algorithms are thus critical to the collection strategy adopted for imaging satellites because slew time has a direct impact on the volume of satellite imagery collected. In other words, a shorter slew time can potentially lead to collection of more satellite imagery within an assigned imaging window period.

Although there has been a significant amount of research that has contributed towards the design of control systems to meet the aforementioned objectives, there is currently a gap in translating the performance enhancements achieved by these maneuver strategies into the operational benefits they can provide for the spacecraft mission. By using a business-analytic approach towards analyzing novel spacecraft maneuver strategies, an objective analysis of the derived operational benefits can be used to support the specific business case for their implementation. At the same time, conducting an operational analysis helps to justify the need to invest in the design of new control systems and ground infrastructure for implementing optimal spacecraft maneuvers.

C. RESEARCH OBJECTIVES AND OUTCOME

This thesis aims to develop new insights into the operational benefits associated with time-optimal maneuver technology from a business perspective. Such an analysis provides an independent justification for the resources expended on the design of control systems for implementing optimized spacecraft maneuvers. This thesis will therefore augment existing technical

feasibility studies [12], [13], [15] and help to influence design considerations for different spacecraft maneuver strategies.

This thesis adopts a business-analytic approach towards analyzing time-optimal spacecraft maneuvers. The primary objectives of the study are as follows:

- A. To demonstrate how the implementation of time-optimal spacecraft maneuvers can translate into enhanced performance for spacecraft and enrich mission objectives.
- B. To provide a framework for quantifying mission effectiveness and operational efficiency with respect to the image collection requirements, as a measure of the benefits achieved from time-optimal spacecraft maneuvers.

In this study, the Analytic Hierarchy Process (AHP) technique [17] is applied to analyze the spacecraft performance. AHP provides a comprehensive and rational framework for structuring the operational analysis. In using the AHP technique, this thesis will break down the complex spacecraft mission goals into a ranked structure made up of simpler objectives, each of which can then be analyzed individually. The AHP approach allows the representation and quantification of key spacecraft performance elements in relation to these sub-goals and supports an investigation into how those performance elements will affect the overall mission goal.

Criteria such as image collection volume and resolution, among others, can be used in the AHP analysis. Furthermore, the Hierarchy Model introduced in this thesis for analyzing imaging satellite operations can be customized to fit different mission goals and collection requirements. Application of this structured framework can help key decision makers in the imaging satellite business to find the best solution which best suits their mission goals. Thus, commercial satellite companies and military space organizations can use the results of this work to gain a better understanding of how time-optimal spacecraft maneuvers can

translate into enhanced performance for their respective spacecraft in specific image collection scenarios.

The remainder of the thesis is outlined as follows:

Chapter II discusses the use of imaging satellites and the key factors that affect satellite imagery collection in the context of commercial and military applications for remote sensing purposes.

Chapter III presents the attitude control attributes of imaging satellite operations and provides examples of research work as well as recent practical demonstrations of time-optimal spacecraft maneuvers. The chapter concludes with an introduction of the two operational scenarios set up in the AGI Systems Tool Kit (STK) environment for subsequent operational analysis and business case analysis.

Chapter IV contains the results obtained from the operational analysis conducted in Operational Scenario 1 (OS1) and the derived operational benefits with the implementation of time-optimal maneuvers to the imaging satellite's operations. The results from the analysis provide the motivation for a more detailed business case analysis.

Chapter V introduces the concept of the Analytic Hierarchy Process (AHP) technique and applies this technique to develop a framework for the business case analysis of imaging spacecraft operations.

Chapter VI presents the application of the AHP-based framework to conduct an AHP analysis and discusses the impact of time-optimal maneuvers to the imaging operations in Operational Scenario 2 (OS2).

Conclusions and recommendations for future work are stated in Chapter VII.

II. IMAGING SATELLITES FOR REMOTE SENSING

Over the past few decades, satellites have been used in the environment of remote sensing industry to obtain a multitude of information about planet Earth. The use of satellites for remote sensing ranges from military applications to tracking global weather patterns, tectonic activity, surface vegetation, ocean currents and temperatures, polar ice fluctuations, pollution, and many other aspects [18].

Significant development had been made in space-based imaging systems and technology since the United States' first operational space-reconnaissance program (Corona).⁴ From the Corona days of using film cameras to record images to the range of cutting-edge sensors that are currently deployed on imaging satellites in the modern space environment, e.g., Electro-Optical (EO), Thermal Infrared (IR) sensor systems and imaging radar systems such as Synthetic Aperture Radar (SAR), space-based imaging technology has come a long way.

After the launch of the first sub-meter resolution commercial imaging satellite (IKONOS) in September of 1999 [20], there has been substantial improvement in the quality of satellite images and this spurred increased competition among the commercial satellite operators. These companies are constantly engaged in technology development to upgrade sensors in order to capture higher resolution imagery as well as the development of space platforms with higher efficiency and technologically superior ground systems. In the past two decades, we have also seen the power of satellite imaging harnessed by the military for augmenting Intelligence, Surveillance and Reconnaissance (ISR) capabilities. In the civilian sector, Google Earth and NASA's Visible Earth have gradually replaced aerial photos and become standard imaging tools used for a

⁴ The Corona program produced a series of US strategic reconnaissance satellites used for photographic surveillance of the Soviet Union, China and other regions. The program started in June 1959 and ended in May 1972. [19]

wide range of commercial applications. Some of these applications are described in the next section to give the reader an appreciation for the breadth and scope of remote sensing applications.

A. CIVILIAN AND SCIENTIFIC APPLICATIONS

1. Maritime Applications

a. Oil Spill Detection

During the last few decades, pollution of the oceans on Earth has become an increasing international concern. Deterioration of ocean water quality, especially in regions subject to heavy shipping, continues at a high rate despite rigorous control measures [21]. Illegal emissions from ships represent a hefty long-term source of harm to the maritime environment. Therefore, monitoring of vessels' illegal discharges is an important component in ensuring compliance with marine legislation and the general protection of coastal environments. In modern days due to the large area coverage required, prompt delivery of satellite SAR images are of particularly great value in detecting oil spills. The size, location and disbursement pattern of the oil spill can be efficiently determined using SAR imagery [22]. Figure 2 shows an example of a satellite image captured by the Moderate Resolution Imaging Spectroradiometer (MODIS) on NASA's Terra satellite in May 2010. The image illustrates the extent of the oil spill from BP's ruptured oil well on the floor of the Gulf of Mexico [23].



Figure 2. NASA MODIS Terra Satellite Image of Oil Slick Surrounding the Mississippi Delta due to BP oil spill. From [23]

b. Sea State Monitoring

Marine conditions change very rapidly and can vary considerably between locations only a few kilometers apart. Maritime weather and sea-state forecasts are critical to activities such as ship routing, fishing, management of offshore operations and coordinating rescue services. Planning of marine operations is heavily dependent on sea state conditions and forecast errors can cause damage to the economy and even cost human lives. Therefore, high accuracy and wide coverage of maritime weather and sea-state forecast services is highly desirable by the maritime and coastal entities. The consistent and geographically homogeneous data required for monitoring and forecasting of maritime conditions can come from analyzing satellite images.

c. Bathymetry Data Acquisition

Satellite SAR imagery, acquired under suitable ocean current and surface wind conditions, provides data for visualization of the ocean bottom topography. This imagery can subsequently be used to produce bathymetry data

through additional data processing and analysis. Therefore, combining satellite SAR imagery can substantially reduce maritime forces' survey times in the production of bathymetry maps with major cost savings [24]. An example of the ocean bottom topography visualization near the Golden Gate Bridge in San Francisco, California, produced from the utilization of bathymetry data is shown in Figure 3.

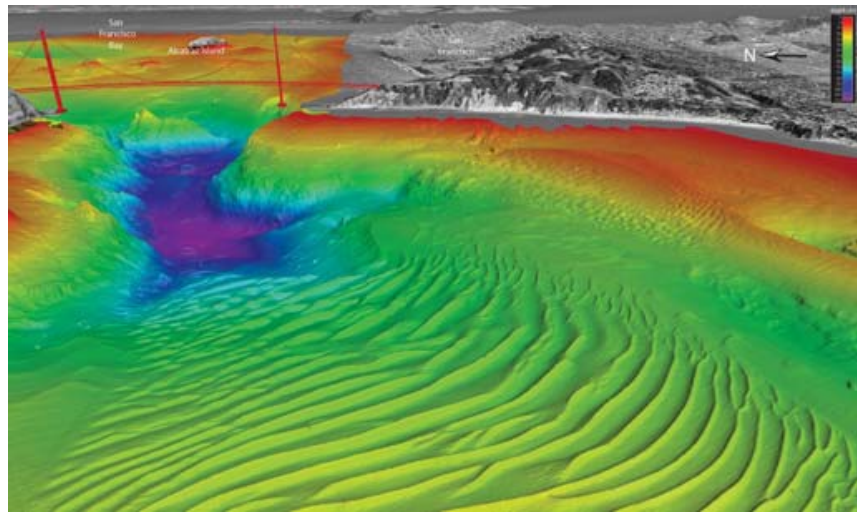


Figure 3. Bathymetry Data Expressed in Shaded Relief Visualization of Ocean Bottom Topography. From [25]

2. Climate Monitoring

Climate scientists recently issued a warning on global warming and predicted that heat waves, rainstorms, tropical cyclones and surges in sea level are expected to become more frequent, more widespread or more intense in the near future [26]. Global climate changes have posed significant challenges to the scientific community. The utilization of satellite-based remote sensors has been identified as a major source of consistent and continuous Earth imagery data for atmospheric, ocean, and land studies at multiple spatial and temporal scales. From space, satellite sensors are able to track and capture images of systemic changes on planet Earth as the spacecraft orbits the planet, hence acting as a reliable climate monitoring system through observation of Earth. Figure 4 points

out how scientists monitor the changes in sea surface height around the world to help measure the amount of heat stored in the ocean and hence predict global weather and climate events such as El Niño [27].

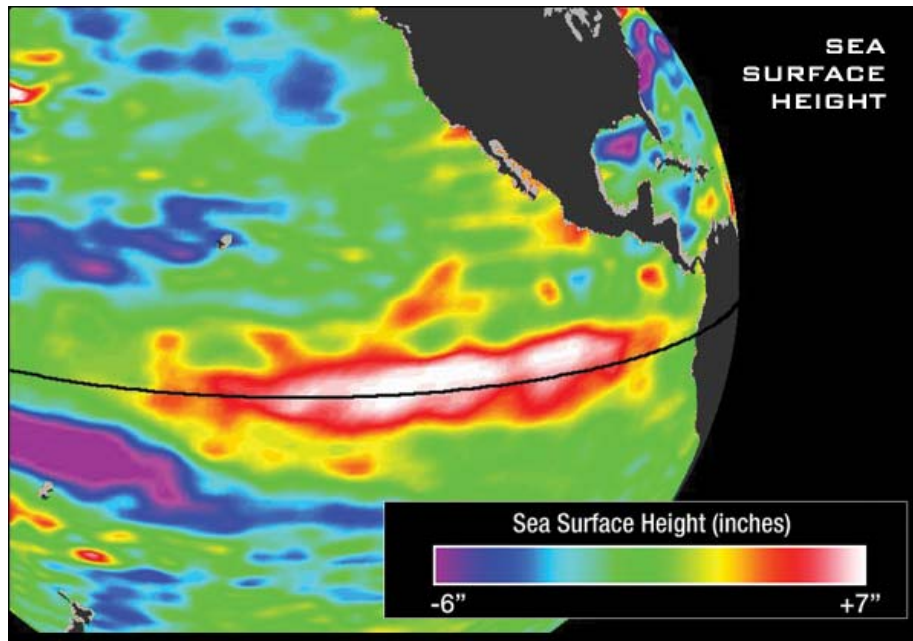


Figure 4. Sea Surface Height Data Obtained from Active Radar Remote Sensing Equipment. From [27]

3. Forestry and Agriculture Monitoring

Remote sensing satellites offer agronomists the ability to monitor crop development independent of weather conditions with multi-temporal analysis. This activity is typically associated with acquiring three input SAR datasets at different times and then assigning the color band according to the state of vegetation development. The color changes that appear in the satellite image will reflect the change in the state of land cover. Thus, crops planted at varying times and developing at varying rates can be identified through the observation of these color changes. Monitoring these data increases the crop area mapping accuracy and acreage estimation [28]. As a result, earth observation data obtained through imaging satellites provides a common data source and standardized methodology for the collection of agricultural statistics.

Besides crop monitoring, satellite SAR data can also provide mapping information of forest extent and forestry type in tropical areas subjected to almost continuous cloud cover conditions. In conjunction with other remote-sensing data, satellite images provide government organizations with the capability to map out forest damage, encroachment of agriculture onto forested areas unsuitable for development and scientific data of timber area inventories. Multi-temporal analysis is also being applied to monitor logging in forested areas [29]. Figure 5 shows a color composite map that presents the coverage of forestation in the tropical rainforests of Southeast Asia from multiple satellite sources.

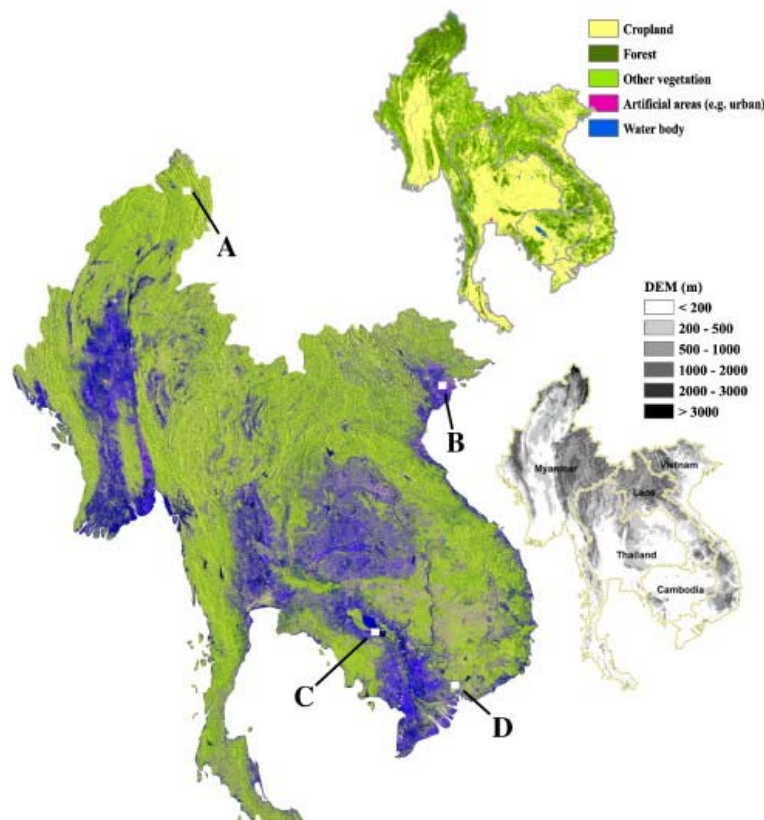


Figure 5. Forestation Coverage Map of Tropical Rainforests in Southeast Asia. From [30]

4. Natural Disaster and Hazard Assessment

Natural disasters can occur at anytime on any place on Earth. Tropical countries in Southeast Asia like the Philippines, Thailand and Indonesia are

vulnerable to floods, tsunamis and earthquakes. From time to time, people living in Europe and United States have also become victims to hurricanes and storms occurring virtually overnight. Whenever a disaster occurs, it is pertinent that the necessary responses including mitigation and rescue operations be executed in a timely manner.

Imaging satellites pass over nearly all regions of the world and provide regular image updates. Satellite imagery can be used not only to detect and monitor disaster areas, but also to assess the damage in the aftermath of a natural disaster. Vital information comes in the form of satellite imagery for the authorities in charge of planning and executing relief and rescue operations. Increasingly, imaging satellites play a critical role in natural disaster and hazard assessment given that the space-borne sensors can provide wide area coverage whilst ground-based equipment only performs localized measurements. For example, Figure 6 shows a satellite image of the nuclear meltdown incident at Japan's Fukushima Nuclear Power Plant in March 2011 after the explosion of the no. 3 and no. 4 reactors.

In addition, satellite monitoring provides unique advantages for post-disaster measures, such as rehabilitation and reconstruction, especially in large areas where other methods like aircraft surveillance and field visits, are not available or are inefficient and expensive. During peacetime, drought monitoring can also be supplemented by satellite data that indicates plant stress due to lack of water and the vitality of vegetation [31].



Figure 6. Satellite Image of Japan's Fukushima Nuclear Power Plant during the Nuclear Meltdown Incident in March 2011. From [32]

B. MILITARY APPLICATIONS

During the Gulf War, Operation Desert Storm⁵ demonstrated that space resources could contribute greatly to military operations. From that time onwards, the United States military has increased efforts in the development of space systems and technology for enhancing military capabilities [34]. As a result, U.S. military doctrine and operations have changed along with the creation of new organizations that emphasize military space applications. Space is now an important component of military operations.

The trend of the U.S. military harnessing space resources continued with the peace-keeping operations in Bosnia whereby commercial, military and NATO satellites were involved in providing communications, navigation and weather information to the war fighters. In particular, multi-spectral satellite imagery from commercial satellites such as LandSat and SPOT were utilized to provide broad area coverage of the war theater. Practical applications included using “unclassified imagery to determine optimal drop zones for supplies in potentially dangerous regions” [35].

A cornerstone of the U.S. military's exploitation of commercial satellite imagery is found in the U.S. Air Force's Eagle Vision program, which focused on

⁵ The Gulf War codenamed Operation Desert Storm was a war waged by U.N.-coalition forces from 34 nations led by the United States, against Iraq in response to Iraq's invasion of Kuwait [33].

transmitting satellite imagery to the war fighters [36]. The key-contributing factor to the program's success was the ease of access to high-resolution commercial remote sensing data. Originally built around using imagery from the Spot satellite, the program now taps on many of the new commercial remote sensing satellites that have been launched in recent years⁶. Today, with its capabilities enhanced by a plethora of modern commercial remote sensing satellites as well as new mission planning ground systems, the Eagle Vision program now even allows users to mix different types of remote sensing imagery and process them together with topographical data to generate 3-D terrain models.

Besides leveraging commercial imaging satellites, the U.S. military has also developed and launched its own battlefield reconnaissance space assets. Most recently in June 2011, U.S. Air Force successfully launched the Operationally Responsive Space-1 (ORS-1) satellite. The ORS-1 program is managed by the Operational Responsive Space Office and its mission is to provide field commanders with an enhanced battle space awareness capability through the feed of orbital space imagery to support combatant command operations [37].

C. CHARACTERIZATION OF SATELLITE IMAGING RESOLUTION

The database of high-resolution satellite imagery is expanding daily as worldwide users continue to tap into this information-rich repository for a host of commercial projects and research studies. Not all satellite imagery is created equal. There are differing levels of resolution tagged to the satellite imagery data that is being collected in accordance with the users' requirements. Resolution selection is often driven by the size of the AOI. This is mainly due to the conflict between resolution and Field of View (FOV), i.e., lower spatial resolution imagery data will be obtained when imaging a larger AOI.

⁶ Eagle Vision currently incorporates remote sensing imagery from Spot, Landsat, Canada's Radarsat and the European radar satellite (ERS). [32]

Besides the disadvantages of higher cost, the amount of data that must be stored increases exponentially with the resolution of data and swath width. As a result, the width across a strip of satellite imagery typically drops with higher resolution data. The most common characterization of different satellite imaging resolutions can be decomposed into the following categories:

1. Spatial,
2. Temporal and
3. Spectral.

1. Spatial Resolution

Spatial resolution specifies the pixel size of satellite images acquired during the imaging satellite collection. Hence, spatial resolution is commonly used to describe the level of detail in the image based on a quantifiable scale of reference. As shown in Figure 7, an image with 1-meter spatial resolution, whereby each individual pixel represents a ground distance of 1 meter by 1 meter, has higher resolution and is comparatively more detailed than a 5-meter resolution image, where each pixel represents a ground distance of 5 meters by 5 meters.

The native Ground Sample Distance (GSD) of images varies based on collection geometry, but with post-processing techniques, images are re-sampled to a uniform resolution before storing the imagery in the database. While 5-meter spatial resolution imagery could suffice for grasping the big picture, this scale of resolution would not be able to show the same level of detail as the higher-resolution 1-meter imagery. The higher-resolution 1-meter imagery will display greater feature detail and show smaller features when zooming into smaller areas in the image.

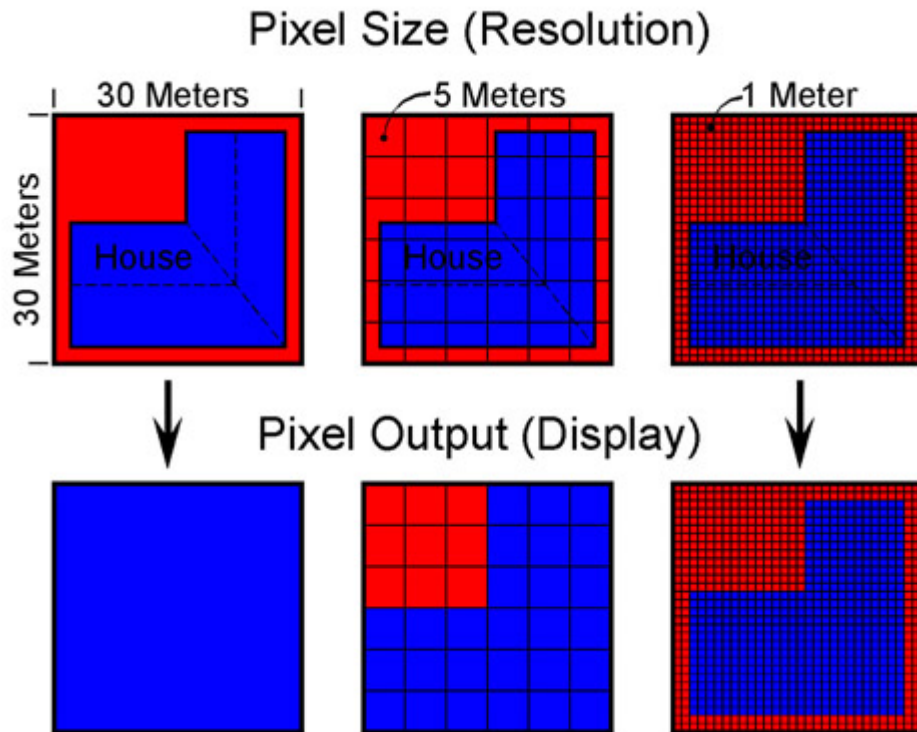


Figure 7. Spatial Resolution Differences. From [38]

2. Temporal Resolution

Temporal resolution simply specifies the revisit frequency for a specific location or AOI. The definition of temporal resolution is broken down into the following categories [38].

- a. High temporal resolution: Less than 3 days.
- b. Medium temporal resolution: 4–16 days.
- c. Low temporal resolution: More than 16 days.

Temporal resolution is strongly correlated with the frequency of flyovers by the imaging satellite and is only relevant in time-dependant studies. One application in the civilian sector that requires multi-temporal resolution is deforestation monitoring. A multi-temporal resolution can help to map out the rate of deforestation and provide consistent status updates [29]. In the military context, the intelligence community could be concerned with the temporal

resolution of satellite imagery in scenarios where repeated satellite coverage could reveal changes in infrastructure, forces' deployment strength or modification of battlefield equipment.

3. Spectral Resolution

The spectral resolution of the imaging satellite sensors specifies the number of spectral bands in which the sensor can collect reflected radiance from the surface of the Earth. Besides the number of bands, the position of spectral bands in the electromagnetic spectrum also plays an important role in determining the spectral resolution of satellite imagery. The science behind determining the spectral resolution is based on the principle of measuring different wavelengths of light in the Electromagnetic spectrum with each imaging band, as shown in Figure 8.

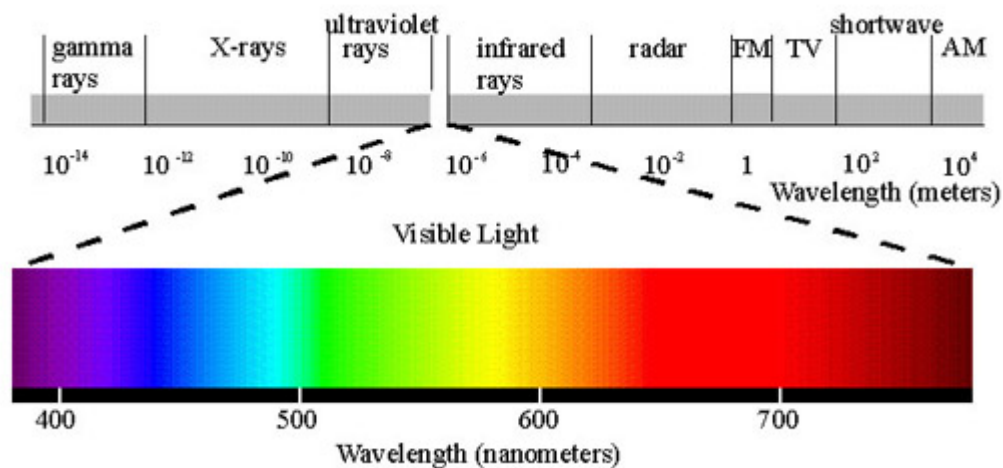


Figure 8. Electromagnetic Spectrum. From [39]

Most commercial imaging satellites capture panchromatic images in a monochromatic gray-scale at high resolution and four multispectral bands, i.e., red, green, blue and infrared [40]. The most common format is typically true or natural color, which is the combination of three-band RGB (red, green, blue). This is because most users of remote sensing data rely on the combination of color and spatial detail for their respective usage. However, advanced users

performing imagery classification or analysis may prefer four-band imagery, because the fourth band, infrared band, is useful for vegetation analysis [28].

4. Commercially Available Satellite Imagery Sources

Table 1 provides a high-level comparison among the high-resolution and medium-resolution satellite imagery sources that are available in the commercial market today.

Table 1. High-Res and Medium-Res satellite Imagery Sources. From [41]

Satellite	Launch Date	Swath Width (km) ¹	Native GSD (m) ²	Output Resolution (meters)	Max View Scale ³	Native Accuracy (meters) ⁴	Bands	Bit Depth	Stereo
IKONOS	Sept 24, 1999	11.3	0.82 x 3.20	1 x 4 ⁵	1:2,500	15	pan + 4 MS	11	Yes
QuickBird	Oct 18, 2001	18 ⁶	0.65 x 2.62	0.6 x 2.4	1:1,500	23	pan + 4 MS	11	No
SPOT-5	May 3, 2002	60	5 x 10 x 20	2.5 x 5 10 x 20 ⁷	1:5,000	48	pan + 4 MS	8	Yes
WorldView-1	Sept 18, 2007	17.7	0.5	0.5	1:1,250	5	pan only	11	Yes
RapidEye	Aug 29, 2008	77	6.5	5	1:12,500	23–45	5 MS (no pan)	12	No
GeoEye-1	Sept 6, 2008	15.2	0.41 x 1.65	0.5 x 2	1:1,250	5	pan + 4 MS	11	Yes
WorldView-2	Oct 8, 2009	17.7	0.46 x 1.85	0.5 x 2	1:1,250	5	pan + 8 MS	11	Yes
Pléiades 1	Dec 16, 2011	20	0.70 x 2.4	0.5 x 2	1:1,250	To be determined	pan + 4 MS	12	Yes

¹ at nadir

² at nadir

³ Estimated value only, as actual max zoom level prior to pixelization will vary based on collection geometry and size, shape and contrast of objects on ground. (If satellite offers multiple resolutions, the max zoom value listed is for the highest available resolution.)

⁴ Horizontal accuracy CE90 without GCPs (except Rapid Eye), excluding terrain and off-nadir effects

⁵ Higher elevation angle imagery available at 0.80 meter x 3.20 meters

⁶ Changed from earlier 16.5 kilometers due to April 2011 orbit raise

⁷ 2.5 meters from 2 x 5-meter scenes

⁸ RapidEye is the only imagery listed where GCPs (but not a DEM) are used with the Basic (1B) imagery, therefore accuracy is higher

in areas where higher accuracy GCPs are available, such as the United States.

5. Resolution Trade-off

Very often, the aforementioned resolution characteristics namely, spatial, temporal and spectral form the limiting factors for the utilization of satellite imagery data for different remote sensing applications. Unfortunately as a result of technical constraints, satellite imaging systems can only offer conflicting relationships:

- a. Between spatial and spectral resolution such that high spatial resolution is associated with low spectral resolution and vice versa.
- b. Between spatial and temporal resolution such that high spatial resolution is associated with low temporal resolution and vice versa.

The limit of the scale of spatial resolution is highly dependent on the elevation angle from the AOI to the satellite during image collection and the technology of the sensor systems. The conflicting relationship between spatial and temporal resolution is due to the low frequency of high elevation angle- imaging opportunities for capturing high-resolution satellite images. Similarly, sensor systems onboard satellites have not reached the state whereby the technology is able to provide high spatial and spectral resolution at the same time. Figure 9 illustrates the three dimensions for satellite image resolution trade-off.

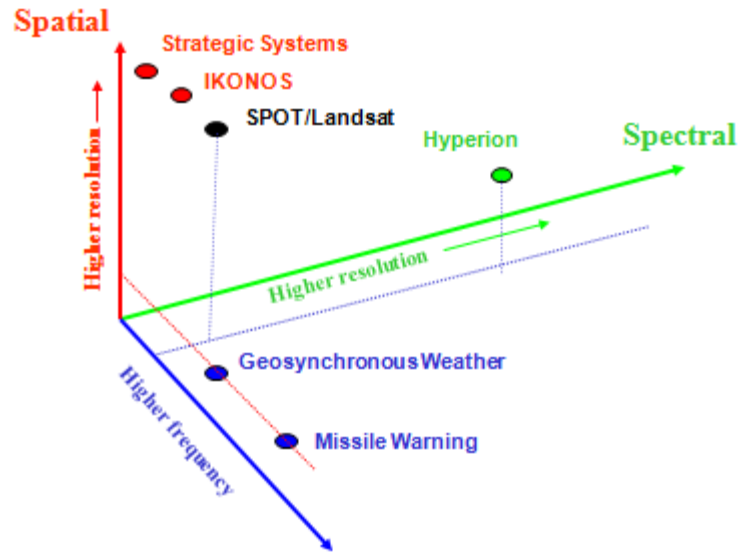


Figure 9. Three Dimensions for Resolution Trade-Off. From [40]

It is often essential to find compromises between the different resolution characteristics according to the required application or to utilize multiple sources of satellite images. The trade-off may result in two different solutions:

- a. Emphasize the most important resolution characteristic which directly impacts the application, with the acceptance of low resolution in the other two aspects, or
- b. No emphasis on one specific resolution characteristic but rather the collection of imagery that satisfies the baseline spatial, temporal and spectral resolution requirements [40].

D. OTHER CRITERIA AFFECTING QUALITY OF SATELLITE IMAGES

1. Elevation Angle

In the context of “elevation angle,” satellite operators often select 90 degrees of elevation as looking straight down from the satellite’s sensor (i.e., perpendicular to Earth’s surface) and zero degrees would imply looking straight ahead from the sensor (i.e., parallel to Earth’s surface). A high-elevation angle is critical for satellite imagery collection, especially in areas of high relief or tall

buildings to minimize the phenomenon of occultation. Collection of high-resolution satellite imagery is often executed with satellite sensors maintaining a minimum elevation angle of 60 degrees [38]. Figure 10 illustrates the definition of elevation angle during a satellite's imaging operations.

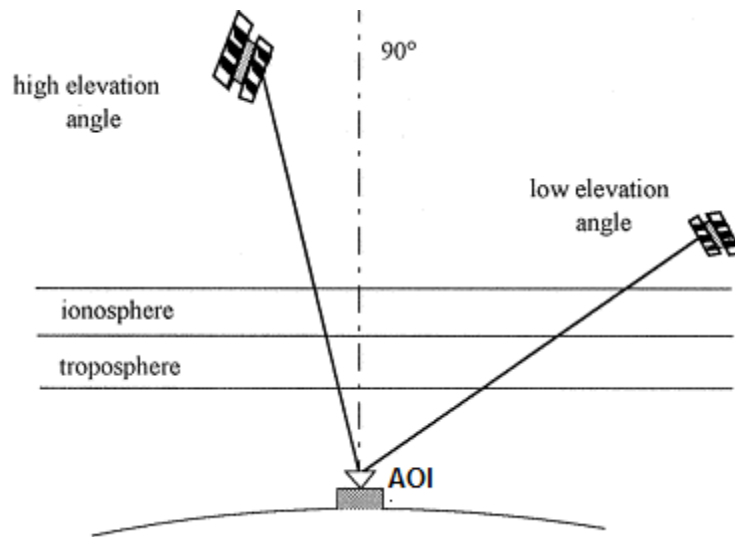


Figure 10. Illustration of Elevation Angle. After [38]

The requirement for a high-elevation angle collection must be ultimately weighed against the corresponding decrease in imaging revisit time. This is because a higher elevation angle requirement decreases the number of suitable imaging satellite access in a given time period, thus reducing the chances of a successful imagery collection.

2. Sun Angle

Sun angle is the elevation angle of the sun above the horizon (see Figure 11). Satellite imagery collected with low sun angles may contain data that are too dark to be of use. Increased shadow areas are problematic for classification and stereo projects. The effect from shadows will be more prominent in high-relief areas and in areas with taller features and infrastructure whereby low sun angles will cast long shadows over the AOI. A typical minimum requirement for sun

angle is 30 degrees, but such a requirement implies that regions in the northern latitudes (regions above 35 degrees latitude) will have black-out periods during the winter months since imagery cannot be collected with a sun angle of at least 30 degrees during this period. Decreasing the minimum required sun angle will reduce the black-out period for regions in the higher northern latitudes.

For the affected land masses, these black-out periods correspond to months with snow cover, making new collects during these times less desirable. Take for example in areas such as Alaska, where low sun angle and snow cover frequently restrict the imaging satellite collection window of opportunity. In such areas, commercial imaging satellites are currently unable to meet the high demand for satellite imagery [42].

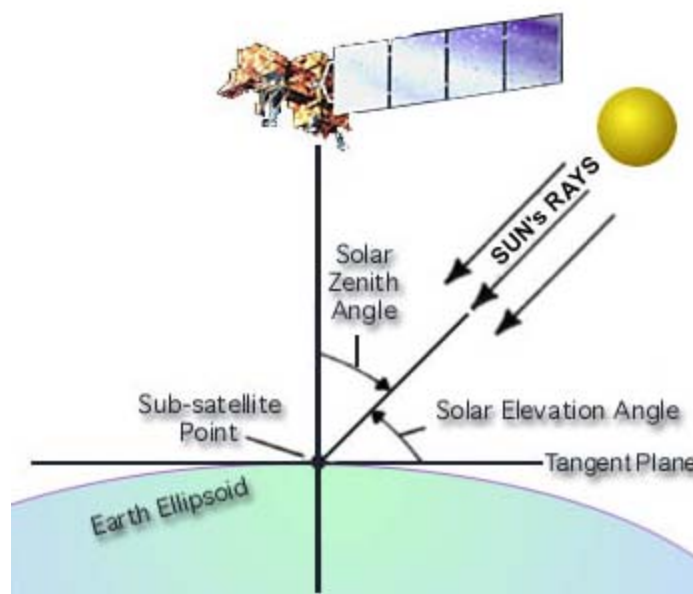


Figure 11. Solar Elevation Angle. After [42]

3. Cloud Cover

In the context of satellite imagery collection, cloud cover commonly refers to the phenomenon of clouds obscuring the sky when observed from the imaging satellite in orbit. In regions of persistent cloud cover, SAR imagery collection will

not be affected as compared to optical imagery collection since radar wavelengths are not significantly affected by clouds. In the commercial satellite imagery industry, if the satellite operator can not deliver the images that meet the product order requirements during the collection window agreed upfront, the customer can either extend the order delivery date or cancel the satellite imagery product order at no charge. With the availability of archived imagery, a preview of the reduced-resolution imagery can be reviewed ahead of product order delivery date. In reality, it is usually unavoidable to collect satellite imagery without small clouds or haze (especially in big cities due to the air pollution).

E. MISSION PLANNING FOR SATELLITE IMAGERY COLLECTION

Imaging satellite systems represent a high capital cost for the satellite operators. From the business perspective, optimizing the collection of satellite images is critical for both meeting customer order requirements and building a sustainable satellite operations business. In modern day, the leading-edge imaging satellites in the industry face multiple challenges in mission planning and scheduling algorithms to maximize the cost-effectiveness of satellite imagery collection. The following sections will highlight some of these challenges.

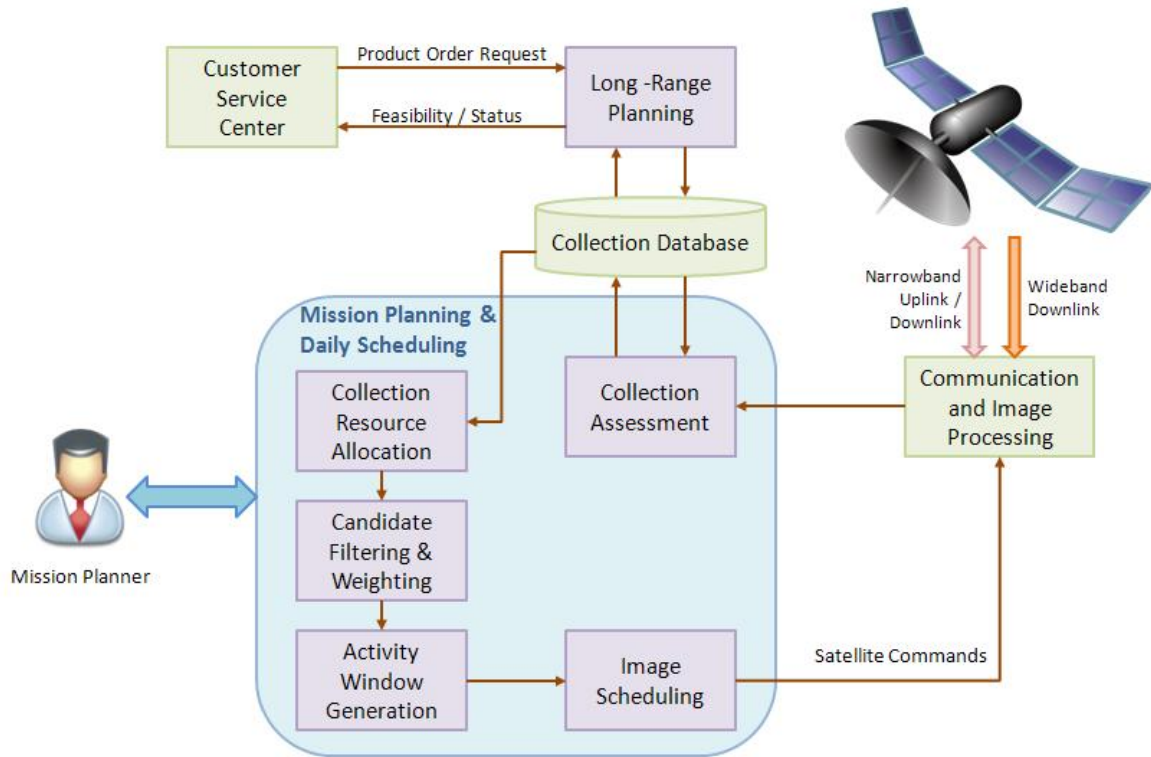


Figure 12. Mission Planning Workflow for Satellite Imagery Collection. After [43]

Figure 12 represents a typical satellite imagery collection workflow which is commonly adopted in the commercial satellite industry. Assisted by an integrated software system at the ground station, the mission planner seeks to optimize the use of satellite imagery collection resources based on the complex and inter-related mission objectives, time constraints and environmental conditions. Mission objectives are primarily driven by the customers' order requirements while time constraints can be due to a combination of the satellite operations and order delivery date.

Before the mission planner can allocate the corresponding collection resources and produce a daily schedule of the satellites' operations, a review of the accepted orders' collection objectives with competing requirements including broad area search, point target collection and mapping will be carried out at the company-wide level. The following parameters then form the primary inputs to the mission planning for the daily satellite operations:

- a. Image requirements such as number, resolution and perspective of images collected
- b. Collection priority level for each AOI target
- c. Satellite access opportunities
- d. Weather forecast
- e. System resource constraints (e.g., satellite agility, on-board memory, power usage profile)

A LEO imaging satellite's daily schedule is likely to be made up of individual imaging opportunities of different regions. In order to optimize the satellite operations, daily collection operations are defined by the product orders that have been contracted and registered with the company. These product orders will typically specify the geographic area of interest, collection geometry, collection priority (if the clients have more than one collection requirement) and time period for imagery collection. Sometimes, the client may also specify the maximum allowable cloud cover limit or this could be left to be determined by the satellite operator in order to meet the minimum requirements for a usable image.

In most established satellite provider companies, long term objectives guide the mission planning and daily scheduling instead of a daily ad-hoc based activity [43]. With the imaging satellites' orbital parameters known upfront and image order requirements extracted from the client orders, optimization algorithms are used to determine the potential windows for image collection. Along this line of thinking, the mission planners and ground operators are able to engage in long term planning and resource allocation (e.g., for a 30-day period) for:

- a. Analyzing the current orders and system loading in order to fulfill existing orders and meet delivery dates,
- b. Identifying product orders with high risk of non-delivery by completion date, and

- c. Assessing the confidence level to accept new product orders based on collection feasibility as well as resource and schedule constraints.

After the acceptance of customers' orders, the satellite provider will peg priority levels to the product orders and this prioritization is one of the key factors that drives the long term planning for daily scheduling [43]. Understandably from the business perspective, and in the interest of the company, level of priority is directly driven by the size of the contract award. Besides influencing the mission planning and resource allocation, this internal exercise makes room for speculative product orders with lower priorities to be accepted with the intent to create a repository of imagery that can be stored in a database for out-of-archive sale to other future customers.

F. OPTIMIZING SATELLITE IMAGERY COLLECTION

Unallocated satellite imaging time provides the basis for assessing the confidence level for acceptance of new product orders. Although, the allocation of imaging time to a specific geographic region is determined by the number of product orders for imaging AOIs in that particular region, unallocated imaging time in collection resource allocation indicates an under-utilization of the satellite on that particular day. An underutilized asset is not ideal for the satellite provider in the economic sense. Apart from the lack of orders, poor visibility caused by cloud cover and satellite downtime due to maintenance issues could also contribute to unallocated imaging time. If product orders are concentrated in a particular geographic region, the satellite provider shall balance the forecasted cloud-free period with the image collection requirements [43]. This will typically lead to under-utilized satellite operations for imagery collection since the remaining periods of the imaging satellite's coverage over other geographic regions will not be used for image collection.

For each geographic region, the ground operators are required to evaluate all active product orders visible to the satellite in order to create a candidate

window period for image collection. Subsequently, all possible candidate windows must be filtered through to select a subset of imaging periods that will maximize the probability of fulfilling the product orders to meet the contractual delivery dates. In the course of this filtering process, an estimated number of the satellite's cloud-free passes over the targeted area of interest will be compared against the computed number of satellite access between the date of product order acceptance and order delivery date to assess mission success probability. However, this is not a fail-proof computational method because the actual number of cloud-free passes is very much dependent on climate changes. As such, there is a need to continuously monitor the probability of mission success until the image collection completion date.

Other parameter constraints that come into the equation for defining mission success probability for each image collection order will include GSD, collection azimuth and elevation, sun azimuth and elevation, wide-band link closure for in-contact imaging, stereo geometry for stereo collection [43]. On the spacecraft platform itself, constraints on satellite power availability, on-board storage and down-linking of collected imagery, camera on-time constraints and satellite thermal constraints will also affect the daily operations that go towards optimizing satellite imagery collection.

In summary, managing the usage of an imaging satellite to maximize business profitability is an extremely challenging task. In this thesis, the planning process will be simplified such that the satellite image collection requirements and imaging period are pre-determined upfront. The approach undertaken in this thesis can, nonetheless be extended in the future to include the additional details described above.

THIS PAGE INTENTIONALLY LEFT BLANK

III. SATELLITE ATTITUDE CONTROL

Due to the need for regular reorientation and maneuvering of the spacecraft to align the onboard sensors for satellite imagery acquisition, attitude control is an important aspect of imaging satellite operations. Modern imaging satellites boast rapid retargeting capability and precise geo-location imaging accuracy. A highly competent attitude control system onboard the spacecraft is used to enable such functionalities in state-of-the-art imaging satellites.

Generally used in spacecraft attitude control systems today, a Control Moment Gyroscope⁷ (CMG) device creates a gyroscopic torque induced by the changing angular momentum from a gimbaled rotor. This gyroscopic torque rotates the spacecraft, thus changing the spacecraft orientation. Since CMGs are typically driven by the onboard EPS, using CMGs for spacecraft attitude control has its advantages provided that maneuvers can be executed with the CMGs functioning within their threshold of angular momentum [44]. Besides CMGs, heritage attitude control systems have also utilized reaction wheel technology. Reaction wheels are electrically driven rotors that are made to spin in the direction opposite to that required for spacecraft re-orientation [45]. A minimum of three reaction wheels must be used in order to exert forces required for space vehicle orientation during spaceflight.

A. MANEUVERING REQUIREMENTS

Commercial imaging satellites must respond to queued-up requests from the ground station to image different areas of the earth within time constraints. To effectively satisfy and manage these requests, geodynamic, camera and spacecraft constraints must be reconciled within a short frame of time to create a workable plan and schedule for image capture during a specific spacecraft pass. In the commercial satellite imagery industry, spacecraft maneuver capability is

⁷ A CMG consists of a spinning rotor along with motorized gimbals that change the direction of the rotor's angular momentum vector to induce a gyroscopic torque.

vital because the speed and response of the spacecraft's target re-acquisition directly impacts the volume of imagery data that can be collected as the spacecraft orbits Earth. The ROI for the satellite operators is very much correlated with 1) the amount of imagery data captured per orbit and 2) timeliness of meeting the customer orders' requirements. Therefore, the overall productivity of the commercial imaging satellites can potentially be increased with the incorporation of a rapid maneuvering capability.

In the context of military and homeland security applications, ISR requirements for satellite imagery collection tend to be even more volatile than the remote-sensing requirements for commercial applications [46]. An ideal satellite imagery exploitation system would serve a variety of users including government organizations, theater commanders, war fighters, analysts etc., and would be capable of end-to-end sensor-tasking, image collection and data management. In this way, regardless of their job scope and location, operational soldiers fighting at the war front, theater commanders on the battlefield and many others are all able to request information from satellites in a planned as well as timely manner. As a result, the capability to update the satellite systems' tasking and resource allocation only minutes before scheduled contacts with the satellite through the telemetry communication system is strongly desired for military spacecraft platforms [46]. Upon receiving updated tasking commands, the imaging satellite will respond to the task schedule by calculating the scan and slew durations required to image each AOI.

During the daily tasking of the satellites' image collection, the most important task lies in executing the essential slew maneuvers to get to the right position (in consideration of the required GSD, collection azimuth and elevation, sun azimuth and elevation) so that the imaging operations can be performed. This involves activate the onboard scanning sensors for image collection and saving the collected images on the onboard memory storage before downloading them to the ground station during the subsequent pass access. It is therefore not

surprising that spacecraft maneuver design has an important role to play in the mission effectiveness of an imaging satellite.

Daily-routine tasks like slewing and maneuvering from target to target are generally executed by turning the spacecraft body about the eigenaxis. This heuristic approach is done primarily to simplify the attitude control logic. Given that maneuvering about the eigenaxis provides the shortest angular path between each spacecraft's attitudes⁸, this maneuvering mechanism implies that the maneuver will likely be the most time-efficient. Despite multiple examples of eigenaxis maneuvering implementation, a number of simulation studies have produced findings which clearly demonstrate that "eigenaxis spacecraft maneuvering is not time-optimal" [13], [15], [47]. In reality, rapid spacecraft reorientation maneuvers are very different from eigenaxis maneuvers. With the appropriate angular rate buildup around the three spacecraft body axes, the spacecraft body can in fact complete the time-optimal reorientation movement over a shorter duration despite traversing a potentially longer angular path distance [15].

B. TIME-OPTIMAL SPACECRAFT MANEUVERS

For a rigid spacecraft with independent three-axis control, the overall benefit of time-optimal maneuvering is strongly tied to the particular rigid spacecraft body configuration under investigation. Reduction in slewing time tends to be larger for spacecraft with highly dissimilar principal inertias as compared to conventional slews because it is "easier to exploit the relationship between the available control authority and the preferred axis of rotation" [48]. Since time-optimal maneuvering takes advantage of the connection between the actuator control space and the spacecraft body's inertia properties, a non-uniform rigid body such as an imaging spacecraft provides an excellent platform for enhanced capability using optimal control techniques.

⁸ The orientation of an aircraft's axes relative to a reference line or plane, such as the horizon.

As discussed in [49], the Legendre pseudospectral optimal control technique can be applied to solve time-optimal reorientation maneuvers for generic spacecraft. For flight implementation, however, “the optimal control problem formulation must be derived from a detailed model of the spacecraft dynamics including any electro-mechanical constraints such as gyro rate limits and the appropriate actuator torque-momentum envelope” [50].

1. ON-ORBIT TIME-OPTIMAL MANEUVER DEMONSTRATION

Time-optimal reorientation maneuvers were demonstrated on board the NASA Transition Region and Coronal Explorer (TRACE) spacecraft in August 2010 [51]. In this real world flight test demonstration, the execution of time-optimal maneuvers showed that reorientation of the TRACE could be completed more rapidly than with conventional slews. In one experiment, an operationally relevant imaging scenario was tested whereby the spacecraft had to maneuver the spacecraft’s instruments to multiple targets as quickly as possible in order to achieve the mission goals.

Results from this experimental spaceflight demonstration in an operationally-relevant environment were collected and presented in [51]. The empirical results were analyzed and key findings were as follows:

- a. Reduction in TRACE spacecraft slewing time for time-optimal maneuvers compared to conventional maneuvers can range from 5% to 20% for each maneuver with an overall performance improvement of 14% for the entire sequence. However, the improvements in agility for other spacecraft configurations could be much higher.⁹ Slew performance improvements of approximately 50% have been demonstrated at Honeywell in recent ground tests on a CMG spacecraft simulator [52].

⁹ Time savings achievable through time-optimal spacecraft maneuvers is dependent on the spacecraft body configuration. In general, a larger reduction in slewing time can be attained for ellipsoid bodies [44].

- b. Reductions in spacecraft slewing time tend to increase with the span of the slew. Therefore, time-optimal maneuvers can be potentially advantageous for operations such as strip collection over large geographic regions.
- c. Time-optimal maneuvers were carried out without modifications to the TRACE spacecraft attitude control system. This implies that time-optimal maneuvers can also be executed on remote-sensing satellites that are already operational.
- d. The simulation results obtained from the ground-based TRACE spaceflight simulation model were generally coherent with the optimal control solution developed for deriving the time-optimal maneuver strategies. This engineering-based model predicted that the spacecraft should perform similarly to the optimal control solution. Hence, the simulation model could be used to verify the feasibility of time-optimal maneuver strategies in alternative future scenarios. As such, the simulation model could be integrated into operational workflow processes for use as reference during mission planning and operational scheduling at the ground station in preparation for executing rapid time-optimal maneuvers.

The experimental demonstration illustrated that apart from improving the agility of TRACE, the implementation of time-optimal maneuvers can contribute towards the mission objectives by maximizing the window of opportunity for data collection by onboard sensing equipment and instruments. This is accomplished through the reduction of slewing time between the various attitudes required to image each target location. Thus, the flight experiment proved that an operational spacecraft can leverage such time-optimal maneuver strategies to “extend the capabilities of existing spacecraft systems, beyond their original design” [50].

C. OPERATONAL ANALYSIS

Precision pointing control and rapid maneuvering capabilities have become mandatory requirements for many space missions. Rapid retargeting could either be an intrinsic component of the mission profile or be required to adjust the attitude of the spacecraft orientation. Especially for imaging satellites, the overall effectiveness of their missions is directly connected to the average slewing and image collection time. While image collection time is contingent on the sensors employed onboard the spacecraft and the stability of the spacecraft, slewing time depends much on the image collection route and spacecraft maneuver strategy.

The successful execution of time-optimal maneuvers on an operational space platform demonstrated the feasibility of integrating time-optimal maneuvering capabilities into practical spacecraft operations like the TRACE demonstration. However, there is a current gap in understanding how these maneuvering performance improvements translate into improvements in operational capability.

Safe to say, satellite operators and other key players in the commercial imaging satellite industry should be very keen to investigate further into the potential operational benefits that could be derived from reduction in spacecraft slewing time. The successful demonstration of time-optimal maneuvers on operational spacecraft also invites further questions. Some of the predictable questions that could be asked are: “Does a 20% improvement in slewing time equate directly to a 20%-higher probability of mission success? If not, how significant is the maneuvering performance improvement with regard to mission success? How will the maneuvering performance improvement differ with different operational scenarios?”

With reference to the TRACE spacecraft demonstration, results have shown that reduction in spacecraft slewing time for time-optimal maneuvers can differ with 1) different spacecraft body configurations and 2) the span of

spacecraft slew. To build on the momentum gathered with the successful time-optimal spacecraft maneuver demonstration, two operational scenarios were conceptualized and set up in the AGI Systems Tool Kit (STK) environment for carrying out the operational analysis which is the main focus of this thesis.

Using the two operational scenarios as the backdrop, this thesis seeks to establish a framework for adopting a business-analytic approach towards the operational analysis of time-optimal spacecraft maneuvers. In particular, the investigation is focused on 1) how maneuvering performance relates to mission effectiveness and operational efficiency for imaging satellites and 2) how time-optimal maneuver strategies can enhance the mission.

D. OPERATIONAL SCENARIO SETUP

X-SAT is a microsatellite that was designed, developed and built by Nanyang Technological University (NTU), Singapore in collaboration with Defence Science Organisation (DSO), Singapore and various other strategic partners. The microsatellite, shown in Figure 13, was launched on Indian Space Research Organization (ISRO) Polar Satellite Launch Vehicle from Satish Dhaman Space Centre in India in April 2011. The primary mission objective of the satellite was to provide an experimental and satellite-based earth observation capability with near real-time downlink capability for imaging over Singapore as well as surrounding regions. The spacecraft carries an electro-optical payload with three multi-spectral band imaging capability. Satellite imagery collection is achieved via a push-broom scanner with three individual scan lines in the green (520 nm–600 nm), red (630 nm–690 nm), and near-infrared (760 nm–890 nm) wavelength range. There is also a Parallel Processing Unit onboard the microsatellite for image processing capability [53].

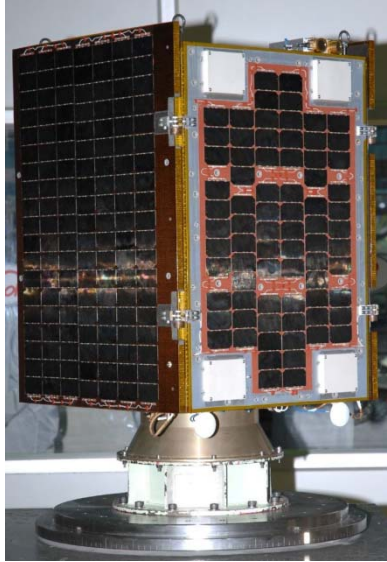


Figure 13. Singapore-developed X-SAT. From [53]

In order to conduct a realistic evaluation of the impact of time-optimal maneuver strategy to the mission effectiveness, the real world X-SAT satellite was used as the imaging satellite of interest for modeling and simulation purposes in the two STK operational scenarios studied as part of this thesis. The mission statement in both STK operational scenarios was:

“To acquire satellite imagery from the Southeast Asia geographic region through the optimization of satellite imagery collection resources.”

Based on X-SAT’s technical specifications and orbital parameters known from open sources shown in Figure 14, the two operational scenarios were set up in the STK environment to address the following objectives:

- a. To investigate the impact of incorporating time-optimal spacecraft maneuver strategies into the workflow process for satellite imagery collection of major cities in the Southeast-Asia region.
- b. To establish a measure of the benefits obtained from time-optimal spacecraft maneuvers for mission effectiveness and operational efficiency.

- c. To understand and study the effectiveness of applying time-optimal spacecraft maneuvers for different image collection scenarios i.e., different scanning and slewing routes.

Overview of XSAT Micro-satellite

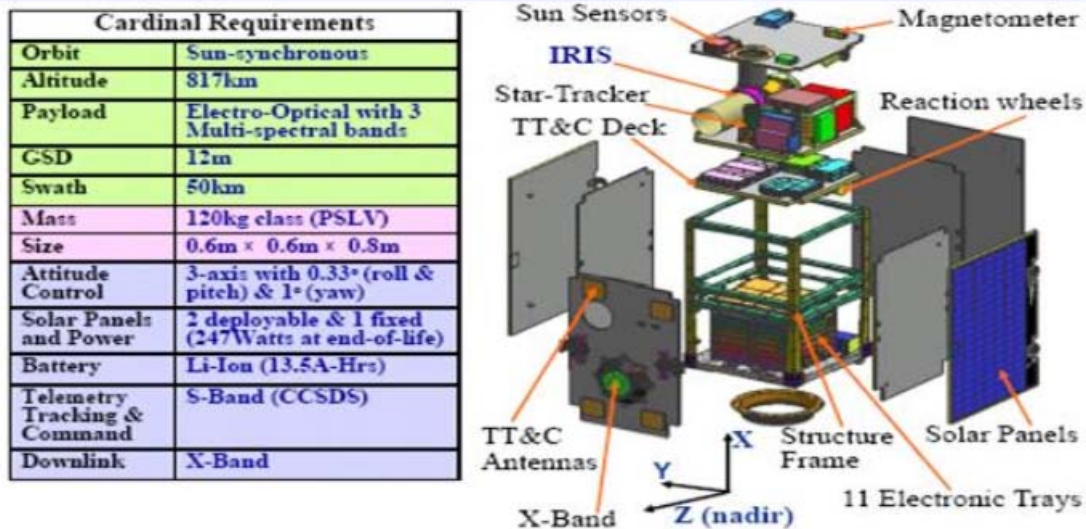


Figure 14. X-SAT Technical Specifications and Orbital Parameters. From [53]

1. Operational Scenario 1

The first operational scenario was set up in STK such that X-SAT was tasked to collect satellite imagery in the Northern parts of the Southeast Asia region (see Figure 15). As per the request from fictitious customer orders, the scenario called for satellite imagery collection in five major cities namely Bangkok, Hanoi, Phnom Penh, Vientiane and Yangon, which are the capital cities of Southeast Asian countries i.e., Thailand, Vietnam, Cambodia, Laos and Myanmar, respectively. Figure 16 highlights the target cities for image collection in OS1.



Figure 15. Southeast Asia Geographic Map

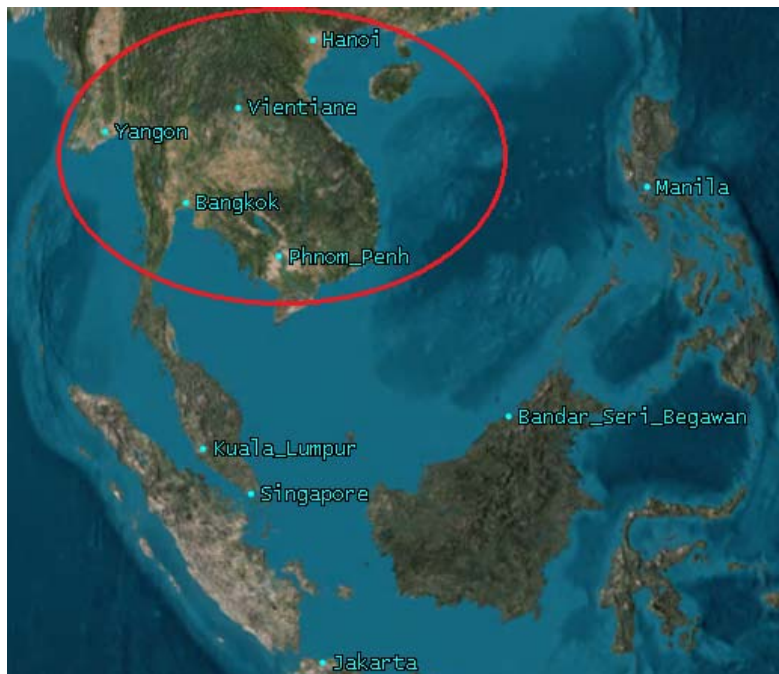


Figure 16. Target Cities in Operational Scenario 1

In order to identify an appropriate window for imaging opportunities of the Northern Southeast Asia region, the orbital parameters of X-SAT were modeled and simulated in STK for analysis. Through the observation of X-SAT's orbit

around Earth, an appropriate window for imaging opportunities was identified to be between 05:10:00 UTCG to 05:15:00 UTCG on November 5th 2012. During this window, X-SAT will cross directly over the Southeast Asia region of interest.

In this operational scenario, X-SAT was tasked to collect satellite imagery for 5 cities. Therefore, there will be a total of 120 different permutations that specify the order of imagery collection route. To simplify the operational scenario and reduce the number of permutations needed for consideration, the following assumptions were made:

- a. Product orders from the customer did not specify the image collection priority level for the 5 cities, i.e., No city is deemed to be more important than the other 4 cities during satellite imagery collection. The collection priority level is therefore the same for all 5 cities.
- b. No collection requirements were specified by the customer, except the requirement of an imaging window of at least 30 seconds for each city. The 30-second window was required to collect a sufficient amount of data to fulfil the customers' requirements.
- c. X-SAT's access opportunities to the five cities were assumed to be equal. Factors such as cloud cover and system resource constraints (e.g., onboard storage capacity, power usage profile) were assumed to be negligible.

2. Operational Scenario 2

The second operational scenario set up in the STK environment also focused on image collection in the Southeast Asia region. However, in this second scenario, X-SAT was tasked to maneuver around and survey a larger region in Southeast Asia. The mission is to capture satellite images from four further-distanced target cities like Bandar Seri Begawan, Hanoi, Manila and Singapore. The appropriate window for imaging opportunities was identified to be from 04:32:00 UTCG to 04:40:00 UTCG on November 2, 2012.

Figure 17 highlights the target cities for image collection in OS2. In view that the span of the X-SAT maneuvers is expected to be large as it shifts from one target to the next, the fictitious customer product order requirement in this case specified a minimum imaging window period of at least 45 seconds for each target city.



Figure 17. Target Cities in Operational Scenario 2

IV. ANALYSIS OF OPERATIONAL SCENARIO 1

A. PRELIMINARY WORK

Prior to conducting the analysis of the first operational scenario defined in this thesis, it was essential to identify the key requirements that will outline the mission goals that drive the best collection order. Based on the assumptions identified upfront for Operational Scenario 1 (OS1), the most ideal order for imagery collection shall be defined to be one such that it has the least satellite slew time between the imaging windows for each of the target cities. The rationale behind this was that if the satellite slew time can be reduced to a minimum during the 5-minute imaging window period, the imaging satellite could then maximize the imagery collection opportunities. Hence, the first task in the analysis of OS1 was to investigate and identify the best collection order out of the 120 possible collection route permutations.

To be very specific in defining the mission goal for this operational scenario, the value of the set of imaging operations was assigned to be equal to the sum of the imaging window periods for X-SAT satellite imagery acquisition across all target cities. X-SAT's slewing performance was modeled to emulate that of typical imaging satellites¹⁰. Through the assignment of five specific 30-second image collection windows to the five respective target cities in this set of imaging operations, the OS1 simulation was run in the STK environment with the software automatically calculating and determining the slews required to meet the imaging windows allocated for each target city. The assignment was carried out by adjusting the target pointing under the "Attitude" section of the X-SAT satellite basic parameters. Figure 18 shows a screenshot from STK which presents how the 30-second image collection windows were assigned to the respective cities.

¹⁰ The slewing rate of X-SAT was modeled to be between 0.7 to 1.1 degrees per second.

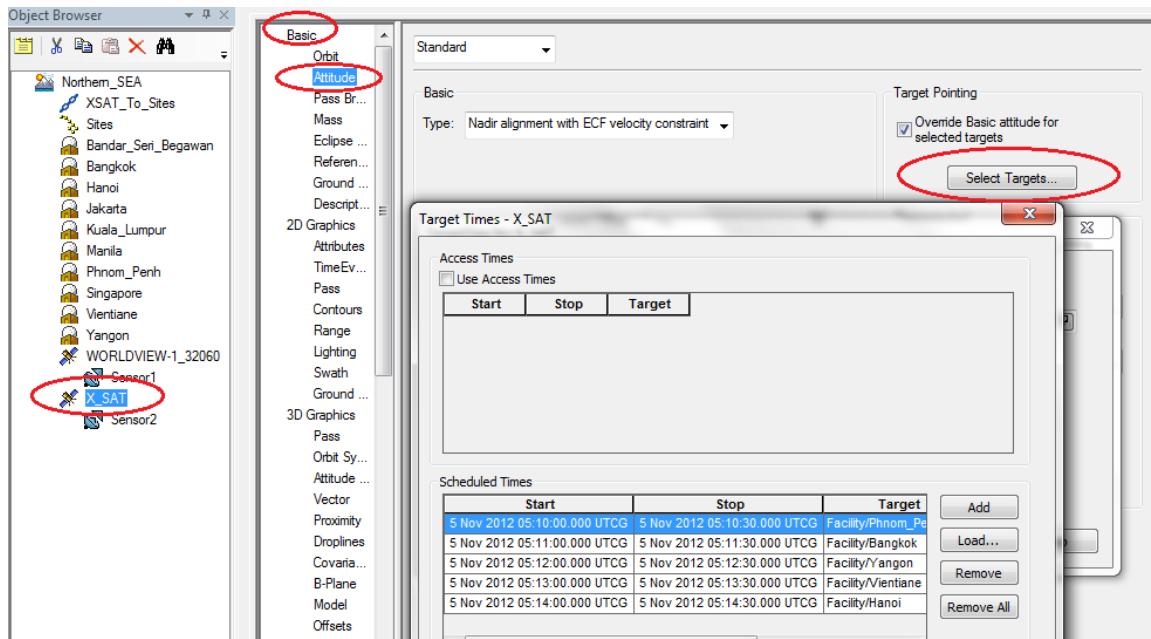


Figure 18. Screenshot of Imaging Window Assignment in STK

Figure 19 shows the screenshot captured from the 3D Graphics window of the STK simulated scenario of X-SAT sensing and acquiring satellite imagery from Bangkok (one of the target cities) during its imaging operations in OS1.

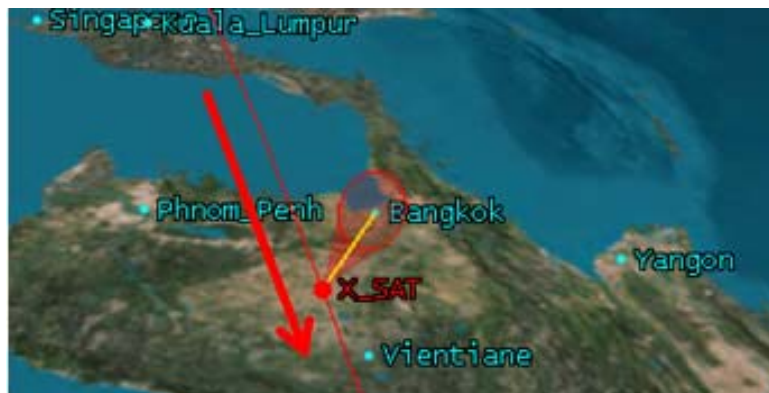


Figure 19. Screenshot of X-SAT Imaging Bangkok City (arrow shows direction of satellite motion along the ground track)

B. DETERMINATION OF IDEAL COLLECTION ROUTE

In view of X-SAT's mission goal and given that there no requirements to dictate the resolution of imagery data and collection priority of the five target

cities, the highest-valued sequence of image collection operations is the one that gives the longest duration of satellite imagery collection across the five target cities. This sequence was determined through the STK scenario simulation.

The volume of satellite imagery collected for all five cities is directly proportional to the total imaging window period across the five cities. This indirectly implies that the ideal imagery collection route in this five-minute imaging window (i.e., 05:10:00 UTCG to 05:15:00 UTCG on November 5, 2012) will be the one with the least slew time incurred as X-SAT maneuvers and re-orientates the spacecraft from one target city to the next. This simple case will set the stage for subsequent engagement in a more detailed study of the operational scenario whereby the identified ideal collection route will be further investigated and analyzed to see how time-optimal maneuvers can bring additional operational benefits to the mission.

Based on the results produced from the STK simulation, the best collection route was identified to be (in descending order):

- a. Phnom Penh (05:10:00 UTCG to 05:10:30 UTCG)
- b. Bangkok (05:11:00 UTCG to 05:11:30 UTCG)
- c. Yangon (05:12:00 UTCG to 05:12:30 UTCG)
- d. Vientiane (05:13:00 UTCG to 05:13:30 UTCG)
- e. Hanoi (05:14:00 UTCG to 05:14:30 UTCG)

The STK results showed that with the satellite imagery acquisition route set up in this collection order, the mission could be completed in the shortest time frame (i.e., 273 seconds) with the largest window available for image collection at each AOI.

C. IMPACT OF TIME-OPTIMAL MANEUVER STRATEGIES

With the ideal imagery collection route being identified, it was then feasible to investigate the impact and potential operational benefits that could be derived from incorporating time-optimal spacecraft maneuver strategies into this operational scenario. Although the slewing time (which equates to non-imaging

time for X-SAT) in this specific collection route, is the least among the 120 different permutations, the maneuver time from target to target can be further reduced through the application of time-optimal maneuver algorithms.

Moving forward, the impact and potential benefits derived from incorporating time-optimal maneuver algorithms in OS1 shall be investigated through the simulation of X-SAT's slewing performance with 1) an approximate 25% reduction in maneuvering time and 2) an approximate 50% reduction in maneuvering time. Figures 20 and 21 show screenshots from STK, which presents how 25% and 50% reduction in maneuvering time was modeled, respectively, in STK through the assignment of closer imaging window periods in OS1.

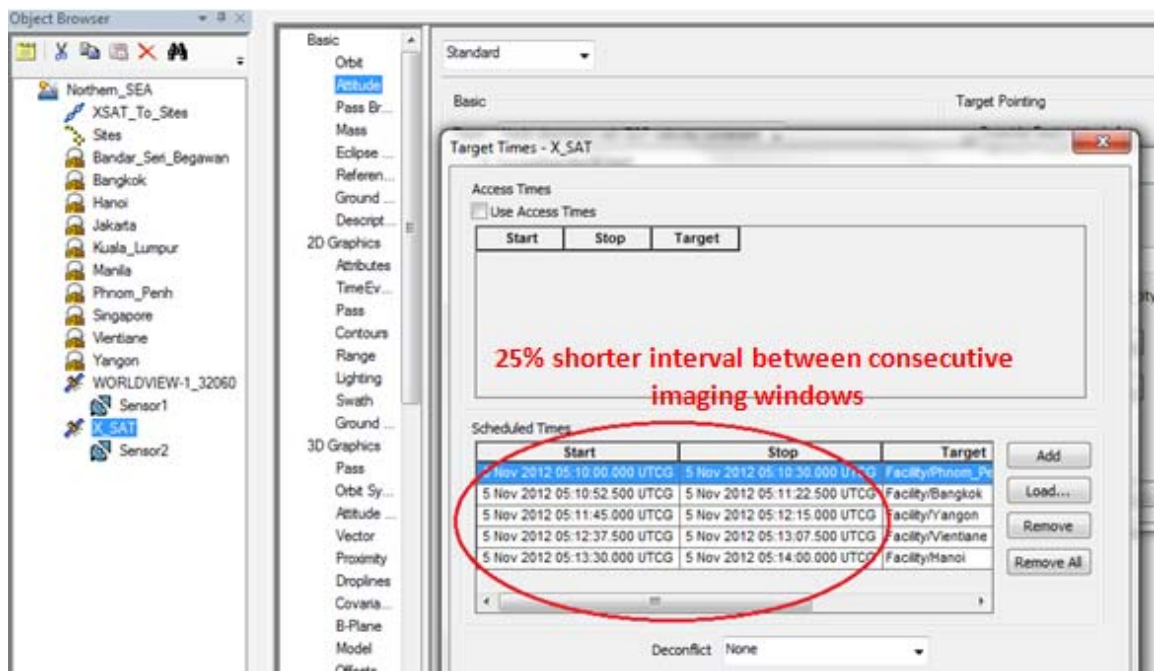


Figure 20. 25% Reduction in Maneuvering Time

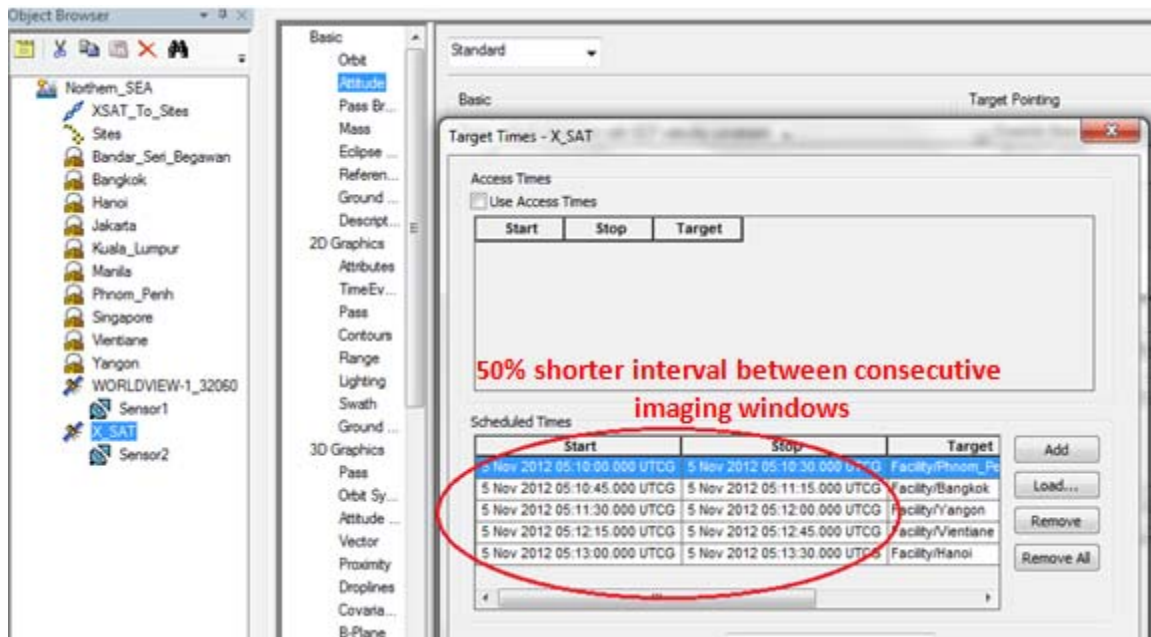
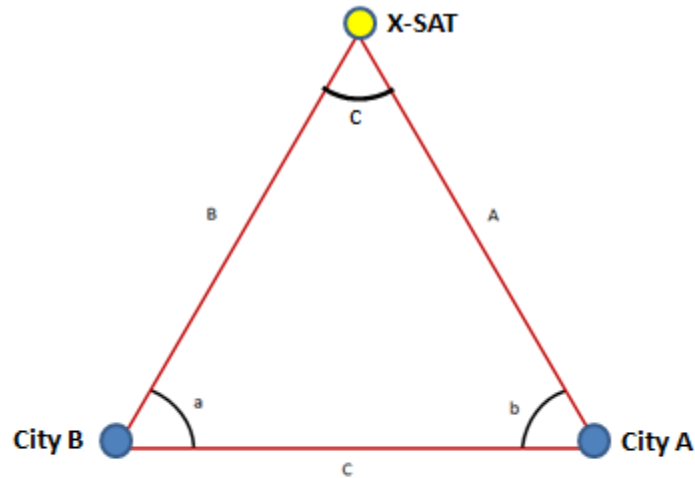


Figure 21. 50% Reduction in Maneuvering Time

The slewing performance associated with the slewing angles required to complete X-SAT's imagery collection mission in this operational scenario is summarized in Tables 2 and 3. Using trigonometric equations, the slew angles between target cities were mathematically calculated based on the following:

- 1) Slant range from target city to X-SAT,
- 2) Distance between target cities and
- 3) Average elevation angles recorded during the imaging period of each target city.

Figure 22 illustrates an example of the slew angle calculation.



Where: A = Slant range from X-SAT to City A
 B = Slant range from X-SAT to City B
 C = Ground distance between City A and City B
 Angle a = Elevation angle from City B to X-SAT
 Angle b = Elevation angle from City A to X-SAT
 Angle c = Slewing angle from City A to City B

Using cosine rule, solve equation: $\cos(c) = \frac{A^2 + B^2 - C^2}{2AB}$ to obtain slewing angle, c.

Figure 22. Slew Angle Calculation Example

Slew times between target cities were determined by measuring the scenario time difference between the last imaging instance of the former target city to the first imaging instance of the latter target city. An example of the slew time measurement from Phnom Penh to Bangkok is presented in Figure 23 for the baseline X-SAT slew performance.

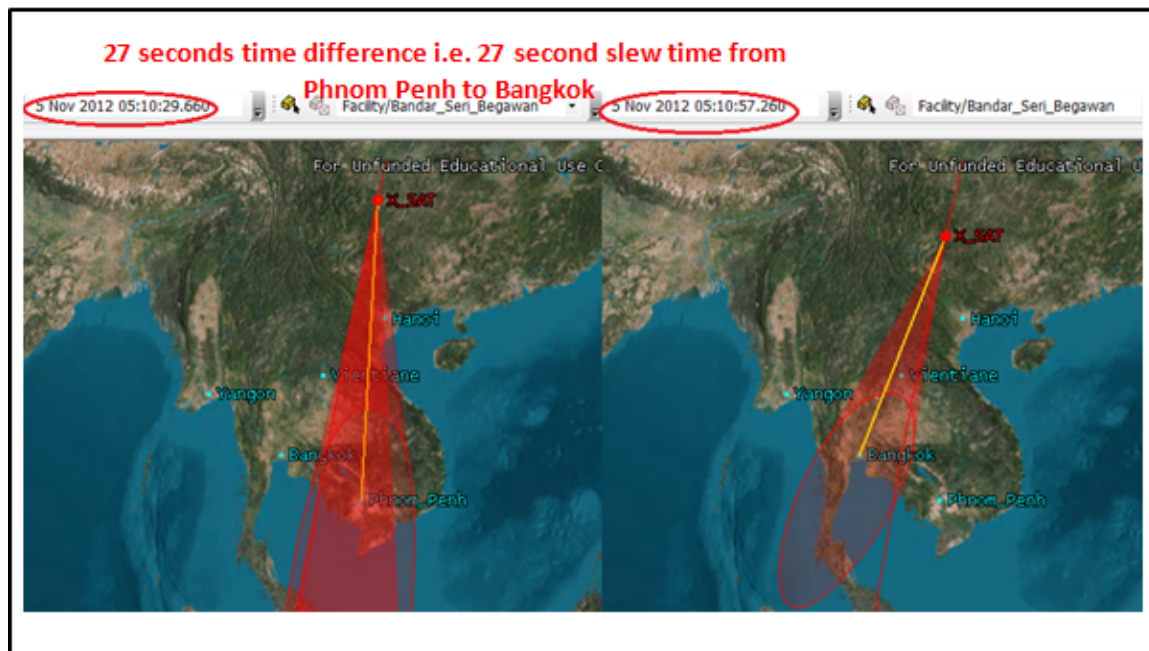


Figure 23. Slew Time from Phnom Penh to Bangkok for Baseline X-SAT Slew Performance

Table 2. X-SAT Slewing Angles and Slewing Time in OS1

Maneuver	Baseline		25% Improvement		50% Improvement	
	Slew Angle (deg)	Slew Time (s)	Slew Angle (deg)	Slew Time (s)	Slew Angle (deg)	Slew Time (s)
Phnom Penh to Bangkok	19.1	27	19.0	20	18.7	14
Bangkok to Yangon	25.2	27	24.4	20	23.6	13
Yangon to Vientiane	32.3	37	30.8	25	29.3	16
Vientiane to Hanoi	20.1	18	23.6	17	28.0	14

Table 3. X-SAT Slewing Rate in OS1

	Baseline	25% Improvement	50% Improvement
Maneuver	Slew Rate (deg/s)	Slew Rate (deg/s)	Slew Rate (deg/s)
Phnom Penh to Bangkok	0.70	0.95	1.34
Bangkok to Yangon	0.93	1.22	1.82
Yangon to Vientiane	0.86	1.24	1.83
Vientiane to Hanoi	1.11	1.39	2.0

In order to critically analyze the mission effectiveness and potential operational benefits brought about from the integration of time-optimal spacecraft maneuver strategies to the operational scenario, there was a need to identify measurable performance indicators for benchmarking X-SAT's operational performance. The performance indicators that were used in the analysis were as follows:

- Imaging Window Period, i.e., Length of time for productive image collection.
- Mission Completion Time, i.e., Time at which image collection has been completed for all target cities.
- Resolution of Satellite Imagery Collected, i.e., Level of details in the collected images.
- In-Track Stereo Imaging Opportunities, i.e., Possibility for stereo image collection for any target city or cities within the imaging window period.

1. Imaging Window Period

With the integration of time-optimal maneuvers to X-SAT's imaging operations, the total duration within the 5-minute mission window available for productive imaging operations increased. Besides meeting X-SAT mission's original requirement of a minimum 30-second imaging period for each target city, there was still sufficient time for X-SAT to collect satellite imagery of other cities which were not originally scheduled, to expand the database.

Assuming that the baseline slew time to the next target AOI will use up 30 seconds¹¹, results of the availability of additional imaging time associated with 25% and 50% improvement in slewing performance is summarized in Table 4.

Table 4. Additional Imaging Time with Varying Improvement in Slewing Performance

	Baseline	25% Improvement	50% Improvement
Total time (i.e., slew and imaging) required to fulfill original mission requirements (s)	273	243	214
Slew time to additional targets (s)	30	22.5 ¹²	15 ¹³
Additional Imaging Time (s)	NA ¹⁴	34.5	71
Total Imaging Window Duration (s)	165	195.5	228
Percentage Utilization of 5-min Mission Window for Image Collection	55%	65.2%	76%

¹¹ Based on an average 1 degree per second slewing rate, 30 seconds could allow X-SAT to slew 30 degrees to collect imagery of other Southeast Asian states like Singapore.

¹² Since there is a 25% improvement in slewing performance, slew time will take only 22.5 seconds.

¹³ Likewise for a 50% improvement in slewing performance.

¹⁴ Not possible because slewing to the additional target will take the mission time past the assigned 5-minute mission window.

The results of Table 4 showed that the value of this set of X-SAT's imaging operations that took place within the assigned 5-minute mission window will be significantly enhanced with the integration of time-optimal maneuver strategies to reduce slewing time. For example, with a 50% improvement in slewing performance, the percentage of the assigned 5-minute mission window utilized for satellite imagery collection jumped from 55% to 76%. This also implies that the revenue collected from this set of imaging operations will also increase significantly with improvements in slewing performance. Based on the original requirements of a minimum 30-second imaging window per AOI target, the results showed that an improvement of 25% in X-SAT's slew performance will lead to additional imaging time of 34.5 seconds, thus enabling the image collection of an additional AOI target. Similarly, 50% improvement in X-SAT slew performance will lead to additional imaging time of 71 seconds, which can accommodate the image collection of two additional AOI targets, thereby significantly increasing revenue generated during the pass.

2. Mission Completion Time

With the integration of approximately 25% and 50% reduction in slewing times, the overall mission completion time in this operational scenario also changed. The results are summarized in Table 5.

Table 5. Mission Completion Time for Imaging Five Target Cities

	Baseline	25% improvement	50% Improvement
Mission Completion Time (s)	273	243	214
Percentage Reduction in Mission Completion Time	-	11%	22%
Percentage Utilization of 5-min Mission Window for Original Mission Requirements	91%	81%	71.3%

The results show that the execution of time-optimal maneuvers in X-SAT's imagery collection operations over the Northern SEA's cities led to an overall reduction in mission completion time. Based on an approximately consistent 50% improvement in slewing performance during its target-to-target maneuver, X-SAT was able to finish the collection of all five target cities to meet the mission goals within 214 seconds which was a 22% reduction in mission completion time compared to the scenario with no improvement in X-SAT's slewing capabilities. This also meant that X-SAT utilized only 71.3% of the available 5-minute mission window period to complete the mission and the remaining 29.7%, i.e., 86 seconds of the mission window period could be utilized to collect imagery of two more AOI targets as highlighted in the earlier section.

Therefore, the decrease in mission completion time associated with incorporating time-optimal spacecraft maneuvers to reduce slewing time implies that the 5-minute imaging window of opportunity could be further optimized to include imaging other AOIs outside of the original requirements. This will enhance the value of this set of imaging satellite operations in the Northern SEA region and provide additional benefits to the satellite operators who can use the previously unutilized portion of the satellite access in the 5-minute window period to expand their imagery database.

3. Resolution of Satellite Imagery Collected

Satellite operators frequently refer to the "elevation angle" of the target area to the imaging satellite during the planning of the imagery collection route. The reason is because this parameter is a key factor in determining resolution of the satellite imagery collected. A typical requirement for high-resolution satellite imagery collection is a minimum elevation angle of 60 degrees, which implies an off-nadir angle of 30 degrees.

To examine the influence of slew maneuvers on the resolution of the collected images, the elevation angles for each target city collection were obtained from STK. While the elevation angles remain very similar for the first three cities (Phnom Penh, Bangkok and Yangon) as shown in Figure 24, the elevation angles differ in greater magnitudes for the last two target cities (Vientiane and Hanoi) as the spacecraft slew performance is improved.

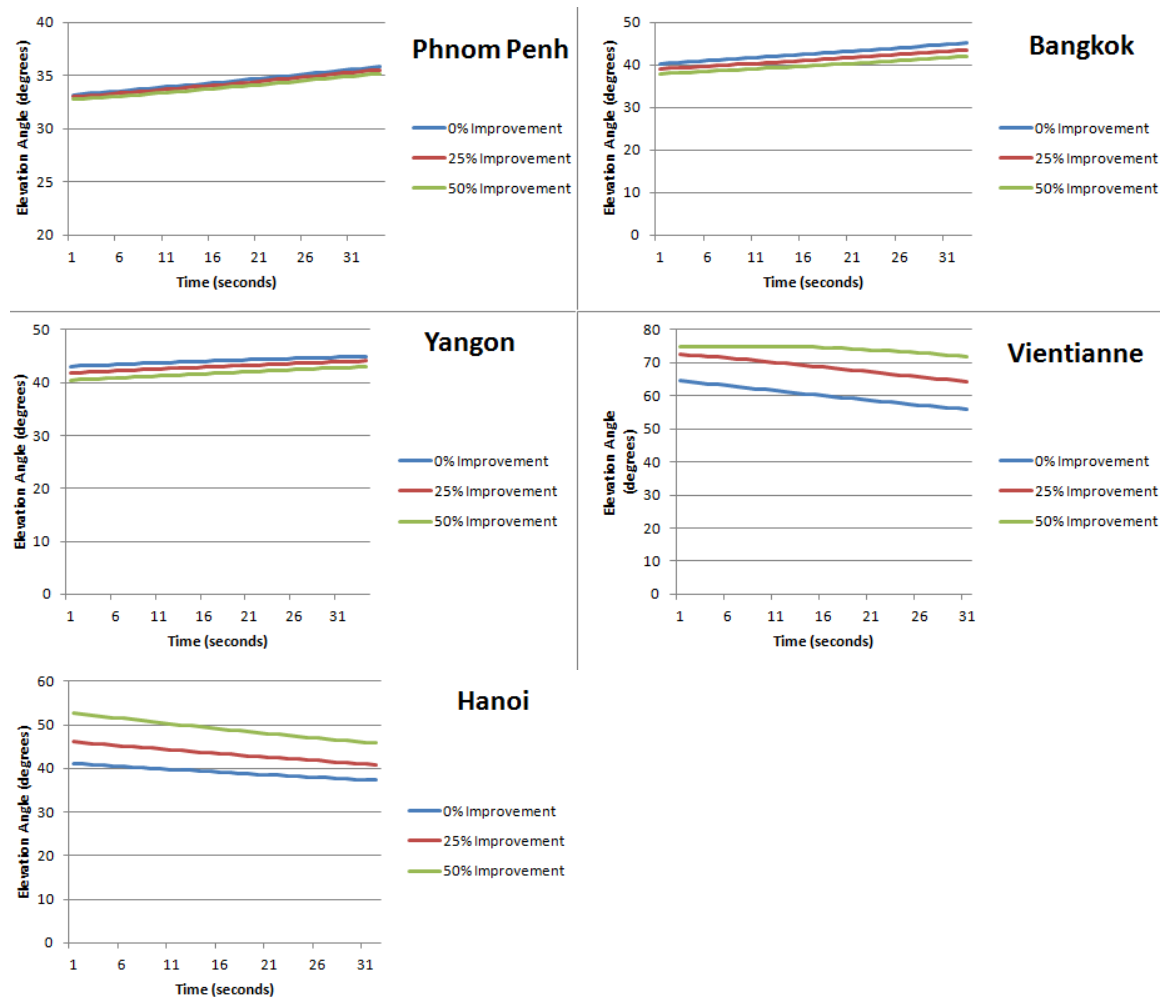


Figure 24. Elevation Angle from Respective Target Cities to X-SAT during Image Collection in OS1

From Figure 24, the results indicated that throughout the imagery collection window period for Vientiane, the elevation angle remained consistently above 70 degrees when the spacecraft slewing time was reduced by 50% and consistently above 65 degrees when the slew time was reduced by 25%. The higher elevation angle recorded during X-SAT's imagery collection operations implied that higher-resolution imagery data could be collected with the integration of time-optimal spacecraft maneuver to X-SAT's operations.

The statistics recorded during X-SAT's imaging of Hanoi demonstrated that the elevation angle did not drop below 40 degrees for both 25% and 50% improvement in spacecraft slewing performance. Furthermore, a 50% improvement in spacecraft slewing performance ensured that the elevation angle stayed consistently above 45 degrees during the imaging period versus an average 38 degree-elevation angle for the baseline spacecraft slewing performance.

To summarize the results presented in Figure 24, it can be inferred that the incorporation of time-optimal spacecraft maneuvers to X-SAT operations has led to a reduction in the target-to-target slewing time, thereby allowing X-SAT to commence the imagery collection of the two cities, Vientiane and Hanoi, at a higher elevation angle before the spacecraft moved further away from the region in its orbit. Figure 25 illustrates this phenomenon. As can be seen, the off-nadir angle is much smaller when the slew time is reduced.

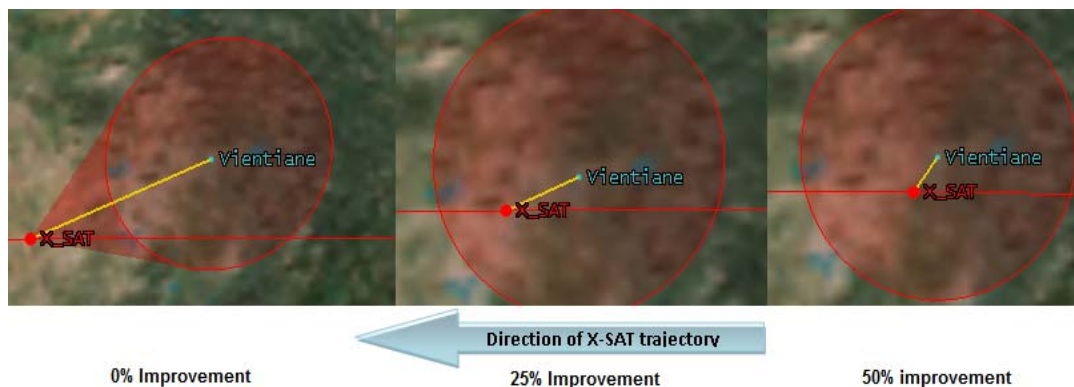


Figure 25. Position of X-SAT at the start of Collecting Vientiane Imagery

In essence, the higher elevation angles during satellite imagery collection translate to enabling the collection of higher-resolution satellite imagery. In real world applications, this would be especially critical for imaging satellites operating over rough terrain because high elevation angles from target AOI to satellite sensor is mandatory for image collection in rough terrain and mountainous areas. In addition, higher-resolution data can also fetch higher revenue income for the satellite providers as such imagery data command a higher selling price in accordance to market norms [41].

So far the analysis has shown that reducing slew time not only allows for acquisition of additional satellite images but also improves the quality of the acquired images.

4. In-Track Stereo Imaging Opportunities

A satellite stereo image product comprises a pair of satellite images of the same area target captured from two dissimilar perspectives at different orbital positions. An in-track stereo imaging opportunity implies that a satellite stereo image could be obtained during the same orbital pass of the satellite over the AOI target [54]. In-track stereo images are highly desired due to the consistent color tone between the pair of images resulting from the similar sun conditions in the same orbital pass, thus enabling collection of better quality images [41].

To this end, it is worthwhile to investigate whether it is possible to obtain any in-track stereo imagery opportunities during the assigned 5-minute mission window in OS1. Although the original mission requirements of collecting satellite images from the five target cities (with a minimum of 30 seconds per city) remain as the fundamental mission goal, availability of such in-track stereo imaging opportunities can further enhance the value of X-SAT's imaging operations in this mission and bring in additional revenue.

From the investigation conducted, it turned out that in-track stereo imaging was feasible only for Vientiane city if an improvement of 50% in slewing performance can be obtained in this operational scenario. From Figure 26, we can see that X-SAT was able to capture images of Vientiane (second last AOI) from two different perspectives at high elevation angles (more than 60 degrees) in the same orbital pass within the assigned 5-minute mission window.

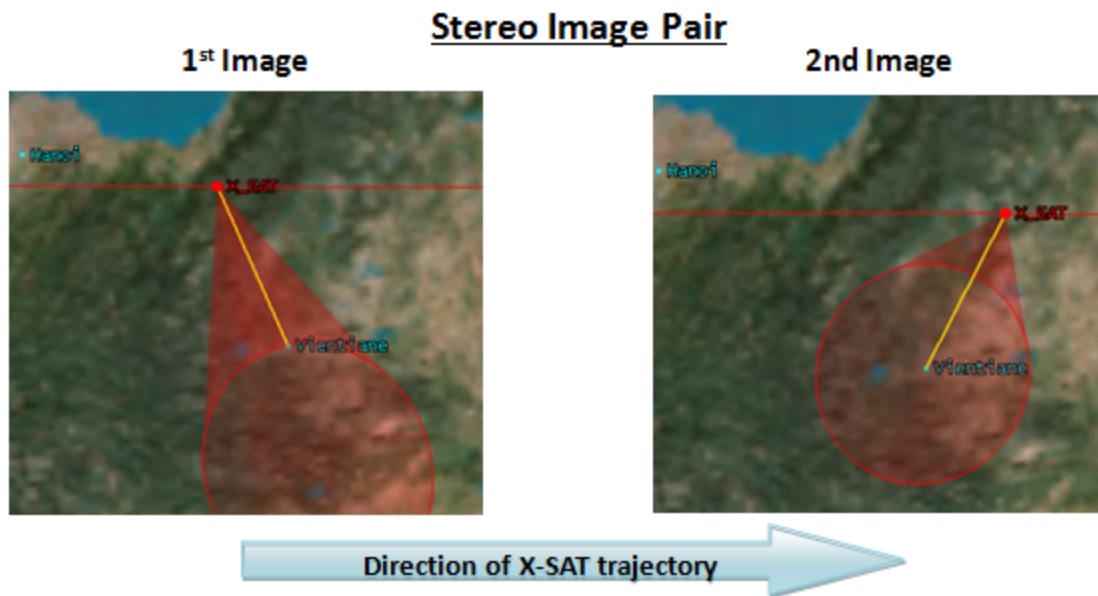


Figure 26. In-Track Stereo Imaging of Vientiane in OS1

This observation illustrated that with an improved slewing rate, the collection of high-demand in-track satellite stereo images can further raise the value of this specific X-SAT's imaging operations in SEA while meeting the baseline mission goals.

D. CONCLUSIONS DRAWN FROM OS1 ANALYSIS

From the analysis of the performance indicators identified earlier¹⁵ to study the impact of integrating time-optimal maneuver to X-SAT imaging operations, the results clearly showed that an improvement in X-SAT slew performance enhanced the value of this specific set of imaging operations while meeting the baseline mission requirements. However, the additional value brought about by the incorporation of time-optimal maneuver strategies was not easily quantifiable in terms of an economic benefit. Therefore, the results of this chapter justified some additional effort directed at establishing a framework that can facilitate the business case analysis of imaging satellite operations. Constructing such a framework is the topic of the next chapter.

¹⁵ The performance indicators are 1) Imaging window period, 2) Mission completion time, 3) Resolution of satellite imagery and 4) In-Track Stereo Imaging Opportunities.

V. A FRAMEWORK FOR BUSINESS CASE ANALYSIS

A Business Case Analysis (BCA) is a fundamental tool used by key stakeholders for the evaluation of feasible alternatives to a problem statement and facilitates sensible decision-making to determine the best-value solution [55]. In the context of business investment and operations, this structural and systematic methodology examines not only the economic ROI, but also other quantifiable and non-quantifiable aspects that support an investment decision. As a decision-making tool, the quality and reliability of the BCA is crucial in enabling the decision-maker to reach an informed selection.

In Chapter IV, the results obtained from conducting the preliminary operational analysis of OS1 illustrated that the incorporation of time-optimal maneuver strategies into the operation of an imaging satellite holds promise for enhancing mission effectiveness. In particular, the augmented operational capability allowed for additional volume of satellite images to be collected, and with better quality. While it was clear that the integration of time-optimal maneuvers to X-SAT's operations in OS1 was advantageous for the baseline image collection sequence, it would be challenging to extrapolate the results and quantify the added value that improvements in slewing performance can bring to the overall image collection operations. Without a strategic framework in place, it will be tricky to convince decision-makers of the value that novel maneuver strategies can bring to imaging spacecraft operations.

Moving forward, it will be useful to explore how an analytical process can be set up to conduct a BCA in the context of imaging satellite operations. A framework based on the AHP technique can be utilized by the satellite operators to determine the best-value collection route permutation as well as to critically study and quantify the impact and value that new maneuvers can bring to imaging satellite operations.

A. ANALYTIC HIERARCHY PROCESS

In view that the Analytic Hierarchy Process (AHP) is a structured technique for organizing and analyzing complex problem statements, it has particular application in group decision making [17]. The application of AHP to complex decision situations is widely used around the world in various fields such as business, industry, healthcare, government and education [17]. Besides recommending the best-value decision, the AHP helps users of the technique to find the solution that best matches their desired end goal based on their interpretation of the problem. The AHP technique enables a comprehensive and rational framework for:

- a. Structuring a problem statement that requires a decision to be made,
- b. Representing and quantifying the elements eligible for analysis,
- c. Relating those eligible elements to the overall goal and
- d. Fairly evaluating the feasible alternative solutions.

At the start, AHP users will typically attempt to decompose their decision problem into a hierarchy of more easy-to-comprehend sub-problems, each of which can be independently analyzed without interfering with the other sub-problems. The second layer of sub-problems can be further broken down into elements that directly influence the parent sub-problem and therefore indirectly affect the overall decision problem. These lower-layered elements of the hierarchy can relate to any aspect of the problem statement. However, it is very important to ensure that no two elements are repeated. Otherwise, it would not be a fair assessment. An example of an AHP hierarchy modeled to evaluate the feasible solutions to a generic “Which car should I buy?” decision problem is presented in Figure 27.

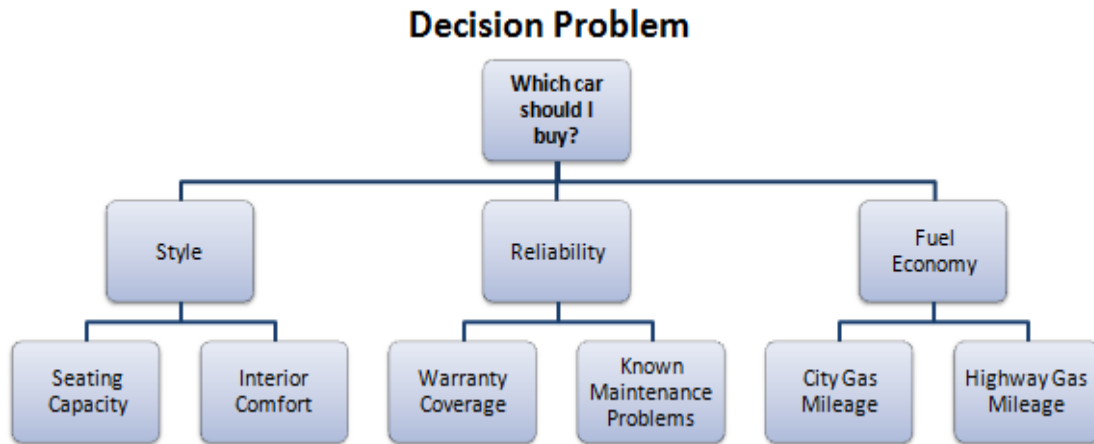


Figure 27. Generic AHP Hierarchy model

Once the hierarchy model is built with the inputs and consensus from all stakeholders, the car buyer shall systematically evaluate the respective elements and assign the relative weights to each element in the hierarchy. Using pair wise comparisons, the relative importance of one criterion over another can be expressed. Elements that are associated with the “must-have requirements” are deemed more important than those associated with the other “good-to-have” requirements and will therefore be assigned higher-value weights so that the importance of the key requirements can be factored into the evaluation process. Under the hierarchy, the total sum of the assigned weights must add up to 100%.

Take for example the “Which car should I buy?” decision problem. If the criterion “Style” was deemed to be twice as important as “Reliability,” “Reliability” deemed thrice as important as “Fuel Economy” and we carry on populating the rest of the hierarchy using pair wise comparison, the resulting AHP hierarchy will look like as shown in Figure 28 (with the assigned weights now included).

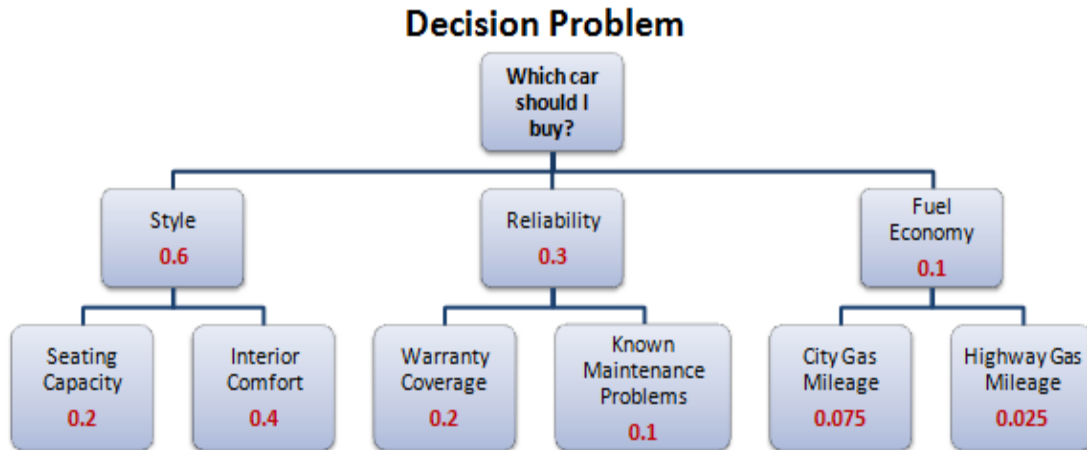


Figure 28. Generic AHP Hierarchy Model with Assigned Weights

Using the aforementioned hierarchy model to evaluate the cars shortlisted for purchase, the options will be ranked accordingly to determine which car will be the best fit in terms of matching the criteria outlined in the AHP hierarchy. Besides using concrete data to assess the options, the car buyer and the other stakeholders can also use their human judgment in performing the evaluation. In the final step of the evaluation process, the AHP technique will convert the evaluations for each element to the respective numerical values that can be processed to rank the options. Based on the options' relative ability to meet the pre-defined requirements of the car buyer, the AHP decision-making tool ultimately enables a straightforward conclusion to decide which car to purchase based on the highest-ranked option.

B. AHP-BASED ANALYSIS OF IMAGING SPACECRAFT OPERATIONS

1. Motivation for using AHP Technique

To enhance the value of the operational analysis conducted in OS1, putting together a framework was deemed necessary to enable a structured approach for conducting a BCA on the impact of implementing time-optimal maneuvers for imaging spacecraft operations. The ultimate goal of this BCA is to provide key stakeholders and decision-makers with relevant insights as to how

time-optimal maneuver strategies support the strategic mission objectives and how the optimal collection route can deviate with the execution of time-optimal spacecraft maneuvers. In applying the structured framework for assessment, pertinent information on the collection route options, operational benefits and economic ROI can be laid out clearly to achieve the best solution for future spacecraft image collection scenarios.

Application of the AHP technique is used to construct a structured framework to facilitate a fair and logical operational analysis of time-optimal maneuvering strategies for imaging spacecraft. Use of the AHP technique will help to organize the complex problem statement and break down into clearly-defined sub-problems for ease of comprehension.

2. An AHP Hierarchy for Imaging Operations

In a typical imaging spacecraft mission, the collection route will be planned upfront by operators at the ground station. Refer to the satellite imagery collection workflow (illustrated earlier in Figure 12), which is commonly adopted in the commercial satellite industry today. Based on the allocated satellite imagery collection resources and filtering of target AOIs' priority levels, the mission planners will generate the window periods for satellite image collection operation tasking. It is a common goal for satellite imagery providers to seek maximum economic returns from their investment. Adopting an AHP-based technique for operational analysis and integrating this decision-making tool into the workflow can therefore be beneficial to the satellite operators in determining the best-value collection route within an assigned or available mission window period.

In most imaging satellite operations, the imaging satellite will typically be tasked to collect satellite images of a few target AOIs, which have been filtered and prioritized by the mission planners. Taking the number of target AOIs tasked to the imaging satellite to be n , this implies that the number of possible collection routes will be equivalent to $n!$. Therefore, the desired end goal in many satellite

imaging operations would be to find the ideal collection route given the $n!$ alternatives. The ideal collection route should generate the highest revenue among the $n!$ number of possible permutations.

In line with the AHP technique, the problem statement “How to determine the best collection route?” can be logically decomposed into sub-problem statements that evaluate the amount of revenue generated from image collection at each target AOI. In this way, the total amount of revenue received from a set of image collection operations will be equivalent to summing up the revenue generated from each target AOI. Thus, a numerical value can be assigned to each permutation for comparative ranking purposes. As a result, the highest-ranked permutation based on the performance elements and the associated weights defined in the AHP hierarchy, will be accepted as the ideal collection route.

It is logical to assume that the revenue generated from imaging each target AOI correlates directly with the image collection volume and the overall image resolution. Therefore, it makes sense to define “Volume of image collection” and “Resolution of imagery data” as elements in the AHP hierarchy structure for “measuring performance per target AOI” which is likened to “calculating revenue generated from each target AOI.” Assuming that there will be $n=4$ target AOIs scheduled for image collection, Figure 29 illustrates how the AHP hierarchy model may look for this set of spacecraft image collection operations.

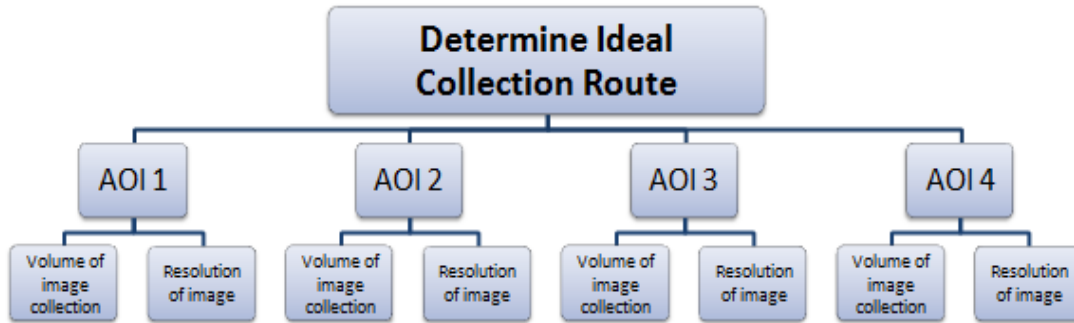


Figure 29. AHP Hierarchy Model for Imaging Spacecraft Operations

The elements covered in the hierarchy structure as shown in Figure 29 is neither exhaustive nor exclusive. Spacecraft mission success hinges on several key parameters and the definition of mission success can differ from scenario to scenario. Depending on the definition of mission success or image collection requirements, other elements relevant for measuring the performance level can be included, if desired, to make the analysis more relevant and complete. This flexible methodology of operational analysis can also be extended to different scenarios (for example, image collection from more target AOIs) to determine the best collection route. The hierarchy structure is also flexible enough such that when the priority of image collection for a particular AOI changes, the weights of the elements can be easily adjusted to reflect the change in AOI collection priority.

With the set up of this hierarchy structure, an operational analysis of the set of imaging operations can be carried out to determine the best-value collection route out of the $n!=24$ possible permutations. To integrate the use of this AHP-based evaluation methodology as part of the workflow, the mission planners shall systematically evaluate the respective elements and assign the appropriate weights to each element in the hierarchy prior to the start of mission. Using pair wise comparisons, the relative importance of one AOI over the other can be expressed and defined in the hierarchy. AOIs deemed to be more important than the others will therefore be assigned higher-value weights so that these AOIs will have a greater influence on the evaluation outcome. Under each

AOI, the weights of relevant elements “Volume of image collection” and “Resolution of image” can also be adjusted accordingly to fit the customers’ requirements.

Depending on the nature and requirements of the image collection operations, the AHP hierarchy model could be updated to look like that shown in Figure 30. The model shown in Figure 30 reflects the following characteristics of this set of imaging operations:

- a. AOI 1 was deemed to be the most important target, followed by AOI 4, AOI 3 and then AOI 2.
- b. AOI 1 is $\frac{4}{3}$ times more important than AOI 4. AOI 4 is twice as important as AOI 3 and likewise, AOI 3 is also twice as important as AOI 2.
- c. Requirements for the volume and resolution of satellite imagery collected for AOI 1 are equally important.
- d. Requirement for image resolution is thrice as important as the volume collected for AOI 3.
- e. Requirement for the image resolution is twice as important as the volume collected for AOI 4. This is true for AOI 2 as well.

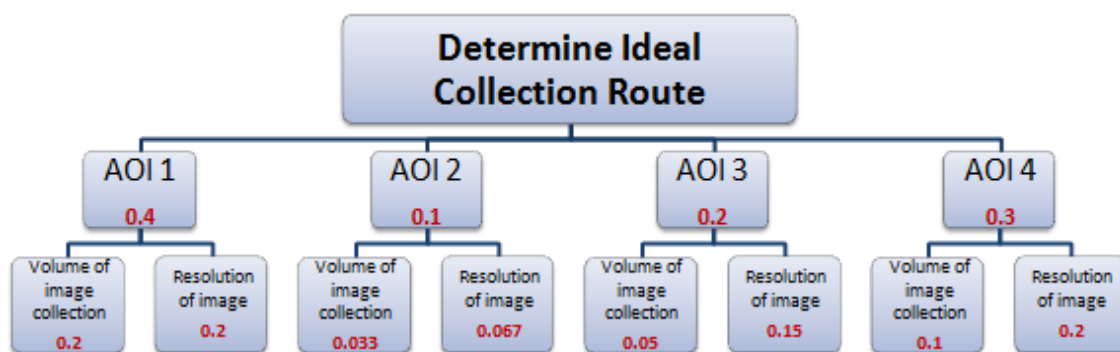


Figure 30. AHP Hierarchy Model for Imaging Spacecraft Operations with Assigned Weights

In essence, putting together such a hierarchy model based on the AHP technique enables a flexible and methodical evaluation process to systematically determine the best-value image collection route for imaging spacecraft missions in different operational scenarios. In applying this AHP-based technique, the satellite operator can achieve maximum economic return.

Operational benefits that could potentially add value to the set of imaging operations in OS1 with the incorporation of time optimal-maneuver strategies were identified earlier in Chapter IV. It was clear that appropriate time-optimal maneuver strategies can reduce slewing time and enhance the value of that specific image collection route in OS1 with the following benefits:

- a. Higher utilization of mission window for image collection,
- b. Higher volume of satellite imagery collected,
- c. Expansion of the imagery database with image collection of additional AOIs outside of original mission requirements,
- d. Higher resolution of satellite imagery data collected and
- e. Additional opportunities for in-track stereo image collection.

However, it was tough to quantify the operational benefits that time-optimal maneuvers brought to X-SAT imaging operations in OS1. Furthermore, the operational benefits gained with improved slewing rate were demonstrated and analyzed only for a specific collection route. A more comprehensive operational analysis of the set of imaging operations across other collection route permutations can be conducted to critically examine and quantify the operational benefits of integrating time-optimal maneuvers to imaging satellite operations.

In the next chapter, a comprehensive operational analysis of OS2 will be conducted using the AHP technique described here to provide an assessment that better quantifies the benefits of time-optimal maneuvers for imaging operations.

THIS PAGE INTENTIONALLY LEFT BLANK

VI. AHP ANALYSIS OF OPERATIONAL SCENARIO 2

The baseline mission requirements in OS2 are to capture satellite images from four Southeast-Asian cities namely Bandar Seri Begawan, Hanoi, Manila and Singapore. During the setup of OS2 in the STK environment, the appropriate window for imaging opportunities was identified to be from 04:32:00 UTCG to 04:40:00 UTCG on November 2, 2012. In order to demonstrate the application of the proposed AHP technique, only OS2 will be analyzed. This decision was made to reduce the amount of raw data to be included as part of this thesis. The approach and analysis outlined in this chapter can, however, also be applied to provide a more detailed analysis of OS1.

A. EXTRACTING RELEVANT DATA FOR ANALYSIS

There are a total of 24 possible collection permutations for X-SAT's mission to collect satellite imagery from four target cities in OS2. The request from fictitious customer orders called for a minimum imaging time of 45 seconds for each target city with no preference in collection order. In this chapter, X-SAT's image collection operations in OS2 will be analyzed by the application of the AHP hierarchy-based framework introduced in Chapter V. Applying the AHP hierarchy structure as a methodological framework for analysis enables the ideal collection route to be determined in an organized manner.

In order to determine the most ideal collection route in OS2, the analysis will require relevant data to measure the "performance" of each permutation of the collection route. After modeling X-SAT and setting up OS2 in the STK simulation environment, data pertaining to the satellite access time coverage for each target city and the elevation angle from each target city to X-SAT at each step in the OS2 scenario was extracted for analysis purposes. The satellite access time to each target city for a specific collection route could be determined

for all four target cities by generating the “Complete Chain Access” report for the “Chain” object type¹⁶. This is illustrated in Figure 31 which shows the screenshot from STK.

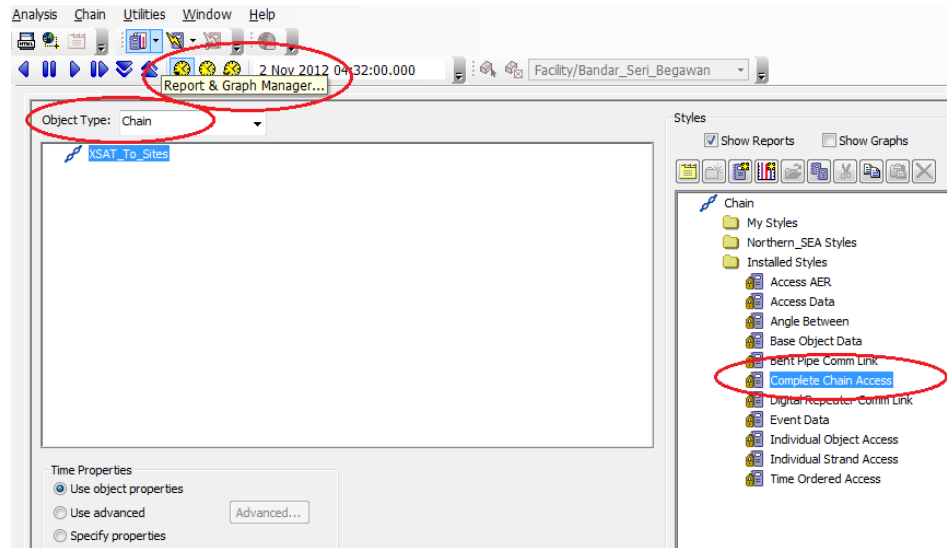


Figure 31. Screenshot from STK for Generating the Satellite Access Time in OS2

Under the same “Report and Graph Manager” section in STK, the Azimuth, Elevation and Range (AER) data for a specific collection route could also be determined by generating the “Access AER” report for a time-step of 1 second. This is illustrated in Figure 32, which shows the screenshot from STK.

¹⁶ Defined by assigning the four target cities to the X-SAT imaging sensor in STK.

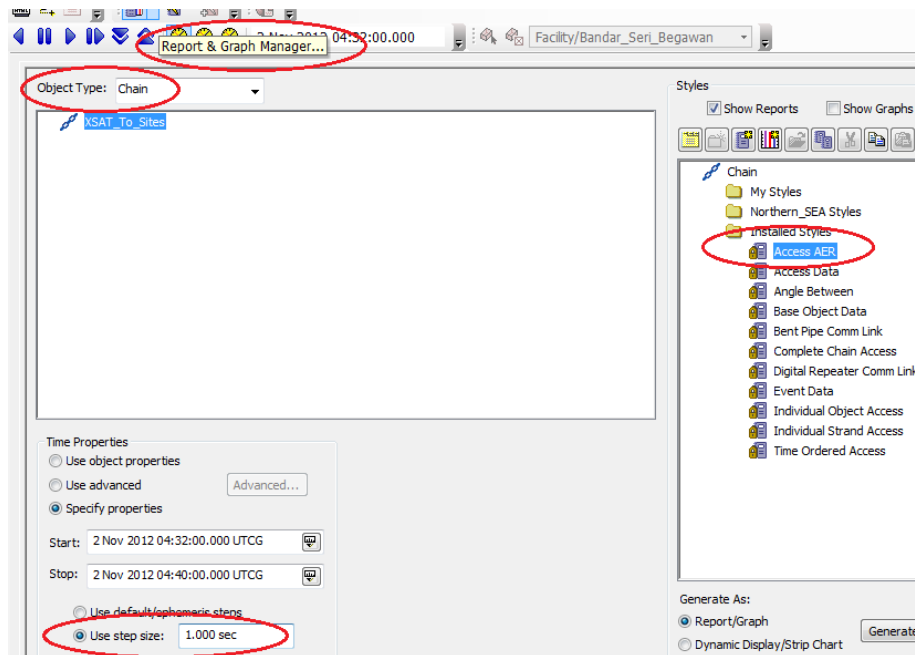


Figure 32. Screenshot from STK for Generating the AER data in OS2

The Satellite Access Time data for the specific collection route i.e., Singapore -> Bandar Seri Begawan-> Hanoi-> Manila, is shown in Figure 33. Figure 34 shows the STK screenshot of AER data collected for Manila city in this specific collection route.

XSAT_Sensor-To-Singapore				
	Access	Start Time (UTCG)	Stop Time (UTCG)	Duration (sec)
	-----	-----	-----	-----
	1	2 Nov 2012 04:32:00.000	2 Nov 2012 04:33:21.171	81.171
XSAT_Sensor-To-Bandar_Seri_Begawan				
	Access	Start Time (UTCG)	Stop Time (UTCG)	Duration (sec)
	-----	-----	-----	-----
	1	2 Nov 2012 04:33:37.451	2 Nov 2012 04:35:06.297	88.847
XSAT_Sensor-To-Hanoi				
	Access	Start Time (UTCG)	Stop Time (UTCG)	Duration (sec)
	-----	-----	-----	-----
	1	2 Nov 2012 04:35:53.584	2 Nov 2012 04:37:10.336	76.752
XSAT_Sensor-To-Manila				
	Access	Start Time (UTCG)	Stop Time (UTCG)	Duration (sec)
	-----	-----	-----	-----
	1	2 Nov 2012 04:37:49.961	2 Nov 2012 04:39:03.853	73.892

Figure 33. Screenshot of X-SAT Satellite Access Time Data from STK

X_SAT/Sensor2 to Manila

Time (UTCG)	Azimuth (deg)	Elevation (deg)	Range (km)
2 Nov 2012 04:37:49.961	216.813	-34.282	1746.600490
2 Nov 2012 04:37:50.000	216.807	-34.279	1746.801874
2 Nov 2012 04:37:51.000	216.667	-34.213	1752.033653
2 Nov 2012 04:37:52.000	216.529	-34.147	1757.277760
2 Nov 2012 04:37:53.000	216.391	-34.082	1762.534079
2 Nov 2012 04:37:54.000	216.254	-34.017	1767.802495
2 Nov 2012 04:37:55.000	216.118	-33.953	1773.082893
2 Nov 2012 04:37:56.000	215.984	-33.889	1778.375160
2 Nov 2012 04:37:57.000	215.850	-33.825	1783.679185
2 Nov 2012 04:37:58.000	215.717	-33.762	1788.994857
2 Nov 2012 04:37:59.000	215.586	-33.699	1794.322066
2 Nov 2012 04:38:00.000	215.455	-33.637	1799.660703
2 Nov 2012 04:38:01.000	215.326	-33.575	1805.010660
2 Nov 2012 04:38:02.000	215.197	-33.513	1810.371832
.
.
.
.
2 Nov 2012 04:38:58.000	209.305	-30.718	2125.625837
2 Nov 2012 04:38:59.000	209.220	-30.679	2131.479261
2 Nov 2012 04:39:00.000	209.134	-30.640	2137.339191
2 Nov 2012 04:39:01.000	209.050	-30.601	2143.205567
2 Nov 2012 04:39:02.000	208.966	-30.563	2149.078329
2 Nov 2012 04:39:03.000	208.882	-30.525	2154.957418
2 Nov 2012 04:39:03.853	208.811	-30.492	2159.979743

Figure 34. Sample Screenshot of Azimuth, Elevation and Range (AER)
Data for Manila City

The AER data similar to that shown in Figure 34 was collected for the other three cities as well for this specific collection route. Subsequently, the AER data could be similarly extracted for the other 23 collection order permutations by repeating and re-running the OS2 scenario for the other collection routes in the STK software. Thus, the full set of Satellite Access and AER data for all 24 collection route permutations could be extracted from STK and used for analysis purposes.

B. APPLICATION OF AHP TECHNIQUE FOR OS2 ANALYSIS

After extracting the relevant data from STK for OS2 analysis, making sense of the available data was essential to draw the appropriate conclusion and determine the best collection route. The challenge was to customize the AHP Hierarchy Model defined earlier for imaging spacecraft operations and to integrate the data collected earlier from STK for measuring the performance level per target city in OS2.

It was not possible to extract from STK, exact data representing the volume and resolution of satellite imagery collected for each target city as proposed in Chapter V. However, the readily-available Satellite Access time data and Satellite Elevation angle data could be utilized in lieu of these metrics to evaluate and quantify the “performance” of the two elements under each target city in the AHP hierarchy model. This follows from making these two reasonable assumptions:

- a. The volume of satellite imagery collected for each target city is directly proportional to the duration of satellite access to each target city. This assumption is justified because the longer that X-SAT has access to the target city, the longer that X-SAT will be able to sense and collect images from that target city. For a more realistic calculation of image collection time for each target city, 10 seconds were uniformly subtracted from the satellite access time for each target city to account for the time required to stabilize the platform before image acquisition and the time required for X-SAT to maneuver away from the current target city in its slew to the next target city. Figure 35 provides an illustrated explanation using Bandar Seri Begawan as the target city.
- b. Resolution of satellite imagery data is directly proportional to satellite elevation angle of access. This assumption is reasonable given that a high elevation angle of satellite access enables the collection of high resolution satellite imagery. The average of the

elevation angles recorded during the satellite access period for each target city will be utilized to quantify the average resolution “performance” for each target city.

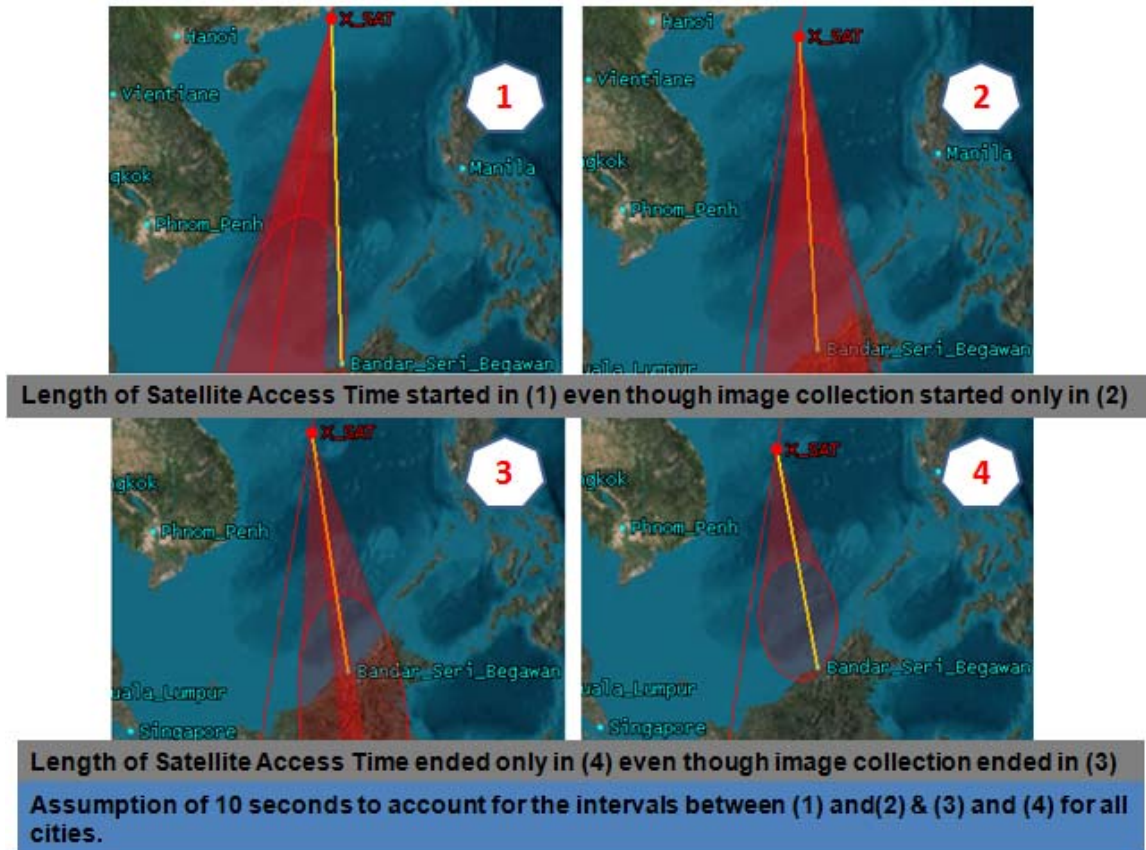


Figure 35. Illustration of Difference between Imaging Time and Satellite Access Time

In view of the discussion above, the AHP hierarchy model for X-SAT imaging operations in OS2 will be slightly modified to take in the relevant data extracted from STK for further analysis. Figure 36 shows the modified AHP hierarchy model.

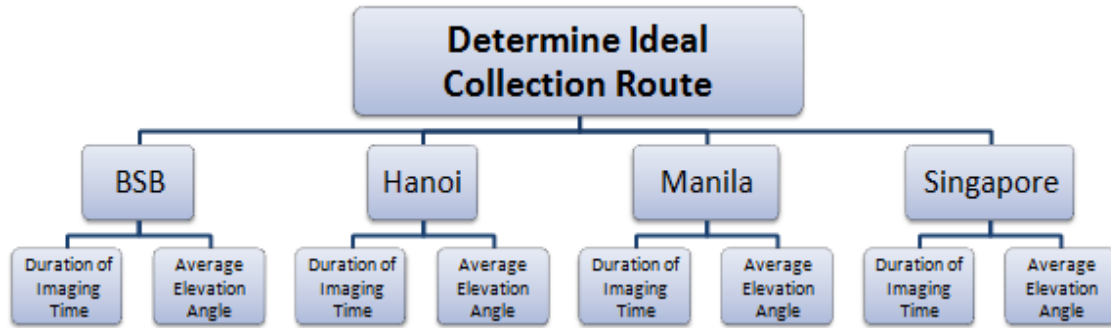


Figure 36. Modified AHP Hierarchy Model for X-SAT Imaging Operations

Given that no specific requirements were specified by the customer orders on the image collection volume and image resolution, all target cities were accorded the same priority level (although this need not be the case in the application of the AHP technique for future operational scenarios). Given the uniform priority, equal weights were assigned to all elements in the AHP hierarchy model as shown in Figure 37.

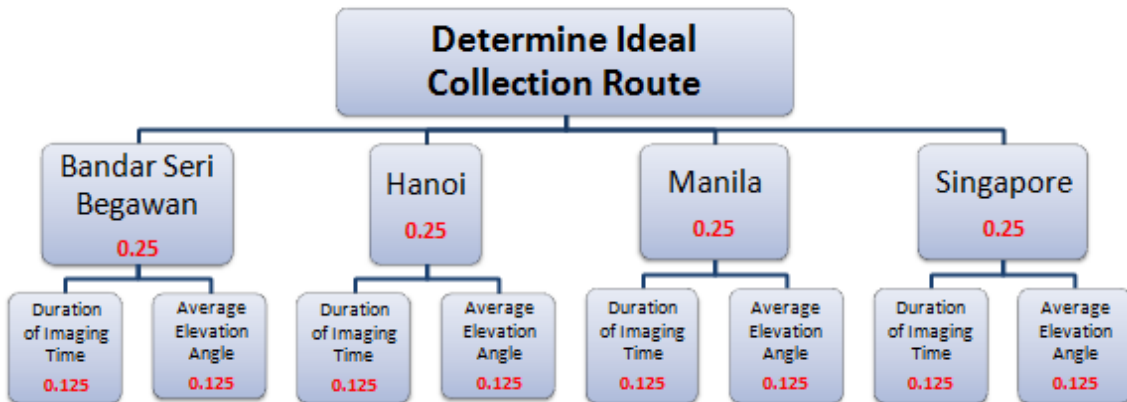


Figure 37. AHP Hierarchy Model for X-SAT Imaging Operations Updated with Assigned Weights

Examples of the data obtained from the OS2 simulation in STK for a few of the collection route permutations are shown in Table 6. Given the inconsistency in benefits derived from “Imaging Time” and “Average Elevation Angle” since the underlying data collected were expressed in different units,

there was a need to normalize the raw data to attain comparable units of measurement to derive the overall benefit score. In this case, the measured benefit increases with the value of “Imaging Time” and “Average Elevation Angle.” The benefit scores for all 24 possible permutations of the collection route are presented in Table 7. Refer to Appendix A for the detailed data.

Table 6. Relevant Data Obtained from STK for Possible Collection Routes in OS2

S/N	Collection Order(1st, 2nd, 3rd, 4th, 5th)--->			
1	Hanoi	Manila	Bandar	Singapore
Imaging Time (sec)	57	67	69	64
Average Elevation Angle (deg)	40.36	47.18	52.56	46.79
2	Hanoi	Bandar	Manila	Singapore
Imaging Time (sec)	58	68	66	60
Average Elevation Angle (deg)	40.39	35.54	41.17	46.99
3	Manila	Bandar	Hanoi	Singapore
Imaging Time (sec)	65	75	64	61
Average Elevation Angle (deg)	38.63	35.02	35.18	46.89
4	Manila	Hanoi	Bandar	Singapore
Imaging Time (sec)	57	63	65	64
Average Elevation Angle (deg)	38.26	42.79	52.95	46.79
5	Bandar	Hanoi	Manila	Singapore
Imaging Time (sec)	58	66	63	60
Average Elevation Angle (deg)	29.30	42.77	41.03	46.99
.
.
.
23	Singapore	Hanoi	Bandar	Manila
Imaging Time (sec)	60	70	70	64
Average Elevation Angle (deg)	27.69	42.86	53.44	32.23
24	Singapore	Bandar	Hanoi	Manila
Imaging Time (sec)	71	79	67	64
Average Elevation Angle (deg)	27.73	34.88	35.09	32.23

Table 7. Results from Application of AHP Hierarchy Model for X-SAT Imaging Operations for OS2

Route	Route_1	Route_2	Route_3	Route_4	Route_5	Route_6
Benefit Score	0.891	0.833	0.831	0.864	0.819	0.845
Route	Route_7	Route_8	Route_9	Route_10	Route_11	Route_12
Benefit Score	0.805	0.810	0.810	0.806	0.795	0.787
Route	Route_13	Route_14	Route_15	Route_16	Route_17	Route_18
Benefit Score	0.866	0.859	0.854	0.822	0.866	0.837
Route	Route_19	Route_20	Route_21	Route_22	Route_23	Route_24
Benefit Score	0.792	0.843	0.766	0.786	0.824	0.786

The analysis to determine the ideal collection route was simplified with the application of the AHP hierarchy model. From the results shown in Table 7, Collection Route_1 provided the highest benefit score of 0.891 among the 24 possible collection route permutations. The specific collection route of: Hanoi-> Manila-> Bandar Seri Begawan-> Singapore provided the highest benefit score and was deemed to be the best collection route.

Applying the AHP hierarchy model to fit in relevant data extracted from the OS2 simulation in STK has enabled a methodical framework to analyze the possible options for the range of image collection routes in this operational scenario. Besides determining the ideal collection route that gives the best-value for X-SAT operation in this set of image collection tasks, the AHP-based framework has provided a means to directly quantify the operational advantages

that the ideal collection route (Route_1), provides over the least ideal collection route (Route_21). The results imply that Route_1 provides approximately 12.5% more operational benefit than Route_21 based on the specified image collection mission requirements.

At the same time, the AHP hierarchy model presents the satellite operators with a flexible and efficient method to derive the ideal collection route in the event that the mission requirements change. In a different scenario where the priority of image collection from one target city has become higher than any other city targets or the priority level is no longer equal across all target cities, the hierarchy model can be modified with the assigned weights updated to reflect the shift in mission goal accordingly.

Likewise, for other satellite imaging missions where the resolution of satellite imagery is deemed more important than the volume collected, the hierarchy model can also be easily modified such that higher-value weights are assigned to the “Average Elevation Angle” performance elements for all target cities. Although the best collection route and operational benefit of different operational scenarios will change along with the change in the weights’ value, the presented framework based on the AHP hierarchy model provides a systematic way to rank the collection route options and determine the ideal collection route efficiently.

C. IMPACT OF TIME-OPTIMAL MANEUVER STRATEGIES

To investigate the impact of integrating time-optimal maneuvers to X-SAT imaging operations in OS2, X-SAT was re-modeled with an approximate 50% improvement in slewing performance¹⁷. The STK simulation scenario was re-run with the re-modeled X-SAT with no change to the mission original requirements. Relevant data similar to those shown in Table 6 were extracted from this revised STK simulation of OS2 and is shown in Table 8 . Refer to Appendix B for the detailed data.

¹⁷ Similar to the approach undertaken in STK for OS1.

Table 8. Relevant Data Obtained from revised STK simulation of OS2 with 50% Improvement in X-SAT slewing performance

S/N	Collection Order(1st, 2nd, 3rd, 4th, 5th)--->			
1	Hanoi	Manila	Bandar	Singapore
Imaging Time (sec)	54	59	62	60
Average Elevation Angle (deg)	40.26	45.84	42.29	37.84
2	Hanoi	Bandar	Manila	Singapore
Imaging Time (sec)	54	60	59	57
Average Elevation Angle (deg)	40.29	33.21	46.09	37.97
3	Manila	Bandar	Hanoi	Singapore
Imaging Time (sec)	58	63	57	58
Average Elevation Angle (deg)	38.35	32.99	39.33	37.97
4	Manila	Hanoi	Bandar	Singapore
Imaging Time (sec)	54	57	60	60
Average Elevation Angle (deg)	38.13	43.49	42.49	37.84
.
.
.
23	Singapore	Hanoi	Bandar	Manila
Imaging Time (sec)	56	60	58	59
Average Elevation Angle (deg)	27.67	43.48	42.33	38.22
24	Singapore	Bandar	Hanoi	Manila
Imaging Time (sec)	61	65	58	58
Average Elevation Angle (deg)	27.69	32.93	39.3	38.22

The extracted data was then substituted into the same AHP hierarchy model for analysis. Using the same methodology, the benefit scores of the AHP analysis were presented in Table 9 . Refer to Appendix B for the detailed data.

Table 9. Application of AHP Hierarchy Model for X-SAT Imaging Operations in OS2 with 50% Improvement in Slewing Performance

Route	Route_1	Route_2	Route_3	Route_4	Route_5	Route_6
Benefit Score	0.912	0.885	0.872	0.892	0.877	0.884
Route	Route_7	Route_8	Route_9	Route_10	Route_11	Route_12
Benefit Score	0.862	0.853	0.854	0.847	0.847	0.849
Route	Route_13	Route_14	Route_15	Route_16	Route_17	Route_18
Benefit Score	0.921	0.917	0.912	0.886	0.923	0.899
Route	Route_19	Route_20	Route_21	Route_22	Route_23	Route_24
Benefit Score	0.854	0.878	0.839	0.849	0.865	0.849

With an approximately 50% improvement in slew performance, Route_17 (i.e., Singapore-> Hanoi-> Manila-> Bandar Seri Begawan) is now the ideal collection route. This result is different from the result from the previous AHP analysis done using the baseline slewing rate. Table 9 shows that the incorporation of time-optimal maneuvers has a direct impact on the imaging satellite's operations such that the overall value of each set of imaging permutations can be significantly changed, thus leading to a different collection route than originally solved. This aspect highlights the importance of this thesis because the interplay between maneuver performance and imaging performance must be considered to fully justify the application of new maneuvers in practice.

To further investigate the impact of time-optimal maneuver strategies to X-SAT image collection operations, the next part of the analysis zoomed in and focused on the average elevation angle statistics recorded during the respective image collection period for each city target.

As per the original requirements, equal weight was assigned to each “Average Elevation Angle” element under each target city. The benefit scores for all 24 possible collection routes were generated for comparison to see whether an improvement in slewing performance enabled better quality image collection. This aspect of the analysis is different from the earlier analysis done because image resolution is the only criteria used here to measure the performance of X-SAT operation in OS2. The benefit scores directly represent the quality (in terms of image resolution) of the total volume of satellite images collected from all four target cities. Hence, the higher the benefit score, the higher is the quality of satellite imagery collected. The comparison results are presented in Table 10. Refer to Appendix C for the detailed data.

Table 10. Benefit Score Comparison for Image Resolution between Baseline and Time-Optimal Maneuvers

Route		Route_1	Route_2	Route_3	Route_4	Route_5	Route_6
Benefit Score	Original Slew	1.000	0.973	0.974	0.996	0.969	0.974
	50% Slew Improvement	0.896	0.935	0.936	0.902	0.952	0.945
Route		Route_7	Route_8	Route_9	Route_10	Route_11	Route_12
Benefit Score	Original Slew	0.945	0.972	0.973	0.972	0.973	0.945
	50% Slew Improvement	0.985	0.943	0.957	0.944	0.966	0.993
Route		Route_13	Route_14	Route_15	Route_16	Route_17	Route_18
Benefit Score	Original Slew	1.000	0.971	0.996	0.974	0.967	0.974
	50% Slew Improvement	0.962	0.990	0.969	0.991	0.997	0.990
Route		Route_19	Route_20	Route_21	Route_22	Route_23	Route_24
Benefit Score	Original Slew	0.960	0.961	0.956	0.934	0.957	0.934
	50% Slew Improvement	0.957	0.942	0.974	0.993	0.948	0.986

The computed benefit scores showed that time-optimal maneuvers do not necessarily improve the quality of satellite imagery collected for all collection routes. Given that the benefit scores were computed by taking into account the average elevation angles recorded across all target cities, the improvement in the elevation angles for some cities may not be substantial enough to produce an overall higher benefit score for time-optimal maneuvers in all 24 collection permutations. Out of the 24 possible collection permutations, X-SAT managed to

achieve better quality image collection in OS2 with the integration of time-optimal maneuvers in 9 of the 24 collection routes namely Route_7, Route_12, Route_14, Route_16, Route_17, Route_18, Route_21, Route_22 and Route_24. Notably, the benefit score comparison for Route_17 (which was earlier determined to be the best-value collection route permutation from the AHP analysis of X-SAT imaging operations with 50% improvement in slew performance) also illustrated that an improvement in slew performance enabled the overall collection of higher resolution (i.e., better quality) satellite images in OS2. This can be attributed to X-SAT's improved agility that enabled the collection of satellite images from Hanoi and Manila at relatively higher elevation angles.

Application of the AHP hierarchy model has provided us with new insights to the improved image resolution that can be collected with integration of time-optimal maneuvers. The analysis has also offered an unambiguous outcome on the specific collection routes in OS2 that can be enhanced with an improvement in X-SAT's slewing performance with respect to the original mission requirements. In order to obtain a more comprehensive appreciation of the economic impact of time-optimal maneuvers to X-SAT operations, another dimension has to be added to the analysis of X-SAT's imaging operations in OS2.

D. BUSINESS CASE ANALYSIS OF X-SAT IMAGING OPERATIONS IN OS2

Based on the AHP hierarchy model defined for imaging satellite operations, the earlier analysis focused on deriving the benefit scores representing the quality of images collected from the target cities in all 24 collection route permutations. Besides the obvious overall benefit of collecting satellite imageries of better quality in nine out of the 24 collection route permutations, another key factor that will contribute towards receiving higher economic ROI is the total volume of satellite imagery collected.

There are opportunities to further optimize the mission value by collecting additional images from neighboring cities in the 8-minute mission window period assigned to X-SAT. After fulfilling the mission's original requirements of collecting satellite imagery from the four target cities, we made the assumption that X-SAT could slew 30 degrees¹⁸ (similar to OS1) to collect more satellite imagery from another target AOI to further expand the existing image database. This leads to an increase in the volume of satellite imagery collected and thereby enhances the value of the operations through a higher utilization of the mission window period.

The increase in imaging time is assumed to be directly proportional to the volume of images collected. In order to present the BCA of X-SAT imaging operations in OS2 more accurately and provide a more comprehensive analysis of the economic benefits for each collection route permutations, the total imaging time available for image collection, was multiplied to the benefit scores (shown earlier in Table 10), to derive the respective Economic Benefit Score (EBS) for all 24 permutations of the collection route. The results are presented in Table 11.

¹⁸ Based on the original slew performance of 1 degree per second for X-SAT, slew time for X-SAT to the additional target AOI will take 30 seconds. With an improvement of 50% in slewing rate, it was assumed that X-SAT will take only 15 seconds to maneuver to the additional target AOI.

Table 11. Computed Economic Benefit Score for All Collection Route Permutations in OS2

Route	Benefit Score	X-SAT Slew Performance	Total Imaging Time	Economic Benefit Score	Route	Benefit Score	X-SAT Slew Performance	Total Imaging Time	Economic Benefit Score
Route_1	1	Original	282	281.79	Route_13	1	Original	274	274.20
	0.896	50% Improvement	366	327.87		0.962	50% Improvement	361	347.47
Route_2	0.973	Original	278	270.18	Route_14	0.971	Original	290	281.63
	0.935	50% Improvement	361	337.68		0.99	50% Improvement	364	360.46
Route_3	0.974	Original	290	282.79	Route_15	0.996	Original	277	275.64
	0.936	50% Improvement	367	343.46		0.969	50% Improvement	363	351.37
Route_4	0.996	Original	274	273.27	Route_16	0.974	Original	280	272.44
	0.902	50% Improvement	361	325.83		0.991	50% Improvement	360	356.68
Route_5	0.969	Original	272	263.03	Route_17	0.967	Original	292	282.28
	0.952	50% Improvement	356	338.99		0.997	50% Improvement	364	362.38
Route_6	0.974	Original	292	284.41	Route_18	0.974	Original	278	270.21
	0.945	50% Improvement	367	346.58		0.99	50% Improvement	358	354.42
Route_7	0.945	Original	314	296.40	Route_19	0.96	Original	288	276.77
	0.985	50% Improvement	377	371.90		0.957	50% Improvement	366	350.74
Route_8	0.972	Original	283	275.48	Route_20	0.961	Original	307	294.62
	0.943	50% Improvement	363	342.33		0.942	50% Improvement	374	352.20
Route_9	0.973	Original	308	299.85	Route_21	0.956	Original	273	261.30
	0.957	50% Improvement	378	361.47		0.974	50% Improvement	357	348.01
Route_10	0.972	Original	293	285.02	Route_22	0.934	Original	310	289.83
	0.944	50% Improvement	369	348.17		0.993	50% Improvement	374	371.58
Route_11	0.973	Original	291	283.25	Route_23	0.957	Original	290	278.01
	0.966	50% Improvement	367	354.87		0.948	50% Improvement	363	344.34
Route_12	0.945	Original	307	289.93	Route_24	0.934	Original	307	286.43
	0.993	50% Improvement	373	370.79		0.986	50% Improvement	372	366.73

From the EBS tabulated, the BCA showed that the integration of time-optimal maneuvers to X-SAT imaging operations in OS2 increases the overall

economic ROI value across all 24 collection route permutations in accordance to X-SAT mission goals, ranging from 16% to 33%. If the EBS is included as another performance metric in the AHP hierarchy model for analyzing imaging satellite operations in future scenarios, the best-value collection route permutation might not be Route_17 and will likely change depending on the image collection requirements.

In the adoption of the AHP hierarchy model coupled with analyzing the opportunity for additional AOI image collection, the BCA has also put forward a framework that can rationalize and quantify the economic value of each collection route permutation for different scenarios with or without the incorporation of time-optimal maneuver strategies to X-SAT image collection operations in OS2.

VII. CONCLUSION AND FUTURE WORK

A. CONCLUSION

The impact of integrating time-optimal maneuver strategies to the Singapore-developed X-SAT image collection operations in the Southeast Asia region was examined in this thesis. The operational benefits that could potentially enhance the value of the set of imaging operations and contribute to the overall mission effectiveness were analyzed and presented for two operational scenarios. In the results obtained from conducting an operational analysis of OS1, the value of the image collection operations was enhanced with time-optimal maneuver strategies. It was concluded that the implementation of time-optimal maneuvers to X-SAT image collection operations in OS1 provided the following benefits:

- a. Higher utilization of mission window for image collection,
- b. Higher volume of satellite imagery collected,
- c. Potential expansion of the imagery database with image collection of additional AOIs outside of original mission requirements,
- d. Improved resolution of satellite imagery data collected and
- e. Opportunities for additional in-track stereo image collection activities.

To further substantiate and quantify the value of the operational benefits, this thesis also presented an AHP-based framework that could be applied to determine the ideal collection route in imaging spacecraft operations. Under this framework and the assumptions made, an AHP Hierarchy Model which could be customized to fit different mission objectives and image collection requirements was also proposed for a comprehensive and strategic BCA of imaging satellite operations.

The proposed AHP Hierarchy model was subsequently applied to analyze X-SAT image collection operations in OS2. Of note, the AHP analysis showed

that the ideal collection route changed with the integration of time-optimal maneuvers. This change can be attributed to the improvement in X-SAT slew agility which has a direct impact on the imaging satellite's operations such that the value of the set of imaging operations can be significantly altered, thus leading to a revised collection route. Besides determining the best collection route, the AHP analysis also gives the respective benefit scores, which provide a way to quantify the operational advantages or disadvantages that one collection route has over the others.

The initial benefit score comparison for quantifying the quality of image collection between X-SAT original slew and X-SAT slew with 50% improvement suggested that an improvement in X-SAT's slew performance may not necessarily improve the quality of image collected across all 24 permutations of the collection routes. However, the subsequent BCA conducted based on the tabulated EBS demonstrated that the integration of time-optimal maneuvers to X-SAT imaging operations in OS2 will increase the overall economic ROI value across all 24 collection route permutations.

This thesis has demonstrated the advantages of implementing time-optimal maneuvers on a real world imaging satellite in the context of a typical operational scenario. Through the establishment and application of an AHP hierarchy model for data analysis, the findings presented herein suggested that time-optimal maneuvers appear to be a worthwhile investment and one that can enhance the value of imaging operations and provide additional revenue for satellite operators

B. FUTURE WORK

Given the flexibility of the proposed AHP hierarchy model applied to imaging satellite operations, the structure and composition of the hierarchy model are not limited to the performance elements presented in this thesis. The performance measurement elements used in the analysis of the two operational scenarios are by no means the only relevant or suitable factors by which satellite

imagery collection missions may be measured. Depending on the mission goals, the proposed hierarchy model can certainly be customized to suit different image collection missions and provide a more accurate BCA of the range of collection route operations feasible for future operational scenarios.

Future work should be undertaken to explore the extraction of more relevant data from STK simulations of different operational scenarios and apply the proposed AHP hierarchy model to these data for analysis. The flexible and methodical AHP-based framework proposed in this report can also be extended to other imaging satellite scenarios in order to analyze relevant data in a fair, logical and consistent manner.

THIS PAGE INTENTIONALLY LEFT BLANK

APPENDIX A. STK DATA AND BENEFIT SCORES FOR BASELINE SLEW PERFORMANCE

S/N	Collection Order(1st, 2nd, 3rd, 4th, 5th)--->			
1	Hanoi	Manila	Bandar	Singapore
Satellite Access Time (sec)	67	77	79	74
Imaging Time (sec)	57	67	69	64
Avg. Elevation Angle (deg)	40.36	47.18	52.56	46.79
2	Hanoi	Bandar	Manila	Singapore
Satellite Access Time (sec)	68	78	76	70
Imaging Time (sec)	58	68	66	60
Avg. Elevation Angle (deg)	40.39	35.54	41.17	46.99
3	Manila	Bandar	Hanoi	Singapore
Satellite Access Time (sec)	75	85	74	71
Imaging Time (sec)	65	75	64	61
Avg. Elevation Angle (deg)	38.63	35.02	35.18	46.89
4	Manila	Hanoi	Bandar	Singapore
Satellite Access Time (sec)	67	73	75	74
Imaging Time (sec)	57	63	65	64
Avg. Elevation Angle (deg)	38.26	42.79	52.95	46.79
5	Bandar	Hanoi	Manila	Singapore
Satellite Access Time (sec)	68	76	73	70
Imaging Time (sec)	58	66	63	60
Avg. Elevation Angle (deg)	29.30	42.77	41.03	46.99
6	Bandar	Manila	Hanoi	Singapore
Satellite Access Time (sec)	74	87	75	71
Imaging Time (sec)	64	77	65	61
Avg. Elevation Angle (deg)	29.40	46.84	35.21	46.89
7	Singapore	Bandar	Manila	Hanoi
Satellite Access Time (sec)	81	92	81	74
Imaging Time (sec)	71	82	71	64
Avg. Elevation Angle (deg)	27.73	35.02	40.94	29.78
8	Singapore	Manila	Bandar	Hanoi
Satellite Access Time (sec)	69	80	78	71
Imaging Time (sec)	59	70	68	61
Avg. Elevation Angle (deg)	27.68	47.11	52.46	29.73

9	Manila	Bandar	Singapore	Hanoi
Satellite Access Time (sec)	75	93	83	71
Imaging Time (sec)	65	83	73	61
Avg. Elevation Angle (deg)	38.63	35.40	35.19	29.75
10	Manila	Singapore	Bandar	Hanoi
Satellite Access Time (sec)	69	84	83	71
Imaging Time (sec)	59	74	73	61
Avg. Elevation Angle (deg)	38.40	29.52	52.09	29.73
11	Bandar	Manila	Singapore	Hanoi
Satellite Access Time (sec)	74	86	75	71
Imaging Time (sec)	64	76	65	61
Avg. Elevation Angle (deg)	29.40	46.83	35.50	29.75
12	Bandar	Singapore	Manila	Hanoi
Satellite Access Time (sec)	82	89	77	74
Imaging Time (sec)	72	79	67	64
Avg. Elevation Angle (deg)	29.53	29.26	40.75	29.78
13	Hanoi	Manila	Singapore	Bandar
Satellite Access Time (sec)	67	73	75	76
Imaging Time (sec)	57	63	65	66
Avg. Elevation Angle (deg)	40.36	47.17	35.54	59.25
14	Hanoi	Singapore	Manila	Bandar
Satellite Access Time (sec)	70	79	81	77
Imaging Time (sec)	60	69	71	67
Avg. Elevation Angle (deg)	40.48	29.37	40.57	59.31
15	Manila	Hanoi	Singapore	Bandar
Satellite Access Time (sec)	67	74	77	76
Imaging Time (sec)	57	64	67	66
Avg. Elevation Angle (deg)	38.26	42.76	35.47	59.25
16	Manila	Singapore	Hanoi	Bandar
Satellite Access Time (sec)	69	78	76	73
Imaging Time (sec)	59	68	66	63
Avg. Elevation Angle (deg)	38.40	29.42	35.21	59.12
17	Singapore	Hanoi	Manila	Bandar
Satellite Access Time (sec)	70	81	81	77
Imaging Time (sec)	60	71	71	67
Avg. Elevation Angle (deg)	27.69	42.83	40.62	59.31
18	Singapore	Manila	Hanoi	Bandar
Satellite Access Time (sec)	69	77	75	73

Imaging Time	59	67	65	63
Avg. Elevation Angle (deg)	27.68	47.10	35.18	59.12
19	Hanoi	Bandar	Singapore	Manila
Satellite Access Time (sec)	68	83	81	70
Imaging Time (sec)	58	73	71	60
Avg. Elevation Angle (deg)	40.39	35.78	35.11	32.10
20	Hanoi	Singapore	Bandar	Manila
Satellite Access Time (sec)	70	87	89	74
Imaging Time (sec)	60	77	79	64
Avg. Elevation Angle (deg)	40.48	29.48	52.68	32.23
21	Bandar	Hanoi	Singapore	Manila
Satellite Access Time (sec)	68	76	74	70
Imaging Time (sec)	58	66	64	60
Avg. Elevation Angle (deg)	29.30	42.77	35.35	32.10
22	Bandar	Singapore	Hanoi	Manila
Satellite Access Time (sec)	82	90	78	74
Imaging Time (sec)	72	80	68	64
Avg. Elevation Angle (deg)	29.53	29.28	35.15	32.23
23	Singapore	Hanoi	Bandar	Manila
Satellite Access Time (sec)	70	80	80	74
Imaging Time (sec)	60	70	70	64
Avg. Elevation Angle (deg)	27.69	42.86	53.44	32.23
24	Singapore	Bandar	Hanoi	Manila
Satellite Access Time (sec)	81	89	77	74
Imaging Time (sec)	71	79	67	64
Avg. Elevation Angle (deg)	27.73	34.88	35.09	32.23

Route	Parameter	Bandar Imaging Time	Bandar Avg Elev Angle	Hanoi Imaging Time	Hanoi Avg Elev Angle	Manila Imaging Time	Manila Avg Elev Angle	Singapore Imaging Time	Singapore Avg Elev Angle	Benefit Score
	Weight	0.125	0.125	0.125	0.125	0.125	0.125	0.125	0.125	
Route_1	Raw data	69	52.56	57	40.36	67	47.18	64	46.79	0.891
	Normalized data	0.8352	0.88619	0.80488	0.94174	0.868	1	0.79415	0.99572	
	Weighted Score	0.1044	0.11077	0.10061	0.11772	0.1085	0.125	0.09927	0.12447	
Route_2	Raw data	68	35.54	58	40.39	66	41.17	60	46.99	0.833
	Normalized data	0.8215	0.5991	0.81916	0.94247	0.8659	0.8726	0.74549	1	
	Weighted Score	0.1027	0.07489	0.10239	0.11781	0.1082	0.1091	0.09319	0.125	
Route_3	Raw data	75	35.02	64	35.18	65	38.63	61	46.89	0.831
	Normalized data	0.901	0.59039	0.9096	0.82084	0.8445	0.8188	0.76426	0.99788	
	Weighted Score	0.1126	0.0738	0.1137	0.10261	0.1056	0.1024	0.09553	0.12474	
Route_4	Raw data	65	52.95	63	42.79	57	38.26	64	46.79	0.864
	Normalized data	0.7861	0.89263	0.89531	0.9984	0.7413	0.8111	0.79415	0.99572	
	Weighted Score	0.0983	0.11158	0.11191	0.1248	0.0927	0.1014	0.09927	0.12447	
Route_5	Raw data	58	29.30	66	42.77	63	41.03	60	46.99	0.819
	Normalized data	0.6932	0.49396	0.93218	0.99812	0.8214	0.8696	0.74549	1	
	Weighted Score	0.0866	0.06174	0.11652	0.12477	0.1027	0.1087	0.09319	0.125	
Route_6	Raw data	64	29.40	65	35.21	77	46.84	61	46.89	0.845
	Normalized data	0.7686	0.4956	0.91914	0.82162	1	0.9929	0.76426	0.99788	
	Weighted Score	0.0961	0.06195	0.11489	0.1027	0.125	0.1241	0.09553	0.12474	
Route_7	Raw data	82	35.02	64	29.78	71	40.94	71	27.73	0.805
	Normalized data	0.9864	0.59035	0.89863	0.69487	0.9225	0.8678	0.88614	0.59015	
	Weighted Score	0.1233	0.07379	0.11233	0.08686	0.1153	0.1085	0.11077	0.07377	
Route_8	Raw data	68	52.46	61	29.73	70	47.11	59	27.68	0.81
	Normalized data	0.8213	0.88451	0.85693	0.69374	0.9068	0.9985	0.7317	0.58915	
	Weighted Score	0.1027	0.11056	0.10712	0.08672	0.1134	0.1248	0.09146	0.07364	
Route_9	Raw data	83	35.40	61	29.75	65	38.63	73	35.19	0.81
	Normalized data	1	0.59686	0.86281	0.69411	0.8445	0.8188	0.91248	0.74894	
	Weighted Score	0.125	0.07461	0.10785	0.08676	0.1056	0.1024	0.11406	0.09362	
Route_10	Raw data	73	52.09	61	29.73	59	38.40	74	29.52	0.806
	Normalized data	0.8759	0.87813	0.85693	0.69374	0.7736	0.814	0.92455	0.62811	

	Weighted Score	0.1095	0.10977	0.10712	0.08672	0.0967	0.1017	0.11557	0.07851	
Route_11	Raw data	64	29.40	61	29.75	76	46.83	65	35.50	0.795
	Normalized data	0.7686	0.4956	0.86281	0.69411	0.9863	0.9928	0.80407	0.75553	
	Weighted Score	0.0961	0.06195	0.10785	0.08676	0.1233	0.1241	0.10051	0.09444	
Route_12	Raw data	72	29.53	64	29.78	67	40.75	79	29.26	0.787
	Normalized data	0.8606	0.49789	0.89863	0.69487	0.8701	0.8639	0.98384	0.62275	
	Weighted Score	0.1076	0.06224	0.11233	0.08686	0.1088	0.108	0.12298	0.07784	
Route_13	Raw data	66	59.25	57	40.36	63	47.17	65	35.54	0.866
	Normalized data	0.79	0.99892	0.80488	0.94174	0.8231	0.9999	0.81416	0.75642	
	Weighted Score	0.0988	0.12487	0.10061	0.11772	0.1029	0.125	0.10177	0.09455	
Route_14	Raw data	67	59.31	60	40.48	71	40.57	69	29.37	0.859
	Normalized data	0.8033	1	0.85269	0.94462	0.9197	0.86	0.86401	0.62495	
	Weighted Score	0.1004	0.125	0.10659	0.11808	0.115	0.1075	0.108	0.07812	
Route_15	Raw data	66	59.25	64	42.76	57	38.26	67	35.47	0.854
	Normalized data	0.79	0.99892	0.90983	0.99783	0.7413	0.8111	0.83208	0.75493	
	Weighted Score	0.0988	0.12487	0.11373	0.12473	0.0927	0.1014	0.10401	0.09437	
Route_16	Raw data	63	59.12	66	35.21	59	38.40	68	29.42	0.822
	Normalized data	0.7614	0.99669	0.93684	0.82171	0.7736	0.814	0.84483	0.62605	
	Weighted Score	0.0952	0.12459	0.11711	0.10271	0.0967	0.1017	0.1056	0.07826	
Route_17	Raw data	67	59.31	71	42.83	71	40.62	60	27.69	0.866
	Normalized data	0.8033	1	1	0.99945	0.9276	0.861	0.748	0.58929	
	Weighted Score	0.1004	0.125	0.125	0.12493	0.116	0.1076	0.0935	0.07366	
Route_18	Raw data	63	59.12	65	35.18	67	47.10	59	27.68	0.837
	Normalized data	0.7614	0.99669	0.92227	0.82093	0.8756	0.9984	0.7317	0.58915	
	Weighted Score	0.0952	0.12459	0.11528	0.10262	0.1095	0.1248	0.09146	0.07364	
Route_19	Raw data	73	35.78	58	40.39	60	32.10	71	35.11	0.792
	Normalized data	0.8823	0.60329	0.81916	0.94247	0.7762	0.6803	0.88763	0.7472	
	Weighted Score	0.1103	0.07541	0.10239	0.11781	0.097	0.085	0.11095	0.0934	
Route_20	Raw data	79	52.68	60	40.48	64	32.23	77	29.48	0.843
	Normalized data	0.9498	0.88808	0.85269	0.94462	0.837	0.6833	0.9599	0.62733	
	Weighted Score	0.1187	0.11101	0.10659	0.11808	0.1046	0.0854	0.11999	0.07842	
Route_21	Raw data	58	29.30	66	42.77	60	32.10	64	35.35	0.766
	Normalized data	0.6932	0.49396	0.93277	0.99812	0.7762	0.6803	0.79714	0.75229	

	Weighted Score	0.0866	0.06174	0.1166	0.12477	0.097	0.085	0.09964	0.09404	
Route_22	Raw data	72	29.53	68	35.15	64	32.23	80	29.28	0.786
	Normalized data	0.8606	0.49789	0.96773	0.82031	0.8324	0.6833	1	0.62307	
	Weighted Score	0.1076	0.06224	0.12097	0.10254	0.1041	0.0854	0.125	0.07788	
Route_23	Raw data	70	53.44	70	42.86	64	32.23	60	27.69	0.824
	Normalized data	0.8461	0.90093	0.98609	1	0.837	0.6833	0.748	0.58929	
	Weighted Score	0.1058	0.11262	0.12326	0.125	0.1046	0.0854	0.0935	0.07366	
Route_24	Raw data	79	34.88	67	35.09	64	32.23	71	27.73	0.786
	Normalized data	0.9482	0.58799	0.94361	0.81875	0.8324	0.6833	0.88614	0.59015	
	Weighted Score	0.1185	0.0735	0.11795	0.10234	0.1041	0.0854	0.11077	0.07377	

APPENDIX B. STK DATA AND BENEFIT SCORES FOR 50% IMPROVEMENT IN SLEW PERFORMANCE

S/N	Collection Order(1st, 2nd, 3rd, 4th, 5th)--->			
1	Hanoi	Manila	Bandar	Singapore
Satellite Access Time (sec)	64	69	72	70
Imaging Time (sec)	54	59	62	60
Avg. Elevation Angle (deg)	40.26	45.84	42.29	37.84
2	Hanoi	Bandar	Manila	Singapore
Satellite Access Time (sec)	64	70	69	67
Imaging Time (sec)	54	60	59	57
Avg. Elevation Angle (deg)	40.29	33.21	46.09	37.97
3	Manila	Bandar	Hanoi	Singapore
Satellite Access Time (sec)	68	73	67	68
Imaging Time (sec)	58	63	57	58
Avg. Elevation Angle (deg)	38.35	32.99	39.33	37.97
4	Manila	Hanoi	Bandar	Singapore
Satellite Access Time (sec)	64	67	70	70
Imaging Time (sec)	54	57	60	60
Avg. Elevation Angle (deg)	38.13	43.49	42.49	37.84
5	Bandar	Hanoi	Manila	Singapore
Satellite Access Time (sec)	64	68	66	67
Imaging Time (sec)	54	58	56	57
Avg. Elevation Angle (deg)	29.25	43.49	46.02	37.97
6	Bandar	Manila	Hanoi	Singapore
Satellite Access Time (sec)	68	73	67	68
Imaging Time (sec)	58	63	57	58
Avg. Elevation Angle (deg)	29.31	45.55	39.33	37.97
7	Singapore	Bandar	Manila	Hanoi
Satellite Access Time (sec)	71	77	70	68
Imaging Time (sec)	61	67	60	58
Avg. Elevation Angle (deg)	27.69	33.00	46.01	33.41
8	Singapore	Manila	Bandar	Hanoi
Satellite Access Time (sec)	65	71	69	67
Imaging Time (sec)	55	61	59	57
Avg. Elevation Angle (deg)	27.67	45.76	42.06	33.41

9	Manila	Bandar	Singapore	Hanoi
Satellite Access Time (sec)	68	78	73	68
Imaging Time (sec)	58	68	63	58
Avg. Elevation Angle (deg)	38.35	33.17	31.61	33.41
10	Manila	Singapore	Bandar	Hanoi
Satellite Access Time (sec)	65	74	72	67
Imaging Time (sec)	55	64	62	57
Avg. Elevation Angle (deg)	38.22	28.75	41.93	33.41
11	Bandar	Manila	Singapore	Hanoi
Satellite Access Time (sec)	68	73	67	68
Imaging Time (sec)	58	63	57	58
Avg. Elevation Angle (deg)	29.31	45.55	31.71	33.41
12	Bandar	Singapore	Manila	Hanoi
Satellite Access Time (sec)	71	75	68	68
Imaging Time (sec)	61	65	58	58
Avg. Elevation Angle (deg)	29.36	28.64	45.94	33.41
13	Hanoi	Manila	Singapore	Bandar
Satellite Access Time (sec)	64	67	70	72
Imaging Time (sec)	54	57	60	62
Avg. Elevation Angle (deg)	40.26	45.79	31.77	58.35
14	Hanoi	Singapore	Manila	Bandar
Satellite Access Time (sec)	66	70	69	70
Imaging Time (sec)	56	60	59	60
Avg. Elevation Angle (deg)	40.33	28.69	45.94	58.55
15	Manila	Hanoi	Singapore	Bandar
Satellite Access Time (sec)	64	68	70	72
Imaging Time (sec)	54	58	60	62
Avg. Elevation Angle (deg)	38.13	43.48	31.75	58.35
16	Manila	Singapore	Hanoi	Bandar
Satellite Access Time (sec)	65	69	68	69
Imaging Time (sec)	55	59	58	59
Avg. Elevation Angle (deg)	38.22	28.71	39.37	58.65
17	Singapore	Hanoi	Manila	Bandar
Satellite Access Time (sec)	66	70	68	70
Imaging Time (sec)	56	60	58	60
Avg. Elevation Angle (deg)	27.67	43.48	45.94	58.55
18	Singapore	Manila	Hanoi	Bandar
Satellite Access Time (sec)	65	69	67	69

Imaging Time (sec)	55	59	57	59
Avg. Elevation Angle (deg)	27.67	45.71	39.33	58.65
19	Hanoi	Bandar	Singapore	Manila
Satellite Access Time (sec)	64	73	72	67
Imaging Time (sec)	54	63	62	57
Avg. Elevation Angle (deg)	40.29	33.32	31.58	38.13
20	Hanoi	Singapore	Bandar	Manila
Satellite Access Time (sec)	66	75	74	69
Imaging Time (sec)	56	65	64	59
Avg. Elevation Angle (deg)	40.33	28.74	42.01	38.22
21	Bandar	Hanoi	Singapore	Manila
Satellite Access Time (sec)	64	69	67	67
Imaging Time (sec)	54	59	57	57
Avg. Elevation Angle (deg)	29.25	43.48	31.67	38.13
22	Bandar	Singapore	Hanoi	Manila
Satellite Access Time (sec)	71	76	69	68
Imaging Time (sec)	61	66	59	58
Avg. Elevation Angle (deg)	29.36	28.65	39.33	38.22
23	Singapore	Hanoi	Bandar	Manila
Satellite Access Time (sec)	66	70	68	69
Imaging Time (sec)	56	60	58	59
Avg. Elevation Angle (deg)	27.67	43.48	42.33	38.22
24	Singapore	Bandar	Hanoi	Manila
Satellite Access Time (sec)	71	75	68	68
Imaging Time (sec)	61	65	58	58
Avg. Elevation Angle (deg)	27.69	32.93	39.30	38.22

Route	Parameter	Bandar Imaging Time	Bandar Avg Elev Angle	Hanoi Imaging Time	Hanoi Avg Elev Angle	Manila Imaging Time	Manila Avg Elev Angle	Singapore Imaging Time	Singapore Avg Elev Angle	Benefit Score
	Weight	0.125	0.125	0.125	0.125	0.125	0.125	0.125	0.125	
Route _1	Raw data	62	42.29	54	40.26	59	45.84	60	37.84	0.912
	Normalized data	0.9123	0.7211 4	0.89143	0.9258 1	0.9385	0.9946	0.9145	0.99661	
	Weighted Score	0.114	0.0901 4	0.11143	0.1157 3	0.1173	0.1243	0.11431	0.12458	
Route _2	Raw data	60	33.21	54	40.29	59	46.09	57	37.97	0.885
	Normalized data	0.8801	0.5662	0.90281	0.9265 4	0.9374	1	0.86391	1	
	Weighted Score	0.11	0.0707 7	0.11285	0.1158 2	0.1172	0.125	0.10799	0.125	
Route _3	Raw data	63	32.99	57	39.33	58	38.35	58	37.97	0.872
	Normalized data	0.9221	0.5624 8	0.94998	0.9044 5	0.9266	0.8322	0.87495	1	
	Weighted Score	0.1153	0.0703 1	0.11875	0.1130 6	0.1158	0.104	0.10937	0.125	
Route _4	Raw data	60	42.49	57	43.49	54	38.13	60	37.84	0.892
	Normalized data	0.8739	0.7244 9	0.94729	1	0.8506	0.8273	0.9145	0.99663	
	Weighted Score	0.1092	0.0905 6	0.11841	0.125	0.1063	0.1034	0.11431	0.12458	
Route _5	Raw data	54	29.25	58	43.49	56	46.02	57	37.97	0.877
	Normalized data	0.7951	0.4987 9	0.96241	1	0.8944	0.9984	0.86391	1	
	Weighted Score	0.0994	0.0623 5	0.1203	0.125	0.1118	0.1248	0.10799	0.125	
Route _6	Raw data	58	29.31	57	39.33	63	45.55	58	37.97	0.884
	Normalized data	0.8539	0.4998 6	0.9491	0.9044 5	1	0.9883	0.87495	1	
	Weighted Score	0.1067	0.0624 8	0.11864	0.1130 6	0.125	0.1235	0.10937	0.125	
Route _7	Raw data	67	33.00	58	33.41	60	46.01	61	27.69	0.862
	Normalized data	0.9846	0.5627 4	0.96408	0.7681 9	0.9551	0.9984	0.93048	0.72941	
	Weighted Score	0.1231	0.0703 4	0.12051	0.0960 2	0.1194	0.1248	0.11631	0.09118	
Route _8	Raw data	59	42.06	57	33.41	61	45.76	55	27.67	0.853
	Normalized data	0.8701	0.7171 4	0.95022	0.7681 7	0.9638	0.9929	0.83326	0.72882	
	Weighted Score	0.1088	0.0896 4	0.11878	0.0960 2	0.1205	0.1241	0.10416	0.0911	
Route _9	Raw data	68	33.17	58	33.41	58	38.35	63	31.61	0.854
	Normalized data	1	0.5656	0.9596	0.7681 8	0.9266	0.8322	0.95008	0.83244	
	Weighted Score	0.125	0.0707	0.11995	0.0960 2	0.1158	0.104	0.11876	0.10406	
Route _10	Raw data	62	41.93	57	33.41	55	38.22	64	28.75	0.847
	Normalized data	0.9103	0.7149 3	0.95022	0.7681 7	0.874	0.8292	0.96894	0.75732	

	Weighted Score	0.1138	0.08937	0.11878	0.09602	0.1093	0.1037	0.12112	0.09467	
Route_11	Raw data	58	29.31	58	33.41	63	45.55	57	31.71	0.847
	Normalized data	0.8539	0.49986	0.9596	0.76818	1	0.9883	0.87219	0.83531	
	Weighted Score	0.1067	0.06248	0.11995	0.09602	0.125	0.1235	0.10902	0.10441	
Route_12	Raw data	61	29.36	58	33.41	58	45.94	65	28.64	0.849
	Normalized data	0.9007	0.50068	0.96408	0.76819	0.9174	0.9968	0.99033	0.75442	
	Weighted Score	0.1126	0.06259	0.12051	0.09602	0.1147	0.1246	0.12379	0.0943	
Route_13	Raw data	62	58.35	54	40.26	57	45.79	60	31.77	0.921
	Normalized data	0.9074	0.995	0.89143	0.92581	0.9079	0.9935	0.90681	0.83673	
	Weighted Score	0.1134	0.12438	0.11143	0.11573	0.1135	0.1242	0.11335	0.10459	
Route_14	Raw data	60	58.55	56	40.33	59	45.94	60	28.69	0.917
	Normalized data	0.887	0.9983	0.92895	0.92728	0.9312	0.9968	0.91399	0.75554	
	Weighted Score	0.1109	0.12479	0.11612	0.11591	0.1164	0.1246	0.11425	0.09444	
Route_15	Raw data	62	58.35	58	43.48	54	38.13	60	31.75	0.912
	Normalized data	0.9074	0.995	0.96068	0.99977	0.8506	0.8273	0.91812	0.83615	
	Weighted Score	0.1134	0.12438	0.12009	0.12497	0.1063	0.1034	0.11476	0.10452	
Route_16	Raw data	59	58.65	58	39.37	55	38.22	59	28.71	0.886
	Normalized data	0.8623	1	0.9608	0.90525	0.874	0.8292	0.90293	0.75607	
	Weighted Score	0.1078	0.125	0.1201	0.11316	0.1093	0.1037	0.11287	0.09451	
Route_17	Raw data	60	58.55	60	43.48	58	45.94	56	27.67	0.923
	Normalized data	0.887	0.9983	1	0.99972	0.9259	0.9968	0.8468	0.7289	
	Weighted Score	0.1109	0.12479	0.125	0.12497	0.1157	0.1246	0.10585	0.09111	
Route_18	Raw data	59	58.65	57	39.33	59	45.71	55	27.67	0.899
	Normalized data	0.8623	1	0.94193	0.90446	0.9303	0.9918	0.83326	0.72882	
	Weighted Score	0.1078	0.125	0.11774	0.11306	0.1163	0.124	0.10416	0.0911	
Route_19	Raw data	63	33.32	54	40.29	57	38.13	62	31.58	0.854
	Normalized data	0.9268	0.56811	0.90281	0.92654	0.9091	0.8274	0.93896	0.83176	
	Weighted Score	0.1158	0.07101	0.11285	0.11582	0.1136	0.1034	0.11737	0.10397	
Route_20	Raw data	64	42.01	56	40.33	59	38.22	65	28.74	0.878
	Normalized data	0.9349	0.71629	0.92895	0.92728	0.9386	0.8294	0.98966	0.75708	
	Weighted Score	0.1169	0.08954	0.11612	0.11591	0.1173	0.1037	0.12371	0.09464	
Route_21	Raw data	54	29.25	59	43.48	57	38.13	57	31.67	0.839
	Normalized data	0.7951	0.49879	0.97492	0.99969	0.9091	0.8274	0.8724	0.83404	

	Weighted Score	0.0994	0.0623 5	0.12187	0.1249 6	0.1136	0.1034	0.10905	0.10425	
Route _22	Raw data	61	29.36	59	39.33	58	38.22	66	28.65	0.849
	Normalized data	0.9007	0.5006 8	0.97499	0.9044 3	0.9256	0.8293	1	0.75471	
	Weighted Score	0.1126	0.0625 9	0.12187	0.1130 5	0.1157	0.1037	0.125	0.09434	
Route _23	Raw data	58	42.33	60	43.48	59	38.22	56	27.67	0.865
	Normalized data	0.8563	0.7218 2	1	0.9997 2	0.9386	0.8294	0.8468	0.7289	
	Weighted Score	0.107	0.0902 3	0.125	0.1249 7	0.1173	0.1037	0.10585	0.09111	
Route _24	Raw data	65	32.93	58	39.30	58	38.22	61	27.69	0.849
	Normalized data	0.9534	0.5615 2	0.95699	0.9036 4	0.9256	0.8293	0.93048	0.72941	
	Weighted Score	0.1192	0.0701 9	0.11962	0.1129 6	0.1157	0.1037	0.11631	0.09118	

APPENDIX C. BENEFIT SCORE COMPARISON BETWEEN BASELINE SLEW PERFORMANCE VERSUS 50% IMPROVEMENT IN SLEW PERFORMANCE

Route	Parameter	Bandar Avg Elev Angle	Hanoi Avg Elev Angle	Manila Avg Elev Angle	Singapore Avg Elev Angle	Benefit Score
	Weight	0.25	0.25	0.25	0.25	
Route_1	Raw data Original Slew	52.56	40.36	47.18	46.79	1
	Normalized data	1	1	1	1	
	Weighted Score	0.25	0.25	0.25	0.25	
	Raw data 50% improvement	42.29	40.26	45.84	37.84	0.896
	Normalized data	0.80458	0.99764	0.9717	0.80872	
	Weighted Score	0.20115	0.24941	0.2429	0.20218	
Route_2	Raw data Original Slew	35.54	40.39	41.17	46.99	0.973
	Normalized data	1	1	0.8932	1	
	Weighted Score	0.25	0.25	0.2233	0.25	
	Raw data 50% improvement	33.21	40.29	46.09	37.97	0.935
	Normalized data	0.93443	0.99765	1	0.808	
	Weighted Score	0.23361	0.24941	0.25	0.202	
Route_3	Raw data Original Slew	35.02	35.18	38.63	46.89	0.974
	Normalized data	1	0.89432	1	1	
	Weighted Score	0.25	0.22358	0.25	0.25	
	Raw data 50% improvement	32.99	39.33	38.35	37.97	0.936
	Normalized data	0.94199	1	0.9929	0.8097	
	Weighted Score	0.2355	0.25	0.2482	0.20242	
Route_4	Raw data Original Slew	52.95	42.79	38.26	46.79	0.996
	Normalized data	1	0.98384	1	1	
	Weighted Score	0.25	0.24596	0.25	0.25	
	Raw data 50% improvement	42.49	43.49	38.13	37.84	0.902
	Normalized data	0.80247	1	0.9964	0.80872	
	Weighted Score	0.20062	0.25	0.2491	0.20218	

Route_5	Raw data Original Slew	29.30	42.77	41.03	46.99	0.969
	Normalized data	1	0.98364	0.8916	1	
	Weighted Score	0.25	0.24591	0.2229	0.25	
	Raw data 50% improvement	29.25	43.49	46.02	37.97	0.952
	Normalized data	0.99839	1	1	0.808	
	Weighted Score	0.2496	0.25	0.25	0.202	
Route_6	Raw data Original Slew	29.40	35.21	46.84	46.89	0.974
	Normalized data	1	0.89517	1	1	
	Weighted Score	0.25	0.22379	0.25	0.25	
	Raw data 50% improvement	29.31	39.33	45.55	37.97	0.945
	Normalized data	0.99722	1	0.9724	0.8097	
	Weighted Score	0.24931	0.25	0.2431	0.20242	
Route_7	Raw data Original Slew	35.02	29.78	40.94	27.73	0.945
	Normalized data	1	0.89137	0.8897	1	
	Weighted Score	0.25	0.22284	0.2224	0.25	
	Raw data 50% improvement	33.00	33.41	46.01	27.69	0.985
	Normalized data	0.94248	1	1	0.99867	
	Weighted Score	0.23562	0.25	0.25	0.24967	
Route_8	Raw data Original Slew	52.46	29.73	47.11	27.68	0.972
	Normalized data	1	0.88994	1	1	
	Weighted Score	0.25	0.22248	0.25	0.25	
	Raw data 50% improvement	42.06	33.41	45.76	27.67	0.943
	Normalized data	0.80163	1	0.9715	0.99954	
	Weighted Score	0.20041	0.25	0.2429	0.24989	
Route_9	Raw data Original Slew	35.40	29.75	38.63	35.19	0.973
	Normalized data	1	0.8904	1	1	
	Weighted Score	0.25	0.2226	0.25	0.25	
	Raw data 50% improvement	33.17	33.41	38.35	31.61	0.957
	Normalized data	0.93693	1	0.9929	0.89809	
	Weighted Score	0.23423	0.25	0.2482	0.22452	
Route_10	Raw data Original Slew	52.09	29.73	38.40	29.52	0.972
	Normalized data	1	0.88994	1	1	

	Weighted Score	0.25	0.22248	0.25	0.25	0.944
	Raw data 50% improvement	41.93	33.41	38.22	28.75	
	Normalized data	0.80497	1	0.9952	0.9742	
	Weighted Score	0.20124	0.25	0.2488	0.24355	
Route_11	Raw data Original Slew	29.40	29.75	46.83	35.50	0.973
	Normalized data	1	0.8904	1	1	
	Weighted Score	0.25	0.2226	0.25	0.25	
	Raw data 50% improvement	29.31	33.41	45.55	31.71	0.966
	Normalized data	0.99722	1	0.9725	0.89331	
	Weighted Score	0.24931	0.25	0.2431	0.22333	
Route_12	Raw data Original Slew	29.53	29.78	40.75	29.26	0.945
	Normalized data	1	0.89137	0.8871	1	
	Weighted Score	0.25	0.22284	0.2218	0.25	
	Raw data 50% improvement	29.36	33.41	45.94	28.64	0.993
	Normalized data	0.99427	1	1	0.97883	
	Weighted Score	0.24857	0.25	0.25	0.24471	
Route_13	Raw data Original Slew	59.25	40.36	47.17	35.54	1
	Normalized data	1	1	1	1	
	Weighted Score	0.25	0.25	0.25	0.25	
	Raw data 50% improvement	58.35	40.26	45.79	31.77	0.962
	Normalized data	0.98485	0.99764	0.9707	0.89379	
	Weighted Score	0.24621	0.24941	0.2427	0.22345	
Route_14	Raw data Original Slew	59.31	40.48	40.57	29.37	0.971
	Normalized data	1	1	0.8832	1	
	Weighted Score	0.25	0.25	0.2208	0.25	
	Raw data 50% improvement	58.55	40.33	45.94	28.69	0.99
	Normalized data	0.98705	0.99617	1	0.97685	
	Weighted Score	0.24676	0.24904	0.25	0.24421	
Route_15	Raw data Original Slew	59.25	42.76	38.26	35.47	0.996
	Normalized data	1	0.9835	1	1	
	Weighted Score	0.25	0.24587	0.25	0.25	
	Raw data 50%	58.35	43.48	38.13	31.75	0.969

	improvement					
	Normalized data	0.98485	1	0.9964	0.89492	
	Weighted Score	0.24621	0.25	0.2491	0.22373	
Route_16	Raw data Original Slew	59.12	35.21	38.40	29.42	0.974
	Normalized data	1	0.89448	1	1	
	Weighted Score	0.25	0.22362	0.25	0.25	
	Raw data 50% improvement	58.65	39.37	38.22	28.71	0.991
	Normalized data	0.992	1	0.9952	0.97582	
	Weighted Score	0.248	0.25	0.2488	0.24395	
Route_17	Raw data Original Slew	59.31	42.83	40.62	27.69	0.967
	Normalized data	1	0.98515	0.8842	1	
	Weighted Score	0.25	0.24629	0.221	0.25	
	Raw data 50% improvement	58.55	43.48	45.94	27.67	0.997
	Normalized data	0.98705	1	1	0.99942	
	Weighted Score	0.24676	0.25	0.25	0.24985	
Route_18	Raw data Original Slew	59.12	35.18	47.10	27.68	0.974
	Normalized data	1	0.89441	1	1	
	Weighted Score	0.25	0.2236	0.25	0.25	
	Raw data 50% improvement	58.65	39.33	45.71	27.67	0.99
	Normalized data	0.992	1	0.9704	0.99954	
	Weighted Score	0.248	0.25	0.2426	0.24989	
Route_19	Raw data Original Slew	35.78	40.39	32.10	35.11	0.96
	Normalized data	1	1	0.8416	1	
	Weighted Score	0.25	0.25	0.2104	0.25	
	Raw data 50% improvement	33.32	40.29	38.13	31.58	0.957
	Normalized data	0.93106	0.99765	1	0.89943	
	Weighted Score	0.23277	0.24941	0.25	0.22486	
Route_20	Raw data Original Slew	52.68	40.48	32.23	29.48	0.961
	Normalized data	1	1	0.8433	1	
	Weighted Score	0.25	0.25	0.2108	0.25	
	Raw data 50% improvement	42.01	40.33	38.22	28.74	0.942
	Normalized data	0.79746	0.99617	1	0.97512	

	Weighted Score	0.19936	0.24904	0.25	0.24378	
Route_21	Raw data Original Slew	29.30	42.77	32.10	35.35	0.956
	Normalized data	1	0.98386	0.8416	1	
	Weighted Score	0.25	0.24597	0.2104	0.25	
	Raw data 50% improvement	29.25	43.48	38.13	31.67	0.974
	Normalized data	0.99839	1	1	0.8958	
	Weighted Score	0.2496	0.25	0.25	0.22395	
Route_22	Raw data Original Slew	29.53	35.15	32.23	29.28	0.934
	Normalized data	1	0.89376	0.8433	1	
	Weighted Score	0.25	0.22344	0.2108	0.25	
	Raw data 50% improvement	29.36	39.33	38.22	28.65	0.993
	Normalized data	0.99427	1	1	0.9787	
	Weighted Score	0.24857	0.25	0.25	0.24468	
Route_23	Raw data Original Slew	53.44	42.86	32.23	27.69	0.957
	Normalized data	1	0.98569	0.8433	1	
	Weighted Score	0.25	0.24642	0.2108	0.25	
	Raw data 50% improvement	42.33	43.48	38.22	27.67	0.948
	Normalized data	0.79216	1	1	0.99942	
	Weighted Score	0.19804	0.25	0.25	0.24985	
Route_24	Raw data Original Slew	34.88	35.09	32.23	27.73	0.934
	Normalized data	1	0.89284	0.8433	1	
	Weighted Score	0.25	0.22321	0.2108	0.25	
	Raw data 50% improvement	32.93	39.30	38.22	27.69	0.986
	Normalized data	0.94421	1	1	0.99867	
	Weighted Score	0.23605	0.25	0.25	0.24967	

THIS PAGE LEFT INTENTIONALLY BLANK

LIST OF REFERENCES

- [1] J. B. Campbell, *Introduction to Remote Sensing*, 3rd ed. New York, NY: The Guilford Press.
- [2] Professional Aerial Photographers Association. "History of aerial photography. [Online]. Available: <http://www.papainternational.org/history.asp>
- [3] Wikipedia. *Low earth orbit*. [Online]. Retrieved Aug 15 2012: http://en.wikipedia.org/wiki/Low_Earth_orbit
- [4] Satellite Imaging Corporation. *WorldView-2 satellite sensor information and specifications*. [Online]. Available: <http://www.satimagingcorp.com/satellite-sensors/worldview-2.html>
- [5] RapidEye. *Resources and downloads, brochures*. [Online]. Available: http://www.rapideye.com/upload/RE_Standard_Image_Products_ENG.pdf
- [6] Satellite Imaging Corporation. *Pleiades satellite imagery and satellite sensor specifications*. [Online]. Available: <http://www.satimagingcorp.com/satellite-sensors/pleiades-1.html>
- [7] H. Y. Lee, T. Kim, W. Park, and H. K. Lee, "Extraction of digital elevation models from satellite stereo images through stereo matching based on epipolarity and scene geometry," *Image and Vision Computing*, vol. 21, pp. 789–796, 2003.
- [8] NASA Jet Propulsion Laboratory. California Institute of Technology. Basics of space flight section II. [Online]. Available: <http://www2.jpl.nasa.gov/basics/bsf11-2.php#>
- [9] B. Wie, D. Bailey, and C. Heiberg, "Rapid multitarget acquisition and pointing control of agile spacecraft," *Journal of Guidance, Control and Dynamics*, vol. 25, no. 1, pp. 96–104, 2002.
- [10] B. Wie and P. M. Barba, "Quaternion feedback for spacecraft large angle maneuvers," *Journal of Guidance, Control and Dynamics*, vol. 8, no.3, pp. 360–365, 1985.
- [11] B. Wie, *Space vehicle dynamics and control*, AIAA, p. 439, 1998.
- [12] S. W. Liu and T. Singh, "Fuel/Time optimal Control of Spacecraft Manuevers," *Journal of Guidance, vol. 20, no. 2: Engineering Notes*, pp. 394–397, 1998.

- [13] K. D. Bilimoria and B. Wie, "Time-Optimal Three-Axis Reorientation of a Rigid Spacecraft," *Journal of Guidance, Control and Dynamics*, vol. 16, no. 3, pp. 446–452, 1993.
- [14] T. Carter and J. Brient, "Fuel-Optimal Rendezvous for Linearized Equations of Motion," *Journal of Guidance, Control and Dynamics*, vol. 15, no.6, pp. 1411–1416, 1992.
- [15] L. C. Lai, C. C. Yang, and C. J. Wu, "Time-Optimal Maneuvering Control of a Rigid Spacecraft," *Acta Astronautica*, vol. 60, pp. 791–800, 2007.
- [16] S. Chakravorty and J. Ramirez, "Fuel Optimal Maneuvers for Multispacecraft Interferometric Imaging Systems," *Journal of Guidance, Control, and Dynamics*, vol.30, no.1, pp. 227–236, 2007.
- [17] N. Bhushan and R. Kanwal, *Strategic Decision Making: Applying the Analytic Hierarchy Process*, UK: Springer-Verlag.
- [18] J. R. Jensen, *Remote Sensing of the Environment: An Earth Resource Perspective*, 2nd Ed. UK: Prentice Hall.
- [19] B. Yenne, *The Encyclopedia of U.S. Spacecraft*, 1st ed. New York, NY: Exeter Books.
- [20] Satellite Imaging Corporation. IKONOS satellite images and sensor specifications. [Online]. Available: <http://www.satimagingcorp.com/satellite-sensors/ikonos.html>
- [21] World Ocean Review. Pollution. [Online]. Available: <http://worldoceanreview.com/en/pollution/>
- [22] C. Brekke and A. H.S. Solberg, "Oil Spill Detection by Satellite Remote Sensing," *Remote Sensing of Environment*, vol. 95, pp. 1–13, 2005.
- [23] NASA Earth Observatory, Natural hazards, images. [Online]. Available: <http://earthobservatory.nasa.gov/NaturalHazards/view.php?id=44070>
- [24] Geoscience Australia, "Shallow Water Bathymetry in the Asia Pacific Region using Remote Sensing." [Online]. Available: http://www.aprsaf.org/data/aprsaf17_data/Day1-eo_11_S_Sagar_1550.pdf
- [25] California State University. Coastal programs and assets. Sea floor mapping. [Online]. Available: <http://www.calstate.edu/coast//programs-assets/seafloor.shtml>

- [26] Environment America Research & Policy Center, "Global warming and extreme weather. *The Science, the Forecast and the impacts on America*, Sep 2010. [Online]. Available: http://www.environmentamerica.org/sites/environment/files/reports/Global-Warming-and-Extreme-Weather_1.pdf
- [27] NASA Mission: Science. Tour of the electromagnetic spectrum. Microwaves. [Online]. Available: http://missionscience.nasa.gov/ems/06_microwaves.html
- [28] M. D. Nellis, K. P. Price, and D. Rundquist, "Remote sensing of cropland agriculture," *DigitalCommons@University of Nebraska-Lincoln*, 2009.
- [29] L. Bruzzone and P. Smits, "Analysis of multi-temporal remote sensing images," *Proc. 1st Int. Workshop on Multitemp 2001*, 2002.
- [30] J. Dong, X. Xiao, S. Sheldon, C. Biradar, N. D. Duong, and M. Hazarika, "A Comparison of forest cover maps in mainland southeast asia from multiple sources: PALSAR, MERIS, MODIS and FRA," *Remote Sensing of Environment*, vol. 127, pp. 60–73, 2012.
- [31] European Space Agency. Disaster monitoring. [Online]. Available: http://www.esa.int/SPECIALS/Eduspace_Environment_EN/SEMGJTANJT_F_0.html
- [32] Coordinates. Smart solutions for disaster management. [Online]. Available: <http://mycoordinates.org/wp-content/uploads/2013/01/fig-211.jpg>
- [33] Wikipedia. Gulf war. [Online]. Available: http://en.wikipedia.org/wiki/Gulf_War
- [34] MAJ E. D. Matthews, USAF, "U.S. space systems: A critical strength and vulnerability," 1996. Available: <http://www.hsdl.org/?view&did=450639>
- [35] T. R. Henry, F. A. Kilpatrick, and J. M. Skinner, "Space image acquisition and processing architecture," *Aerospace Conf., 1998 IEEE*, vol. 2, pp. 165–172, 1998.
- [36] CPT J. A. Hartmetz, USAF, "Eagle Vision—Exploiting commercial satellite imagery," *DISAM Journal*, 2001. [Online]. Available: http://www.disam.dsca.mil/pubs/v.23_4/hartmetz.pdf
- [37] C. Voorhees, "ORS-1 Imaging satellite scheduled for liftoff," 2011, DoDlive.mil. [Online]. Available: <http://science.DoDlive.mil/2011/06/28/ors-1-imaging-satellite-scheduled-for-liftoff/>

- [38] Satellite Imaging Corporation. Characterization of satellite remote sensing systems. [Online]. Available: <http://www.satimagingcorp.com/characterization-of-satellite-remote-sensing-systems.html>
- [39] The Joy of visual perception. Physics of the visual stimulus. Electromagnetic spectrum. [Online]. Available: <http://www.yorku.ca/eye/spectru.htm>
- [40] R.C. Olsen, *Remote Sensing from Air and Space*. Bellingham, WA: SPIE Press.
- [41] LANDinfo Worldwide Mapping LLC. "Buying optical satellite imagery: Top 10 things to consider." [Online]. Available: <http://www.landinfo.com/buying-optical-satellite-imagery.html>
- [42] NASA Landsat 7. [Online]. Available: http://landsathandbook.gsfc.nasa.gov/data_properties/prog_sect6_3.html
- [43] W. Martin, "Satellite image collection optimization," *Lockheed Martin Space Systems Company*, 2002.
- [44] C. Clark, Dr. K. Worrall, and E. Yavuzoglu, "A Control moment gyroscope for dynamic attitude control of small satellites," *24th Annual AIAA/USU Conf. on Small Satellites*, 2010.
- [45] NASA Office of the Chief Technologist. NASA spinoff—reaction/momentum wheel. [Online]. Available: <http://spinoff.nasa.gov/spinoff1997/t3.html>
- [46] MAJ W. S. Bell, USAF, "Commercial eyes in space: implications for u.s. military operations in 2030," *Blue Horizons Paper*, Air War College, 2008.
- [47] A. Fleming, P. Sekhavat, and I. M. Ross, "Minimum-time reorientation of a rigid body," *Journal of Guidance, Control and Dynamics*, vol. 33, no. 1, pp. 160–170, 2010.
- [48] R. Proulx and I. M. Ross, "Time-optimal reorientation of asymmetric rigid bodies," *Advances in the Astronautical Sciences*, vol. 109, pp. 1207–1227, 2001.
- [49] I. M. Ross and M. Karpenko, "A review of pseudospectral optimal control: From theory to flight," *Annual Reviews in Control*, vol. 36, no. 2, pp. 182–197, 2012.
- [50] M. Karpenko, S. Bhatt, N. Bedrossian, and I. M. Ross, "Design and flight implementation of operationally relevant time-optimal spacecraft maneuvers," *Advances in the Astronautical Sciences*, p. 142, 2011.

- [51] M. Karpenko, S. Bhatt, N. Bedrossian, A. Fleming, and I. M. Ross, "first flight results on time-optimal spacecraft slews," *Journal of Guidance Control and Dynamics*, 35(2), pp. 367–376, 2012.
- [52] M. Karpenko, S. Bhatt, and B. Hamilton, "Application of pseudospectral optimal control for shortest-time spacecraft attitude maneuvers," *Workshop on Guidance, Navigation and Control Applications in the Aerospace Industry, IEEE Conf. on Decision and Control, Maui, HI*, 2012.
- [53] Nanyang Technological University. Satellite Research Centre – X-SAT Micro-Satellite. Available:
<http://www.sarc.eee.ntu.edu.sg/Project/Pages/XSAT.aspx>
- [54] Satellite Imaging Corporation. IKONOS stereo satellite imagery. [Online]. Available: <http://www.satimagingcorp.com/svc/ikonos-stereo-satellite-images.html>
- [55] Defense Acquisition University, "Business case analysis," Defense Acquisition University Online. [Online]. Available:
<https://acc.dau.mil/CommunityBrowser.aspx?id=32524>

THIS PAGE LEFT INTENTIONALLY BLANK

INITIAL DISTRIBUTION LIST

1. Defense Technical Information Center
Ft. Belvoir, Virginia
2. Dudley Knox Library
Naval Postgraduate School
Monterey, California